1973

Study of Ames Laboratory Research Reactor physics characteristics by few group design techniques

Joseph Samuel Crudele
Iowa State University

INFORMATION TO USERS

This dissertation was produced from a microfilm copy of the original document. While the most advanced technological means to photograph and reproduce this document have been used, the quality is heavily dependent upon the quality of the original submitted.

The following explanation of techniques is provided to help you understand markings or patterns which may appear on this reproduction.

1. The sign or "target" for pages apparently lacking from the document photographed is "Missing Page(s)". If it was possible to obtain the missing page(s) or section, they are spliced into the film along with adjacent pages. This may have necessitated cutting thru an image and duplicating adjacent pages to insure you complete continuity.

2. When an image on the film is obliterated with a large round black mark, it is an indication that the photographer suspected that the copy may have moved during exposure and thus cause a blurred image. You will find a good image of the page in the adjacent frame.

3. When a map, drawing or chart, etc., was part of the material being photographed the photographer followed a definite method in "sectioning" the material. It is customary to begin photoing at the upper left hand corner of a large sheet and to continue photoing from left to right in equal sections with a small overlap. If necessary, sectioning is continued again — beginning below the first row and continuing on until complete.

4. The majority of users indicate that the textual content is of greatest value, however, a somewhat higher quality reproduction could be made from "photographs" if essential to the understanding of the dissertation. Silver prints of "photographs" may be ordered at additional charge by writing the Order Department, giving the catalog number, title, author and specific pages you wish reproduced.

University Microfilms

300 North Zeeb Road
Ann Arbor, Michigan 48106

A Xerox Education Company

Study of Ames Laboratory Research Reactor physics characteristics by few group design techniques

by

Joseph Samuel Crudele

A Dissertation Submitted to the
Graduate Faculty in Partial Fulfillment of
The Requirements for the Degree of
DOCTOR OF PHILOSOPHY

Major: Nuclear Engineering

Approved:

Signature was redacted for privacy.

In Charge of Major Work

Signature was redacted for privacy.

For the Major Department

Signature was redacted for privacy.

For the Graduate College

Iowa State University
Ames, Iowa

1973

TABLE OF CONTENTS

I. INTRODUCTION

Considerable effort has been placed on the analysis of light-water reactors to the point of its being nearly an exact science. Much less effort has been placed on the analysis of heavy-water, highly-enriched reactors resulting in slightly less confidence and slightly greater error in results.

The Ames Laboratory Research Reactor (ALRR) (1) is a heterogeneous reactor using highly enriched MTR type fuel assemblies. It is moderated and cooled by heavy water. The fuel elements are arranged in a pattern that makes it difficult to analyze. However, methods were used using R-θ geometry with existing codes.

When the six control rods are fully withdrawn, the bottom of the cadmium sections are 11 inches above the top of the fuel region. In a light water reactor, this amount of water would make the remaining rods worthless. However, in the D_2O system, the rods still have a total reactivity worth of approximately 0.6 percent Δk_{eff}. To account for this effect, a uniform poison that contributed a reactivity change equal to the remaining worth of the six rods was assumed to exist in the rodded region.

The LEOPARD code as modified for plate type fuel elements by Kim (2) was used to obtain microscopic and macroscopic cross sections. LEOPARD combines the 54 fast group cross section data from MUFT-5 for the fast neutron data with the 172 thermal group cross sections from KATE-1 for the thermal neutron data

into one convenient code. These fine mesh data are coalesced into three fast and one thermal group values for four group analysis plus a single set of fast parameters for use with the thermal group data for two group analysis. The two group constants can be used for initial parameter studies to reduce cost. The four group data can then be used for more accurate results. Not much accuracy is gained in thermal reactors by using more than four neutron groups.

The two-dimensional diffusion code EXTERMINATOR-2 was used for unit cell calculations and for the R-θ reactor studies. It is a simple code to use that is fairly fast in operation.

The FOG code was used for its buckling iteration feature that enabled getting group dependent axial buckling terms for the EXTERMINATOR-2 R-θ analysis. The FOG poison search feature enabled determining the added poison cross section required in the region with the control rods fully withdrawn.

The main emphasis in this dissertation is the analysis of the ALRR 13 element, cold clean, minimum-critical-mass reactor and the full 24 element core using diffusion theory codes with R-θ geometry. Emphasis is placed on accounting for the worth of the fully withdrawn control rods.

An experiment was conducted using boron-aluminum strips to calibrate control rods and to determine the excess reactivity of the 24 element core. Comparisons are made between measured and calculated results.

II. LITERATURE SEARCH

This chapter describes some of the highly enriched fueled heavy water moderated reactors in the United States and reviews the methods used in their design and analysis. The reactors considered are the Massachusetts Institute of Technology Reactor (MITR), the Georgia Tech Research Reactor (GTRR) and the National Bureau of Standards Reactor (NBSR). All of them use MTR plate type fuel elements with aluminum cladding. The older MITR reactor was based on hand calculations. The newer reactors were able to rely on machine calculations to a greater extent.

The ALRR will be discussed in detail in Chapter III.

A. MITR

The Massachusetts Institute of Technology Reactor (3,4) has been operating since 1958 and the discussion will be limited to the initial core.

The initial reactor designed for 1 MW operation was a heavy water moderated and cooled, heterogeneous highly enriched uranium reactor. The MTR type fuel elements are spaced in an open array in a 4-foot diameter by 7-foot high aluminum tank of D_2O. The tank is surrounded by a 2-foot ring of graphite. Outside of this ring is a thermal shield and a biological shield of dense concrete. The shields are pierced on top, bottom and sides by many openings which penetrate to the reactor tank for experiments. No experimental openings breach the

D_2O tank.

The primary core consists of 19 fuel elements, 1 in the center, 6 in a hexagonal pattern around the center at a radius of 6.375 inches and 12 in a circular pattern outside at a radius of 13.25 inches. There is approximately a 6.5-inch spacing between elements. This is the minimum critical spacing; therefore, any motion of fuel will decrease reactivity. This loading pattern forms an active core region about 30 inches in diameter and 2-foot high. The core is suspended in the 4-foot diameter tank which is filled to a depth of 6 feet with 99.8 mol percent D_2O. The heavy water thus forms 2-foot-thick top and bottom reflectors and about a 9-inch-thick radial reflector.

The active portion of the fuel elements is 23.375 inches long. Each fuel element consists of 18 plates having a radius of curvature of 5.5 inches and are fastened into 0.187-inch-thick grooved side plates. The inner 16 plates have a 0.020-inch thick aluminum fuel alloy clad on both sides with 0.020 inches of aluminum, giving a total plate thickness of 0.060 inches. The two outside dummy plates are 0.060-inch thick-aluminum. The spacing between each plate is 0.117 inch and the distance across the 16 fuel plates and the two dummy side plates is 3.068 inches. The fuel plates, including the end cladding, are 24.625 inches long.

The original fully loaded fuel elements each contained an average of 105 grams of U-235 as 93-94 percent enriched uran-

ium distributed over an active length of 23.375 inches. The later cores also contained 162 gram elements. The fuel element is supported at the top by a 3-inch diameter upper adapter tube which connects the fuel element to a shielding plug at the top of the reactor. The lower adapter screws into cylindrical adapter section at the bottom of the fuel element and connects the fuel element to the inlet plenum stub tubes.

There are 6 shim-safety rods and 1 regulating rod. The absorber section of the shim-safety rod is a hollow cylinder of cadmium 0.040-inches thick, 2.15-inches outside diameter, and 26.125-inches long. The cadmium is clad both inside and outside with 0.050-inch-thick aluminum. The absorber portion of the regulating rod has the same dimensions as the safety and control rods except that only one-third of the circumference of the control cylinder is cadmium. The control rods travel vertically and their traveling distance is 27.2 inches. In the full up position, the cadmium in the shim-safety rods is 3 inches above the active fuel region in the core. The original control rod was a full circle of cadmium but its worth was more than one dollar in reactivity so the circumference was reduced to one-third of the original size.

The top shield is a 5-foot diameter rotary plug with a radial slit to facilitate removal of one fuel element at a time. To service any fuel element, all control rods must be fully down.

There are 40 experimental ports of various sizes up to 12

inches and included is a medical therapy room beneath the reactor intended for cancer research. A thermal column consisting of a 5' x 5' array of graphite penetrates to the graphite annulus.

The design calculations, which were based on two-group diffusion theory calculations of a heavy water reactor with an appreciable amount of aluminum in the core and reflector, have not been checked extensively. Experimental values for age of fission neutrons in heavy water are available, but the data dealing with the thermal diffusion coefficients are ambiguous in that the purity of the heavy water in which the measurements were taken is not usually given, and calculations show that the thermal diffusion length is a strong function of the light water concentration. In a reflector region consisting of heavy water and structural aluminum, the heavy water properties are strongly affected by the aluminum. Since Fermi age, thermal and fast diffusion coefficients, and thermal diffusion length measurements are lacking for mixtures of heavy water and aluminum, these constants for each mixture have been calculated for the U-235 fission spectrum from their definitions with microscopic cross section data. The results are summarized in Table II-1 as a function of the volume ratio of aluminum to D_2O for 99.75% pure D_2O.

Thermal and fast flux distributions have been obtained in a four region spherical reactor for various core sizes and heavy water reflector thickness parametric studies. The four

Table II-1

Two-group Constants Used for MITR Non-fuel Regions

Volume Ratio Al/D_2O	Age cm^2	Fast Diffusion Coefficient cm	Thermal Diffusion Coefficient cm	Thermal Diffusion Length cm
0	126	1.28	.830	104.5
.1	144	1.34	.895	28.3
.3	182	1.45	1.019	19.5
.5	220	1.55	1.128	17.1
.7	262	1.65	1.230	16.1
.9	298	1.73	1.322	15.6

regions are heavy water, fuel, heavy water, and graphite.

To obtain an order of magnitude of the critical mass of the MITR, the disadvantage factor for a unit cell in the fuel lattice has been calculated by Morgan (5). The disadvantage factor is defined as the ratio of volume-averaged thermal neutron flux in the fuel of a unit cell. This calculation has been made on the basis of two-group diffusion theory in three ways, each of which differs from the others in the assumptions made regarding the variation of the fast neutron flux in the cell and the amount of the net leakage of thermal neutrons out of the cell. Under the assumption that the fast neutron flux is constant in the cell and that there is no net leakage of thermal neutrons from the cell, the disadvantage factor has been found to be equal to 1.197. If the spatial variation of the fast neutron flux in the cell is taken into

account, and if the net thermal neutron leakage is taken to be zero, the disadvantage factor is found to be 1.185. Finally accounting for the spatial variation of the fast neutron flux and the leakage of thermal neutrons out of the cell gives a disadvantage factor of 1.160.

For a cold clean reactor with no allowance for the disadvantage factor and poisons, the critical mass is estimated to be 1244 grams with the two group diffusion theory model. To account approximately for the thermal neutron flux depression within each fuel element the value of 1244 is multiplied by the disadvantage factor 1.160 to yield an estimated critical mass of 1445 grams in the case of the cold clean reactor.

The MITR startup measurements (6), however, yielded a critical mass of 1950 grams, which is 35 percent higher than the predicted value.

Extensive calculations of the MITR were performed after startup using Monte Carlo calculations and 1/2 core symmetry. The typical 19 fuel-element core was analyzed with the fuel elements considered as homogenized squares. The rods were considered to be 3 inches above the top of the fuel. K_{eff} were obtained for neutron lifetimes (ℓ) ranging from 1.3 to 1.99 msec and water purity of 99.8 mol percent D_2O. The age to 1.4 ev was 101.6 cm^2 and to 0.025 ev was 128.6 cm^2. The calculated critical mass was 12,150 mβ at 20°C (one β is the value of delayed neutrons). The measured value was only 652 mβ for

an error of 11,500 mβ which corresponds to a mass difference of 560 grams of U-235. This is about the same mass difference as that obtained for the initially predicted and measured values.

Mathews (7) performed two group diffusion calculations using the TWENTY-GRAND code. He used a quarter core, 51 region, X-Y geometry with 20x20 meshed and zero-flux boundary conditions. In his calculation, the fast group constants were generated from the GAM-1 code, and the thermal group constants were computed by hand for a neutron temperature of 383°K. Axial bucklings were derived from the measurements in Reference (4). Comparison of his calculations and measurements shows that measured disadvantage factors are 7 percent higher than calculated values. The calculated traverse through elements indicates that calculated values are higher within fuel elements and also slightly higher in the moderator region than the cobalt wire measurements. The average thermal flux disadvantage factor obtained from all the measurements was 1.395, which is approximately 13 percent higher than the calculated value of 1.235 in Reference (4).

B. GTRR

The Georgia Tech Research Reactor (8) has been operating since 1964. It initially operated at 1 MW for several years but is now operating at 5 MW. The GTRR is a heavy water moderated and cooled reactor using highly-enriched uranium fuel.

The basic reactor consists of a 6-foot diameter aluminum vessel containing about 1100 gallons of heavy water in which the fuel assemblies and control elements are installed. The fully loaded core contains 19 fuel assemblies arranged in a triangular array on a 6-inch pitch. This core forms a vertical right cylinder approximately 2 feet in diameter and height. Surrounding the core is a 2-foot-thick layer of D_2O coolant which serves as a neutron reflector. Additional neutron reflection is obtained from a 2-foot-thick graphite region on the sides and beneath the reactor vessel.

Degradation of the D_2O by light water is minimized by maintaining an atmosphere above the D_2O that is essentially free of water vapor. This is accomplished by maintaining a helium gas blanket at about 1 inch of water pressure above atmospheric. The volume between the outer reactor vessel wall and the inner thermal shield face is called the graphite region. It is filled with 4-inch x 4-inch stringers of grade AGOT graphite. The annular biological shield, containing appropriate penetrations for the reactor experimental facilities, extends approximately 5 feet outward from the thermal shield and completes the reactor structure.

The standard fuel element for the GTRR contains 16 individual curved aluminum-uranium alloy plates. The fuel matrix is 0.020 inches thick, 2 1/2-inches wide, and 23 1/2-inches long. Each plate is clad with type 1100 aluminum alloy 0.015-inches thick, 2.848-inches wide, 25-inches long and has a

5 1/2-inch radius of curvature. Each plate will contain approximately 11.7 grams of U-235.

The maximum size core is comprised of 19 assemblies (elements) of 16 plates each. The fuel bearing section of the assemblies is a completely enclosed box 2.959 inches by 2.772 inches by 27 1/2-inches long. Coolant flow passages, nominally 0.106 inches thick by 2.583-inches wide, are obtained by inserting the edges of the fuel plates into longitudinal slots machined in the side plates. The fuel plates are permanently fastened to the side plates.

In addition to the standard element described above, two special removable plate elements are being secured. These will be identical to the standard element except that the lower locating end-fitting and lower fuel spacer (comb) can be removed by screws. This will permit the central 10 fuel plates (which are not permanently fastened) to slip out of their grooves in the side plates.

The reactor is controlled by means of four shim-safety elements and one regulating element. The shim-safety elements are flat, hollow blades consisting of cadmium metal 0.040-inch thick, clad inside and out with aluminum 0.083-inch thick. These blades weigh approximately 20 pounds and are 5.5-inches wide by 1-inch thick. The hollow center is filled with helium and sealed. The cadmium section has a length of 45.5 inches, and the length from pivot point to end is 60.75 inches. The regulating rod is a 24-inch-long tube of cadmium metal, 1.380-

inch I.D. and 1.420-inch O.D., jacketed inside and out with 0.040 inch of aluminum.

The shim-safety blades are mounted at the top of the reactor vessel, and swing through the core between adjacent rows of fuel assemblies. The blades are driven through their full travel of 55° of arc by horizontal shafts which are engaged through electromagnetic clutches to the drivemotors. The drive assembly incorporates a spring which is compressed as the shim-safety blade is withdrawn, thus insuring rapid insertion of the blade when the clutch is de-energized by a scram signal. The rods are largely inserted within 0.4 seconds after rod motion commences.

The purpose of the shim-safety blades is to control large amounts of reactivity. The worths of these blades range from 9.7% to 15.2%. While these blades may be inserted individually or as a group, withdrawal is limited to individual element movement at a maximum speed of 0.2 degree/second.

The regulating rod operation is in a vertical direction through the core and is intended for fine control only. It is immobilized by a reactor scram. The twelve-inch total motion results in the bottom of this rod moving from the core centerline in the "in" position to the top of the core in the "out" position. The regulating rod is used for power level control and adjustment after a critical position has been attained by the shim-safety blades. Its reactivity worth is about 0.4%. The speed of this rod is fixed at 0.2 inch/second, which

limits the maximum rate of reactivity change to less than 0.01% per second.

The biological shield consists of layers of boral, steel, lead, and concrete surrounding the graphite reflector. The first layer is a 1/4-inch-thick sheet of boral staked to the inside of the steel shield tank enclosing the graphite. A 3 1/2-inch thick layer of lead, containing the copper tubes of the shield cooling system, is cast in the annular space between the external surface of the steel shield tank and an outer steel retainer. By pouring molten lead into this region, an adequate thermal bond between the shield tank and the cooling tubes has been assured. This section of the shield is commonly termed the thermal shield. Its major function is to reduce heating in the concrete portions of the biological shield as a consequence of absorption of radiation from the core.

The outermost portion of the biological shield is a thick layer of concrete completely enveloping the reactor. In order to minimize the thickness of this layer, very dense concrete is used in preference to lighter, ordinary concrete in that portion of the shield immediately surrounding and adjacent to the core proper.

The shield contains a large number of both horizontal and vertical penetrations to accommodate the various experimental facilities. Addition penetrations are provided for the passage of control element drive shafts, coolant and service piping,

service wiring, ventilation, and instrumentation. All penetrations through the shield are stepped and are equipped with permanent steel liners. Where these penetrations extend into the D_2O or graphite regions, the liners are seal-welded to the shield tank. Major openings in the shield, such as the thermal column, are equipped with movable shielding doors or shutters. All other experimental holes are provided with stepped shielding plugs to prevent hazardous radiation streaming.

The reactor is equipped with numerous horizontal and vertical experimental facilities to be used for the extraction of beams of fast and slow neutrons and for the performance of irradiations within the facilities. The top of the reactor contains a total of 46 vertical penetrations of which 41 are for experimental use, including fuel element positions. Twenty-seven of these are located in the D_2O region within the reactor vessel. The remaining 14 are dispersed through the graphite reflector region. Nineteen of the D_2O region openings are fuel assembly positions, any of which could be used for irradiations.

The reactor contains 22 horizontal openings, a thermal column, and a biomedical irradiation facility. Stations H1 through H10 are horizontal beam ports, all of which lie in the horizontal plane passing through the center of the reactor. Stations H1, H3, H7, H8, and H10 are so located that they look directly at fuel elements and thus give good fast or epithermal neutron beams.

A thermal column, 5-foot square, is provided as an extension of the graphite reflector. It is fitted with a shutter and with heavy shielding located at the outer face. The shutter opens horizontally giving a port 4 inches by 4 inches or 16 inches by 16 inches. A number of removable graphite stringers which extend up to the reactor tank wall are provided in the thermal column.

A shielded room for bio-medical research is located on the side of the reactor opposite the thermal column. This facility is designed to allow accurate exposures of biological specimens to a wide-angle beam of thermal neutrons with a relatively low background of fast neutrons and gamma rays. It is fitted with bismuth gamma shield, water tanks for neutron attentuation, a collimator, shutter, and provisions for a converter plate system. The opening in the reactor is surrounded by the shielded room. The use of a converter plate will permit the fast flux to be increased to about 10^{10} $n/cm^2/sec$ with a corresponding decrease in thermal flux and increase in gamma rays.

For the 5 MW physics design calculations, the two group, two dimensional diffusion theory was used. Both R-Z and X-Y geometries were used with the EXTERMINATOR code. The cross sections and constants input to the two group, two dimensional diffusion calculations were generated from the TEMPEST-11 and FORM codes.

As a check calculation, both THERMOS and TEMPEST-11 codes

were used for generation of thermal group constants, and it was found that the Wigner-Wilkins light moderator approximation in the TEMPEST-11 code yielded the best agreement with the THERMOS results. Subsequent thermal group calculations, therefore, were performed using the Wigner-Wilkins light moderator approximations in the TEMPEST-11 code. All fast group constants were generated by the FORM code which is a Fortran version of the MUFT-4 code. The total bucklings used in both FORM and TEMPEST-11 was chosen as 0.0045 cm^{-2}, one-third of which is the axial buckling and the remainder the radial buckling.

The above calculational model has been used for the initial 10 element, 1 MW GTRR core to test its usefulness. This initial core arrangement went critical with shim blades almost fully withdrawn. In the EXTERMINATOR calculation, the core was represented by six R-Z regions, of which only one is the fuel region. The resulting effective multiplication factor agreed within 1.5 percent of the critical value.

The two-dimensional X-Y calculations for a 1 MW, 10-element core was made in order to determine the critical buckling, which accounts for the transverse leakage in this model. This buckling was assumed constant for subsequent X-Y calculations for the 5 MW core.

In order to determine the reactivity effect of xenon and samarium on the equilibrium 5 MW core, the steady-state concentrations of Xe and Sm were first computed. Then the effect

of these poisons on thermal cross-section was assessed by use of TEMPEST 11 and Δk_{eff} was calculated by use of the X-Y geometry EXTERMINATOR code.

Both the two-dimensional X-Y and R-Z calculational methods were used to determine the temperature coefficient for the 1 MW GTRR core, and these results were compared with experiment to choose the preferred method for the 5 MW calculation. The temperature coefficient for the 1 MW core calculated with the R-Z EXTERMINATOR was -0.0383%/°C at 45°C compared to the measured value of -0.0535%/°C at the same temperature.

C. NBSR

The National Bureau of Standards Reactor (9) is a highly enriched U-235 fueled, heavy water moderated, cooled and reflected reactor designed to produce neutrons and gamma rays for research. The reactor is designed to operate at 10 thermal megawatts.

The core is suspended in an aluminum tank 7 feet in diameter and 16-foot high, filled with 99.75 mol percent pure heavy water. The core tank is surrounded by a thermal shield of 2 inches of lead and 8 inches of steel with a 1-inch gap between the core tank and the inner face of the thermal shield.

Although the grid plates provide for 37 fuel element positions and four 2.5-inch semi-permanent irradiation thimbles, the basic NBSR core has fuel elements in 30 locations and the extra seven positions are especially adapted for 3.5-

inch experimental thimbles. One of the 3.5-inch thimble positions is used for a regulating rod. The fuel elements are located on 7-inch centers in a hexagonal array, and each fuel element is located within a rectangular cell of 6.000 by 6.928 inches.

The four shim-safety arms are mounted on hanger brackets just under the grid plate, two on each side, and swing through the core vertically between fuel elements. The drive shafts penetrate the reactor vessel below water level and drive the shim arms directly.

The core is split into an upper and lower section by the use of fuel elements with an unfueled center section. This unfueled section is 7 inches and the horizontal centerline of the unfueled section is 140 inches from the top of the reactor or 23 9/16 inches from the top of the lower grid plate. The upper and lower section of core is 44 inches in diameter and 11 inches thick, and thus, the overall dimension of the core is 44 inches in diameter and 29 inches high.

The fuel assemblies are MTR type elements that consist of 19 curved plates and two side plates. The 19 curved plates have a radius of curvature of 5.5 inches and are fastened into 0.188-inch-thick grooved side plates. The inner 17 plates have a 0.020-inch-thick aluminum fuel alloy clad on both sides with 0.015 inches of aluminum, giving a total plate thickness of 0.050 inches. The two aluminum outside plates are 0.065-inches thick and form a box section, which surrounds the fuel

plates, with the two aluminum side plates. The spacing between the plates is 0.116 inches. The distance across the 17 fuel plates and 2 outside plates is 3.068 inches and the straight line width of a fuel element is 3 inches.

The fuel plate, including the aluminum end cladding, is 32 inches long. The central region of the plate is of unfueled aluminum 7-inches high, and it separates the two fueled regions, each being 11-inches high. The aluminum side and outside plates extend beyond 32 inches of the fuel plate length and join the upper and lower adapter sections to form a closed flow path for the heavy water which flows through the fuel element.

The fuel matrix is an uranium aluminum alloy containing approximately 18 percent enriched uranium. The average enrichment of the fuel is 93.5 percent U-235. The fuel elements of the initially critical NBSR core contained an average of 170 grams of U-235 each, distributed over the upper and lower active sections of the element. This corresponds to a loading of 10 grams of U-235 in each fuel plate. The subsequent 30 element core, however, contained seven 205-gram elements. The enrichment and dimension of the 205-gram element are the same as those of the 170-gram element, but the uranium loading per fuel plate is increased accordingly.

Primary control of the NBSR is accomplished by the use of four semaphore type shim safety arms. Fine control is accomplished by the use of a single vertical type regulating rod.

Each shim-safety arm is one inch by 5 inches by 52 inches active length. The absorber section of the shim safety arms is a hollow form of 99.9 percent pure cadmium 0.040-inches thick and 52-inches long. The cadmium is clad both inside and outside with 1100 series aluminum. The interior of the hollow section is filled with helium.

Each NBSR shim safety arm has an operational travel of 41 degrees with the maximum deflection of 42.6 degrees and the maximum withdrawal of 1.5 degrees. Shim arm catchers were added later to provide safe operation of blades.

The originally designed regulating rod was a helium filled aluminum cylinder, 2.7 inches in length. However, the rod was subsequently replaced by a solid aluminum rod 2.5 inches in diameter and 29 inches in length for purpose of obtaining a desired rod worth. The regulating rod is located in one of the 3.5-inch vertical thimbles directly in the core. The regulating rod travels 29 inches vertically and the drive mechanism is mounted in the top plug.

The heavy water level in the reactor vessel is normally maintained at 117 inches above the top of the core by the 3-inch overflow pipe, and the radial heavy water reflector is 20-inches thick. The bottom reflector is approximately 2-foot thick. The large space above the core allows transfer of fuel elements to the fuel element chute.

Surrounding the core tank is a thermal shield and a 14-sided high density concrete biological shield. One of these

faces contains a thermal column that consists of a graphite section 54 x 52 inches in cross section by 37-inches deep.

A cryogenic facility provides a large re-entrant port that can be used to place a large volume of low temperature moderating material close to the core. It will be used to increase the intensity of low energy neutrons for certain neutron scattering experiments. This will be accomplished by refrigerating a large block of ice to about 25°K by means of cold helium gas. The cryogenic facility is to be filled with a heavy water tank mounted on the end of the large rolling plug during the early stages of reactor operation. The water tank is penetrated by two 6-inch inside diameter tubes which mate with the two cryogenic beam ports in the biological shield.

Other experimental facilities consist of 11 horizontal beam tubes, 17 vertical thimbles and 4 pneumatic tubes.

The design procedures used by Kim (2) are based on the theory and technique used for the design of light water moderated power reactors. For generation of few group neutron cross sections, the modified LEOPARD code was chosen over the HAMMER code because of simplicity in input data preparation, savings in computation time, and unique features available only in the code. For the diffusion theory spatial calculations, the FOG and EXTERMINATOR-2 codes were selected instead of the WANDA and PDQ-5 codes because of easy access to the digital computer for which the former codes were programmed.

The diffusion theory spatial calculations were used instead of the transport calculation to reduce requirement for computer time, and the four neutron energy group scheme was chosen because the number of neutron energy groups above four usually does not provide appreciable improvement over the four group scheme relative to the added computer time. The calculated k_{eff} of the 20 element NBSR at 68°F is 1.00389 compared to the measured value of 1.00806 at 70°F, and the corresponding values for the 30 element NBSR are 1.12275 and 1.11235, respectively. These results give agreement between the calculated and measured values within 0.5 percent for the 20 element core and within one percent for the 30 element core. The results of application of the proposed design procedures to the NBSR have established their usefulness in predicting the initial excess reactivity of high-enriched heavy water moderated reactors.

The neutron leakage from the 20 element NBSR core at 68°F ranged from 31.2 to 36.0 percent of the total neutron removal, while the leakage from the 30 element core at the same temperature ranged from 28.1 to 29.5 percent of the total neutron removal. The calculated worth of 10 dummy fuel elements in the 20 element core was 0.53 percent $\Delta\rho$ compared to a measured value of about 0.5 percent. The calculated worths of upper reflector above the heavy water dump for the 20 element core agreed well with the measured values.

The calculated temperature coefficient was much lower

than the measured coefficients for both 20 and 30 element cores. It was -0.0000498 $\Delta\rho$/°F compared to a measured value of -0.0000917 $\Delta\rho$/°F for the 20 element core. Thus, the agreement between calculated and measured temperature coefficients is very poor. The calculated void coefficient of reactivity is based on a uniform change in density of the heavy water moderator throughout the reactor and it ranged from 0.02554 $\Delta\rho$/(5% void) for the 20 element core to -0.01895 $\Delta\rho$/(5% void) for the 30 element core at 68°F. The calculated worth of a single regulating rod of 2.125-inch diameter at 68°F was -0.0056 $\Delta\rho$ compared to a measured value of -0.006 $\Delta\rho$ for the 20 element core. The worth of fully inserted four shim-safety arms in the 30 element core at 68°F was computed to be -0.298 $\Delta\rho$ compared to about -0.405 $\Delta\rho$ as measured during the low power test at 70°F; however, there is a question as to the accuracy of the measured worth. The proposed method for control rod worth calculation seems adequate.

III. DESCRIPTION OF THE ALRR

A. General Information

The Ames Laboratory Research Reactor as described in the ALRR Hazards Report (1) is a heterogeneous arrangement of highly enriched uranium-aluminum fuel assemblies, using aluminum as structural material and heavy water as its moderator, reflector and main coolant. The reactor was designed for initial operation at a power level of 5 MW with provisions for possible conversion to considerably higher power level.

A cutaway view of the ALRR is shown in Figure III-1 and a plan view of the reactor is given in Figure III-2. These figures show the core, reflectors, control rods and experimental facilities.

The biological shield surrounding the core has the form of an irregular 10-sided prism that is 15-foot high, 22-foot across its maximum horizontal dimension and 19 foot across its minimum horizontal dimension. A nominal 6-foot thick of high density concrete surrounds the core radially.

A total D_2O inventory of approximately 16,200 pounds (1770 gallons) is maintained in the system. The D_2O coolant water enters through a plenum at the bottom of the fuel, passes up through the fuel into the reactor vessel and then out an overflow tube, attached to the bottom of the vessel, that maintains the water at a constant level. The inlet temperature is about 117°F and the outlet temperature is about 125°F under

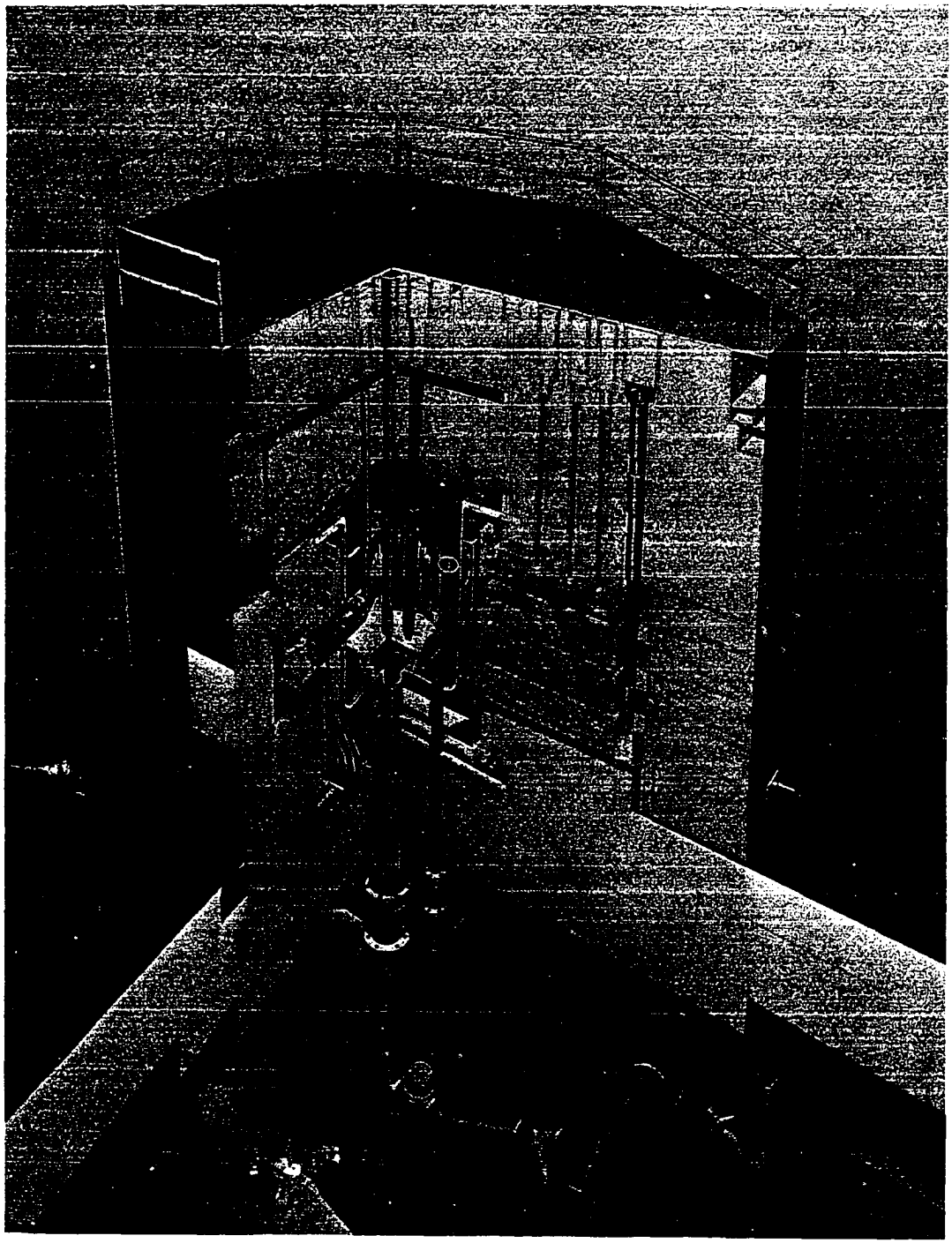

Figure 3-1. ALRR cutaway view

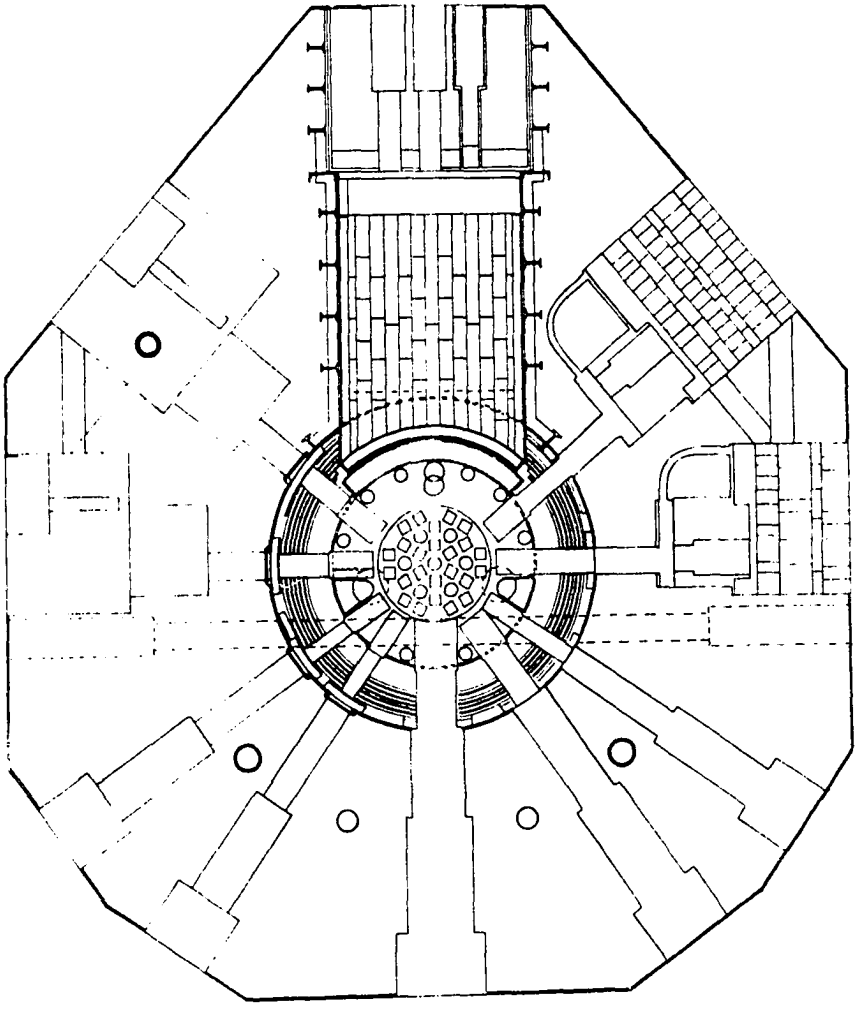

Figure III-2. ALRR plan view

normal 5 MW operation ($\Delta T = 7.85°F$). D_2O leak detectors are strategically located throughout the system and leak detection is annunciated in the control room.

The secondary cooling system provides the necessary light water coolant for the secondary side of the heat exchanger for the D_2O system. The major components of this system are the cooling tower and its associated fans and the main cooling pumps.

A helium atmosphere is maintained above the water within the reactor and thermal shield to minimize production of corrosive acids that occur from the interaction of nuclear radiation with air and water vapor.

B. Reactor Core

The core geometry is a right cylinder, approximately 24-inches high and 32 inches in diameter, composed of a maximum of 24 fuel assemblies. The assemblies are arranged in circular patterns with their centerlines forming three concentric circles of 5.25 inches (6 assemblies) 10.5 inches (6 assemblies) and 13.89 inches (12 assemblies). The reactor core, including its heavy water, is contained in 5-foot diameter by 6-foot high aluminum tank. The tank was initially filled with 99.75 mol percent pure heavy water. The position of the core within the tank provides a heavy water reflector of approximately 15 inches on the side, 30 inches on the top and 18 inches on the bottom.

The fuel elements are supported by a lower aluminum grid plate with orifices that direct the heavy water from the lower plenum up through the fuel elements. A thin grid plate guides the upper end of the fuel elements. Aluminum hold down units hold each fuel element simply and firmly in place on the fuel element positioning stop by means of a removable concrete and lead filled plug.

C. Light Water Thermal Shield

The core tank is coaxially contained within a second tank which is approximately 8 feet in diameter. The resulting annulus between the two tanks comprises the thermal shield region. This annulus is occupied by light water and six coaxially positioned, 1-inch thick stainless steel shells. This shield results in 12 inches of light water and 6 inches of stainless steel.

The heavy water tank protrudes into the thermal shield tank in the region of the graphite thermal column to increase the flux in the thermal column.

D. Fuel Assembly

A cross section and vertical view of the ALRR fuel elements are shown in Figure III-3. It is an MTR type fuel element that consists of 17 curved plates and two side plates. The 17 curved plates have a radius of curvature of 5.5 inches and are attached to two 0.188-inch grooved side plates. Fuel is contained in the 15 inner plates that have a 0.020-inch

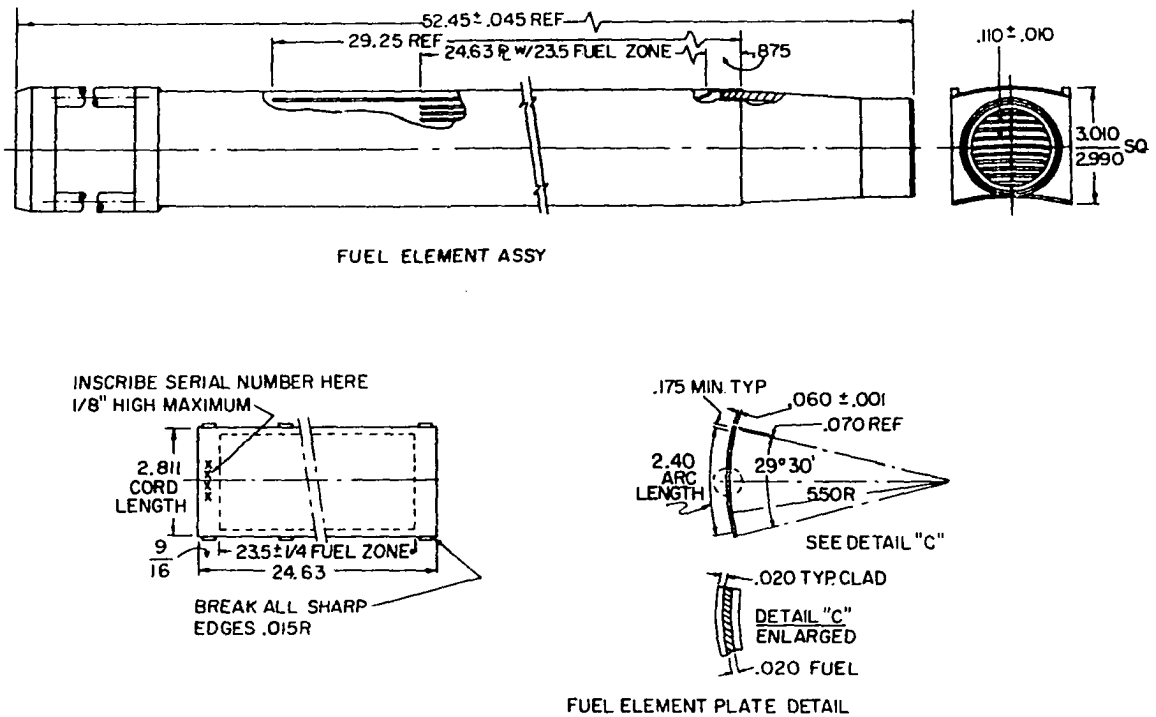

Figure III-3. ALRR fuel element

thick aluminum fuel alloy with 0.020-inch thick aluminum cladding giving a total thickness of 0.060 inch. The two outside plates are also 0.060 inches thick and form a box section, which surrounds the fuel plates, with the two aluminum side plates. The average spacing between the plates is 0.110 inches. The unit forms a 3-inch by 3-inch box assembly. The total length of the completed fuel assembly, including hold-down extension bar and bottom transition nozzle, is approximately 52.5 inches.

The fuel plates are 24.63-inches long, and the fuel region has an average length of 23.5 inches and an average width of 2.478 inches. The fuel matrix is an uranium-aluminum alloy and each fuel plate used in the initial elements contained an average of 11 grams of U-235, providing a nominal inventory of 165 grams per fuel assembly. The average enrichment of the fuel is 93.5 percent U-235.

The lower adapter acts as an inlet nozzle and a valve. Coolant enters the internal passage of the bottom adapter, flows up through the lower portion of the box section, through the curved fuel plate channels and then through the upper box and out the top adapter into the heavy water moderator and reflector regions.

E. Reactor Control Rod System

Control of the reactor is maintained by vertical insertion and removal of six control rods, each in the form of a hollow cylinder of pure cadmium, 20-inches long and 2.75-

inches inner diameter, with a wall thickness of 0.060 inch. The cadmium is completely encased with stainless steel cladding.

The six control elements are radially positioned in the core such that their vertical centerlines form a circle of approximately 9.1-inches radius. Five of the six elements, identified as shim rods, can be raised either individually or simultaneously in any combination after the regulating rod described below has been raised to its servo range. The sixth element, designated as the regulating rod, is operated independently from the others. It has the capability of automatic operation when within its servo range which is set from 75% to 100% withdrawn. In the automatic mode, it is driven in or out by the linear power channel through a servo loop to maintain the reactor power constant within small limits. All control rods have strokes of 28 inches, the fully withdrawn positions of their cadmium sections being 11 inches out of the core. They are magnetically latched into the rod drive systems, and dropped into the core by gravity on a scram signal generated by the reactor automatic safety system, or a shutdown signal initiated by the reactor operator.

The control element is connected by an extension coupler to an armature against which the scram magnet is placed to allow the drive to pick up and then move the control element.

In the original control rods, the scram magnet was raised and lowered by a vertical rack, which was operated within a

guide tube by a pinion gear rotated by a horizontal drive shaft. The horizontal drive shaft penetrated the shield radially and intersected the control rod vertical certerline at a position a few inches above the D_2O level. When a scram occurred, the deenergized magnet released the vertical extension and control rod assembly which dropped into the core free of the vertical rack and horizontal drive shaft. A snubber piston provided a slowing down of the rod as it was about to seat. This reduced the shock of the rod drop.

These rods have been replaced by a vertical drive, lead screw system with the poison section and length of travel similar to the replaced units.

F. Experimental Facilities

A total of 35 experimental facilities penetrate the shielding to permit access to core radiations in a manner which suits the particular research requirements of the Ames Laboratory Staff.

Ten horizontal facilities, with center-lines located about 3'-6" above the reactor floor level, extend radially from the core to the reactor faces. These consist of four beam tubes of 6-inch diameter equipped with rotary shutters and cave arrangements which make them particularly suitable for neutron diffraction work; three beam tubes of 4-inch diameter with vertical shutters, which are designed particularly for irradiation work; two beam tubes, one of 11-inch and one

of 7 1/2-inch diameter, for loop work; and a 4' x 4' x 6' thermal column equipped with nine horizontal access plugs.

Six additional horizontal facilities are provided, consisting of four pneumatic rabbits for fast sample insertion to the core periphery while the reactor is operating, and two grazing tubes, one 4" and one 6" in diameter, extending completely through the reactor, tangent to the core.

Nineteen vertical facilities extend downward from the top of the reactor to regions of various levels of neutron flux. Nine of these are located over the thermal column with all but two terminating at the top face of the graphite; the remaining two penetrate 4 inches into the graphite and are fitted with rotary shutters at the reactor top to permit insertion and removal of samples while the reactor is operating. A large 1' x 4' opening provides vertical access to the entire back face of the thermal column graphite. Eight of the remaining nine vertical thimbles extend into the D_2O reflector along the periphery of the core tank and one extends into the core along the core vertical centerline. This central thimble and two of the reflector thimbles can be used for the insertion of converter tubes for fast neutron irradiation work. One of the reflector converter units is presently provided with a liquid nitrogen cryogenic facility for fast neutron irradiations at low temperatures.

IV. METHODS USED TO ANALYSE THE ALRR

The purpose of this research is to determine the criticality and reactivity of the initial 13 element minimum critical mass reactor and the reactivity of the initial, cold, clean 24 element core. Reactor physics calculations generally involve two large areas of computation. One is the generation of effective few group cross sections for small regions called cells or lattices. Within each cell, somewhat detailed calculations of energy spectrum and spatial neutron distributions are performed. The other is the combination of small regions into a large region representing the reactor for purpose of obtaining the integral parameters of the reactor such as reactivity.

A. Generation of Neutron Cross Sections

The LEOPARD (10) code was used to generate the neutron cross sections. It combines MUFT (11) for the fast neutron spectrum with KATE (12) for the thermal neutron cross sections.

MUFT is a fast neutron spectrum code and solves the multigroup transport equation for the first two coefficients of the directional neutron flux and the isotropic and anisotropic components of the slowing down densities due to a cosine-shaped neutron source. Hydrogen may be treated exactly or in a Selengut-Goertzel (SG) approximation (13). Both age and Grueling-Goertzel approximations (self-consistent age) (14) are available for energy degradation by heavy elements. Slow-

ing down of neutrons by inelastic scattering and removal of neutrons resulting from capture and fission resonances is included (13).

Although the MUFT (MUFT-5) code allows up to a total number of 80 multigroups, the present practice is usually limited to 54 groups. Except for resonance absorptions, it is assumed that the group width is small enough as compared to the flux and cross section variation to permit replacing the average of product by the individual averages. The absorption cross section is defined to be the sum of a smooth contribution and resonance contribution.

The resonance capture can be computed exactly, in terms of the observed absorption cross section, in only two cases:

1) Moderation by hydrogen, absorber atomic weight infinite.

2) Moderation by any scatterer, all absorption and scattering cross sections independent of energy.

However, the actual case in which we are interested is

3) Moderation by any scatterer, all cross sections energy dependent, and this case cannot be solved rigorously. In the MUFT solution, it assumes that the resonances are sufficiently spaced and no absorptions occur between resonances. It is further assumed that the resonances are sufficiently far from the source energy region, so that the fluctuation in the collision density due to the source have damped out, and that the resonances are sufficiently narrow so that a neutron will

suffer no more than one collision within any one resonance. The MUFT code assumes that all inelastically scattered neutrons appear in the first 25 multigroups, and inelastic scattering which fails to remove a neutron from a given group is neglected. The cross section for (n,2n) reactions is also included in the inelastic scattering matrix. In the integration of the slowing down densities, it has been assumed that they vary linearly with lethargy within any one group. Once the multigroup equations are solved for flux, current, and slowing down densities, the MUFT code coalesces the multigroups into a fewer number of groups under specified few group (or broad group) breakpoints.

The energy breakpoints for few group schemes out of the 54 multigroups are optional and must be supplied by the user. These breakpoints are included in LEOPARD. For the nuclides which determine the MUFT spectrum, the cross sections and related constants for 54 energy groups are supplied as data library which are permanently stored on a magnetic tape.

The neutron energy ranges from 10 Mev to 0.625 ev in the MUFT spectrum calculation. The 54 group structure currently used in MUFT data library is shown in Table IV-1. The particular structure was used since the original version of MUFT and the number and size of the group have been devised with high leakage, light water moderated lattices in mind.

Table IV-1

Energy Group Structure Used in MUFT Code

Group Number	Energy (ev)	Lethargy	Lethargy Width
0	10×10^6	0	
1	7.79	0.25	0.25
2	6.07	0.50	
3	4.72	0.75	
4	3.68	1.00	
5	2.86	1.25	
6	2.23	1.50	
7	1.74	1.75	
8	1.35	2.00	
9	1.05	2.25	
10	821×10^3	2.50	
11	639	2.75	
12	498	3.00	
13	387	3.25	
14	3.02	3.50	
15	235	3.75	
16	183	4.00	
17	143	4.25	
18	111	4.50	
19	86.5	4.75	
20	67.4	5.00	0.25
21	40.9	5.50	0.50
22	24.8	6.00	
23	15.0	6.50	
24	9.12	7.00	
25	5.53	7.50	
26	3.35	8.00	
27	2.03	8.50	0.50
28	1.23×10^3	9.00	0.50
29	750×10^0	9.50	
30	454	10.00	
31	275	10.50	
32	167	11.00	0.50
33	130	11.25	0.25
34	101	11.50	
35	78.7	11.75	
36	61.3	12.00	

Table IV-1 (continued)

Group Number	Energy (ev)	Lethargy	Lethargy Width
37	47.8	12.25	0.25
38	37.2	12.50	
39	29.0	17.75	
40	22.6	13.00	
41	17.6	13.25	
42	13.7	13.50	
43	10.7	13.75	
44	8.32	14.00	
45	6.50	14.25	
46	5.10	14.50	
47	3.97	14.75	
48	3.06	15.00	
49	2.38	15.25	
50	1.855	15.50	0.25
51	1.440	15.7538	0.2538
52	1.125	16.00	0.2462
53	0.835	16.30	0.3000
54	0.625	16.5884	0.2884

The KATE-1 code is a current version of a digital computer program for calculating Wigner-Wilkins and Maxwellian averaged thermal constants. It solves the Wigner-Wilkins (15) differential equation for a homogeneous medium moderated by chemically unbound hydrogen atoms in thermal equilibrium. The differential equation provides a faster and simpler numerical method for calculating thermal neutron spectra than would a multigroup solution to the integral transport equation.

The energy mesh points currently used in the KATE code is so-called "fine mesh spacings." These energy mesh spacings are built into the code and are shown in Table IV-2.

Table IV-2

Energy Mesh Spacings in KATE Code

Energy Range, ev	Energy Interval, ev
0-0.005	0.0001
0.006-0.05	0.001
0.06-E_{max}	0.01

E_{max}, the maximum thermal cutoff energy, in Table IV-2 must not exceed 2 ev. Almost all of the isotopic data are stored in tabular form in the KATE data library corresponding to the energy mesh points given in Table IV-2.

The LEOPARD (10) code, which was mentioned earlier, combines the MUFT and KATE codes into one with some modifications. In the LEOPARD code, the non-thermal spectrum calculation is based on a consistent B-1 approximation. In the thermal group, the KATE type calculations are performed at 172 energies between 0 and 0.625 ev. However, an approximate method of treating space energy effects by means of multigroup disadvantage factors is incorporated. Disadvantage factors are calculated using the intergral transport method by Amouyal, Benoist, and Horowitz (16) for each of 172 groups, and flux and volume weighted macroscopic cross sections are then determined at each energy. These energy dependent macroscopic cross sections are used in a normal spectrum calculation similar to KATE, and spectrum averaged, one thermal group, cross sections are com-

puted. The original version is restricted to cylindrical fuel rod configurations. The code was modified by Kim (2) to include plate type fuel elements.

For the analysis of plate type fuel elements which are commonly used in the highly enriched uranium, heavy water reactors, the routine which computes the thermal flux disadvantage for a cylindrical unit fuel cell for each of 172 thermal neutron energy groups must be modified. A method proposed by Bhalla (17) for slab geometry has been extended and incorporated into LEOPARD. It was adopted mainly because it can calculate the disadvantage factors accurately with an extremely simple method. Simplicity of the method is very important in the LEOPARD code, because there are 172 thermal groups for which the disadvantage factors must be determined without adding appreciable computer time. The method by Bhalla will be discussed briefly in the following paragraphs.

Bhalla's method is based on a simple expression given by Theys (18), for an arrangement of slab fuel cell given in Figure IV-1(a). Theys' treatment is based on the Integral Transport Theory and the theory by Amouyal and others (16). In Theys' notation, the flux disadvantage factor is given by

$$\bar{\phi}_1/\bar{\phi}_o = G + a\Sigma_o^a \left[\Sigma_1^{tr} (b-a) + 0.13\right] \qquad \text{(IV-1)}$$

where $G = \bar{\phi}_a/\bar{\phi}_o$ = fuel disadvantage factor.

In Equation IV-1, $\bar{\phi}_1$ and $\bar{\phi}_o$ are the average neutron

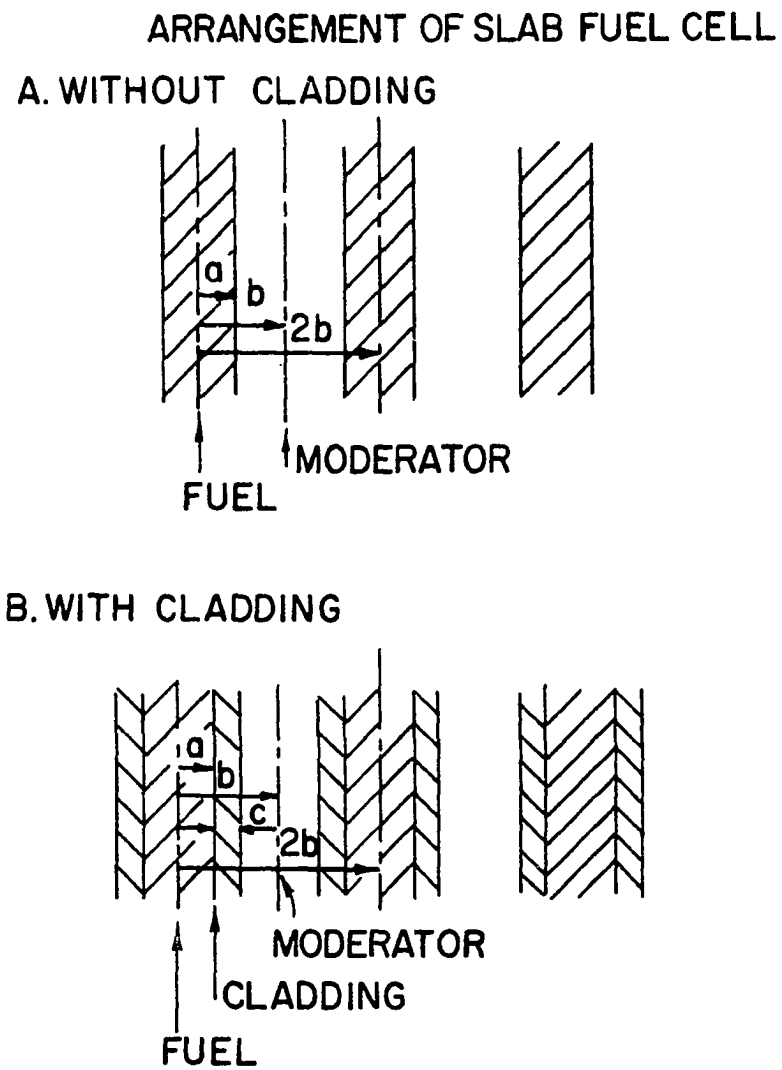

Figure IV-1. Arrangement of slab fuel cell

fluxes in the moderator region and the fuel element, respectively. ϕ_a is the neutron flux at the surface of the fuel slab. The subscripts o and 1 refer to the fuel element and the moderator, respectively. The half thickness of the fuel slab is given by a, and the pitch of fuel plate by 2b. Σ_o^a is the macroscopic absorption cross section of the fuel element and Σ_1^{tr} is the transport cross section of the moderator region.

Instead of using the approximation for G as given by Theys, Bhalla uses the following expression

$$G = a\Sigma_o^a/\alpha \qquad \text{(IV-2)}$$

by blackness theory (19), substitutes this for G in Equation IV-1, and obtains

$$\bar{\phi}_1/\bar{\phi}_o = a\Sigma_o^a\left[\frac{1}{\alpha} + \Sigma_1^{tr}\,(b-a) + 0.13\right] \qquad \text{(IV-3)}$$

Equation IV-3 is a very simple expression of calculation of $\bar{\phi}_1/\bar{\phi}_o$ provided the $1/\alpha$ term can be obtained easily. α is the ratio of current to the flux at the surface of the fuel slab according to the transport theory, and it can be calculated from

$$\alpha(a\,\Sigma_o^a,\ \Sigma_o^s/\Sigma_o^t) = \frac{F_o}{2[2-F_1]} \qquad \text{(IV-4)}$$

F_o and F_1 in Equation IV-4 are neutron capture fractions, and they are defined and conveniently tabulated by Schiff and Stein (19) as a function of $a\Sigma_o^a$ and Σ_o^s/Σ_o^t. A Fortran subroutine which computes G using Equations IV-2 and IV-4 with the tabulated values of F_n was added to the LEOPARD code.

So far we have considered slab unit cells where only fuel plate and surrounding moderator are involved. For a real plate type fuel element, the fuel matrix is usually separated from the moderator by the cladding, as shown in Figure IV-1(B), and hence, the flux rise through the cladding material must be accounted for in the calculation of flux depression in the fuel region of unit cell. Modification of Equation IV-3 for presence of cladding results in the following equation:

$$\bar{\phi}_1/\bar{\phi}_o = \frac{a\Sigma_o^a}{\alpha} + \Delta\phi_2/\bar{\phi}_o + a\Sigma_o^a \left[1 + \frac{V_2\Sigma_2^a\bar{\phi}_2}{V_o\Sigma_o^a\bar{\phi}_o}\right][\Sigma_1^{tr}(b-a-c) + 0.13] \qquad \text{(IV-5)}$$

where subscripts o, 1, and 2 refer to fuel, moderator, and cladding regions, respectively. The first term on the right hand side of Equation IV-5 is the fuel disadvantage factor (ratio of fuel surface to fuel average flux) as defined previously. $\Delta\phi_2$ is the flux rise through the cladding, and the third term is the ratio of clad surface to moderator average fluxes. V refers to region volumes, and a, c, and b are fuel half thickness, cladding thickness, and fuel center-to-moderator center distance, respectively.

In Equation IV-5, Σ_o^a in the original derivation has been replaced by $\Sigma_o^a[1 + V_2\Sigma_2^a\bar{\phi}_2/V_o\Sigma_o^a\bar{\phi}_o]$. Thus the fuel absorption cross section has in effect been increased to account for both fuel and cladding absorption. The blackness of the non-moderator region, as seen from the moderator, is thereby preserved in calculating flux rise across the moderator region.

The flux rise across the cladding is calculated for a thin plate by diffusion theory approximation

$$\Delta\phi_2/\bar{\phi}_o = K_2^2 C \Sigma_o^a/\Sigma_2^a \qquad \text{(IV-6)}$$

where K_2 is the inverse thermal diffusion length and C is the thickness of the cladding region.

The average flux for the cladding region is now given by

$$\bar{\phi}_2/\bar{\phi}_o = \frac{a\Sigma_o^a}{\alpha} + \frac{\Delta\phi_2}{2\bar{\phi}_o} \qquad \text{(IV-7)}$$

Once the flux ratios $\bar{\phi}_1/\bar{\phi}_o$ and $\bar{\phi}_2/\bar{\phi}_o$ are determined, the fluxes are normalized to a volume average of unity. Hence

$$V_o\bar{\phi}_o + V_1\bar{\phi}_1 + V_2\bar{\phi}_2 = 1 \qquad \text{(IV-8)}$$

The foregoing calculations are performed for cross sections corresponding to each energy level of the 172 thermal groups ranging from 0 to 0.625 ev.

The thermal group spectrum is determined by the macroscopic absorption cross section at each energy level. The macroscopic cross section at each energy level is calculated by summing the flux-weighted cross sections and nuclide concentrations over all elements and regions in the unit cell. The Wigner-Wilkins neutron spectrum is then calculated by these macroscopic cross sections at each energy level. Finally, the macroscopic cross sections at each energy level are weighted with the spectrum flux to obtain one thermal group macroscopic cross section for the unit cell.

B. Spatial Effect Calculations

1. One dimensional model

The FOG (20) code solves the one dimensional neutron diffusion equation in slab, cylindrical or spherical geometry. A maximum of four energy groups is permitted but slowing down is permitted only from one group to the next lowest energy group. This is consistent with the types of fast neutron group cross sections generated by the MUFT code. The boundary conditions in FOG consist of zero flux, zero current, fixed flux or logarithmic boundary conditions.

FOG provides options for so-called "criticality search" in addition to reactivity and flux calculations. These options search, for a given reactivity are:

1) Transverse buckling
2) Concentration of homogeneous poison for certain regions of core
3) Dimensions for region or core
4) Position of a poison boundary.

The FOG code has an added buckling search option for a fully reflected, right circular cylindrical reactor. In this option, a radial calculation is performed assuming that the core consisted of one region, and an average group dependent radial buckling is determined based upon the net leakage from the radial flux distribution. These bucklings then become transverse bucklings of the next axial calculation for the

same reactor. Then the axial bucklings are computed from the axial flux distribution and inputed into the radial calculation. This alternate radial and axial one dimensional calculation continues until the bucklings and core reactivity converge within given criteria.

2. Two dimensional model

One dimensional calculations normally neglect the effect of irregular core or region boundaries and assume a high degree of separability of spatial effects. Two dimensional calculations, however, greatly reduce the degree of assumed directional separability of spatial effects. Fuel assemblies, large fraction of core, or an entire core may be represented in great detail. The irregularly shaped control rods, water channels, and fuel regions can be represented explicitly. Two dimensional calculations are performed in X-Y, R-Z, R-θ, or hexagonal (triangular) geometry depending on the arrangement of core regions and the availability of computer codes.

The two dimensional models still solve the basic few group neutron diffusion equation except that the space variable is now a two dimensional variable and the neutron down scattering term must be modified in case of multigroup down scattering.

The EXTERMINATOR-2 (21) code is a two dimensional neutron diffusion code. It is a multigroup code that allows down-scatter from any of up to 50 groups to any other group. Three

outer-boundary conditions may be specified: zero flux, zero current, or periodic condition. The logarithmic boundary condition may also be specified either along boundaries or internal to the mesh. The total composition dependent neutron balance for each energy group and composition average fluxes are provided with the normal flux and power distributions. The code also has options for constant source, poison search, and nuclide concentration search calculations, and adjoint flux and perturbation calculations can be performed. The effect of pointwise equilibrium xenon on the fluxes and effective multiplication factor can also be computed. The input data are normally in macroscopic form, but microscopic cross sections can be used as input to the code. When the microscopic cross sections are used, flux-weighted broad group microscopic cross sections can be computed.

C. Compilation of Reactor Data

1. Basic data

For any design work, accurate and complete input data are necessary for producing useful design. This statement is particularly true for the design of nuclear reactors where the safe operation is the utmost importance. Some erroneous basic data which go into design calculations can produce entirely different reactor physics characteristics.

A complete list of mechanical, thermal-hydraulic, and nuclear data for a reactor is required for preparation of

input to reactor calculations. These data are usually furnished by reactor manufacturers if the reactor is designed already, or they must be assumed or proposed values.

The thermal power level determines the absolute flux and power distribution of the reactor. The pressure, temperature, and type of coolant determine properties of coolant for neutron spectrum and cross section calculations. The rest of the data are essential for calculation of overall core reactivity and spatial distribution of flux and power. The reflector composition and dimension, of course, are important for determining the neutron spectrum in the reflector region and the leakage of neutrons from the core.

The fuel assembly and fuel plate data are used for computation of volume fractions of materials in the various regions within the fuel element, and these, in turn, are used for determination of multigroup neutron spectrum and subsequently, sets of few group cross sections for the regions. The thickness and composition for fuel plate, fuel matrix, cladding and coolant channel will enter in the calculation of thermal neutron flux depression (thermal flux disadvantage factors) in the fuel matrix and cladding prior to the calculation of neutron spectrum for fuel plate cells. The few group cross sections for the various regions within a fuel element are, then, put into the two dimensional cell calculation for the fuel element as a single cell.

Because the MUFT and KATE (SOFOCATE) codes are conveniently combined into a single computer code which provide elimination of redundancy in preparation of input data for two separate programs, the LEOPARD code will be used as the standard tool for generation of few group cross sections, with some modifications and additions when they become necessary. Description of the original LEOPARD code was previously given.

The code has built-in cross sections for 27 nuclides for 172 thermal and 54 fast neutron groups. This feature of the code eliminates drudgery connected with compilation and checking of cross section data from those who use the code infrequently.

The LEOPARD code requires only the most basic input data. The reactor geometry, compositions, and temperatures are supplied by the user. The code corrects the input data according to the temperature and computes nuclide concentrations. The density of moderator can also be computed from temperature and pressure of the system. These options are possible because the code contains built-in values of thermal expansion coefficients for each element in the library and an empirical expression for density of water as a function of temperature and pressure. The code assumes that every reactor contains a large array of unit fuel cell which contains one fuel region, a metallic clad attached to the fuel, and a moderator. In a real reactor, this geometry is adequate within a large fraction of a fuel assembly, or within a large fuel bundle, but

there are some regions which cannot be included in the unit cell geometry. These are control rod channels, water slots, assembly cans, structures, etc. The LEOPARD code accounts for this by allowing a fictitious region to be defined and described in a manner entirely analogous to the description of the real regions within the unit fuel cell. The absorption of thermal neutrons by these "non-unit cell" regions are accounted for by the fraction occupied by these regions and the ratio of the thermal flux in these regions to that for the unit cell.

The two dimensional neutron diffusion code is used for two purposes in our study. The first is to perform a "cell" type calculation to obtain a set of effective few group cross sections for a group of small regions (hereafter they will be called "subregions") such as the fuel element cell which consists of fuel plate cells, plate supporting structures, and extra amount of moderators other than those in unit fuel plate cells. In this calculation, it is assumed, for purpose of obtaining effective few group cross sections, that the core consists of infinitely large number of similar fuel element cells, and the boundaries of each cell are set to zero current condition. The number of spatial points involved in this type of calculation is usually small.

The second is to solve the neutron diffusion equation for the whole core under the assumption that the spatial effects can be separated into two directions, and that the effects of the transverse direction can be accounted for by the trans-

verse bucklings. From the whole core two dimensional calculation, we can obtain the core excess reactivity and distributions of flux and power. Two dimensional calculations are commonly done in the X-Y geometry; however, R-Z or R-θ geometry can be used if the arrangement of core internals provides symmetry with one of the axes. The two dimensional R-θ geometry that was used assumes that the core is uniform in the Z direction which is true for this core. The transverse bucklings required in the two dimensional R-θ geometry can be calculated from the shape of the axial flux distribution. However, to get a good axial flux distribution, the core few group cross sections for the axial calculation must include the effect of radial R-θ variations of fluxes on the R-θ plane. Hence, the axial one-region core cross sections are obtained by weighting region cross sections with region volumes and average fluxes which were obtained by the two dimensional calculation over the core and reflector regions.

The buckling iteration feature of the FOG code was used to obtain a consistent set of group dependent axial buckling terms for the reactor being analyzed in R-θ geometry by the EXTERMINATOR-2 code.

The group dependent, region average, radial buckling, which is calculated from the radial flux distribution, is then used as the radial buckling in the axial calculation. Corresponding expressions for the axial buckling are obtained and the values are determined from the axial flux distribution.

These resulting values are then used as the axial buckling for the next radial calculation. This alternating, radial and axial diffusion calculations continue until convergence of either core eignevalue (excess reactivity) or individual bucklings is achieved within specified limits. The above procedure assumes that the core region (the fuel region) is represented by one region, and the iteration is performed only on the bucklings of the core regions.

This principle of buckling search is recommended when the geometry of a reactor permits its use. For complicated arrangement of reactor structures, this method still provides approximate values which are better than simple geometrical bucklings. In this approach a two dimensional, R-θ multiregion few group, neutron diffusion calculation will be performed over the entire reactor. If possible, symmetry of the reactor will be utilized to the maximum for purpose of saving valuable computation time. In the first two dimensional, R-θ, calculation, assumed axial bucklings are used. The resulting two dimensional flux distribution is used to obtain a set of few group cross sections for one-region core by weighting the cross sections of individual regions in the core with their respective volumes and average fluxes.

The one-region core, few group, cross sections from the results of the R-θ calculation then become the cross sections for the one-region core of a cylindrical reactor with which the buckling iteration is to be performed. Although only one

core region is allowed in the iteration problem, there is no restriction on the number of reflector regions in the problem. The axial bucklings are determined together with the radial bucklings according to the procedure described in preceding paragraphs.

The two dimensional R-θ diffusion calculation is repeated with the new set of axial bucklings for the core regions from the buckling iteration problem, and again flux weighted one-region core cross sections are determined for the next buckling iteration problem. This combination of two dimensional and buckling iteration calculation proceeds until the axial bucklings for the two dimensional calculation converge within a given criterion. The two dimensional flux distribution and the resulting core excess reactivity corresponding to the converged axial bucklings are then the final solutions. Similarly, the axial calculation will provide the axial flux distribution.

V. ANALYSIS OF ALRR

In this chapter, the analysis of the ALRR will be described. The core and reflector regions will be divided into small regions and few group cross sections will be generated for fuel element cells and homogenized non-fuel regions. Spatial calculations will be made on the initial cold clean minimum critical mass reactor and on the full size 24 element core. Various parameter studies will be included as well as calculations to check various assumptions used.

A. Few Group Neutron Cross Sections

1. Arrangement of reactor regions

Figure V-1 shows the geometric relation between the core, control rods and some of the experimental thimbles of the ALRR. It shows 24 fuel elements and the six shim-safety rods. In this study, all rods are considered in their full-up position.

The details of fuel element cells are shown in Figures V-2 to V-4. Figure V-2 is the cell for a 24 element core, Figure V-3 is for an eighteen element core and Figure V-4 was used for the initial 13 element core. The 13 element core was not symmetric and one element was shifted from an off-center to an on-center position to give 1/2 core symmetry. The 18 element cell was used in a calculation to show that this shift caused less than 0.0016 Δk_{eff} change in reactivity which is very small for these calculations. These figures show only a quarter of a cell because they are symmetric about the two

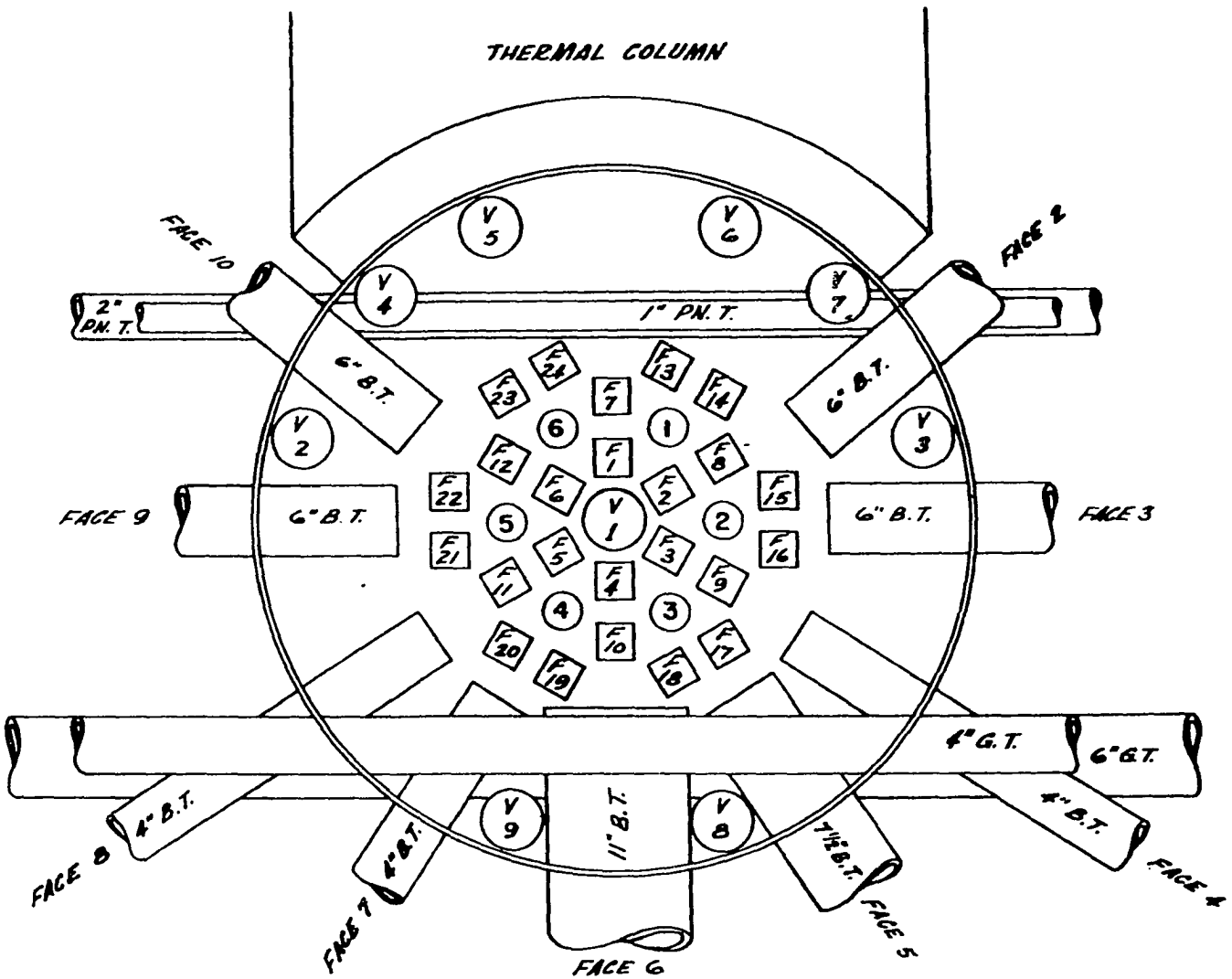

Figure V-1. Geometric relation between the core, control rods and some of the experimental thimbles

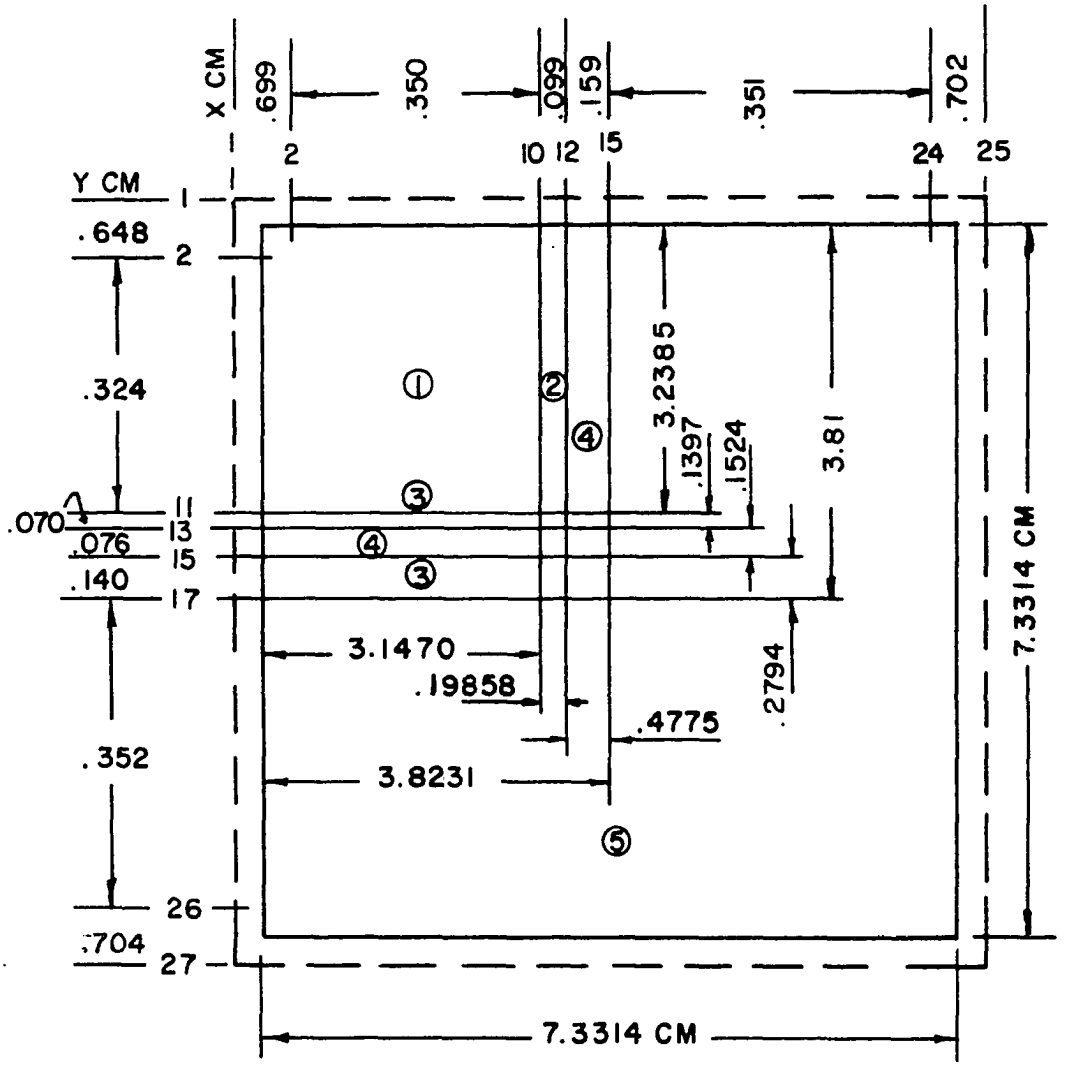

Figure V-2. 24 element cell - 215 cm^2

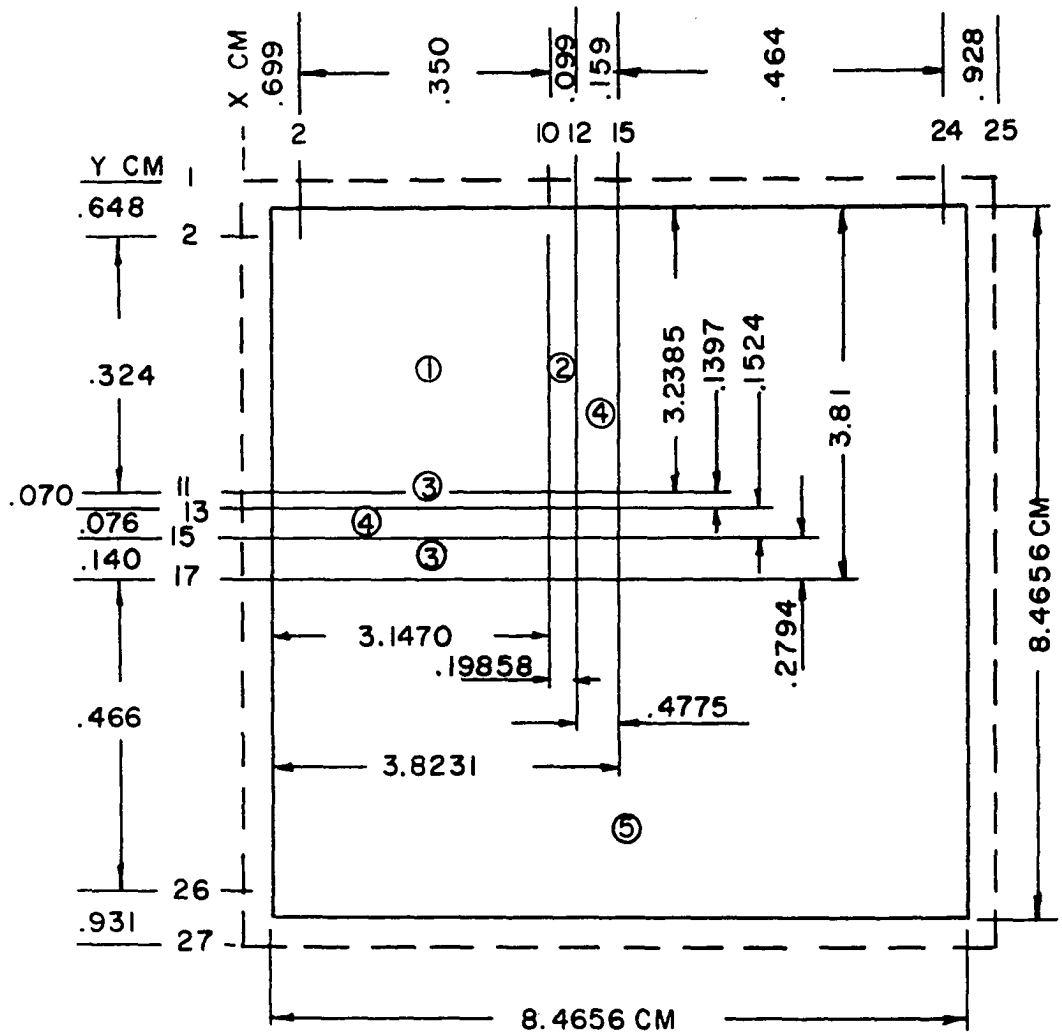

Figure V-3. 18 element cell - 287 cm^2

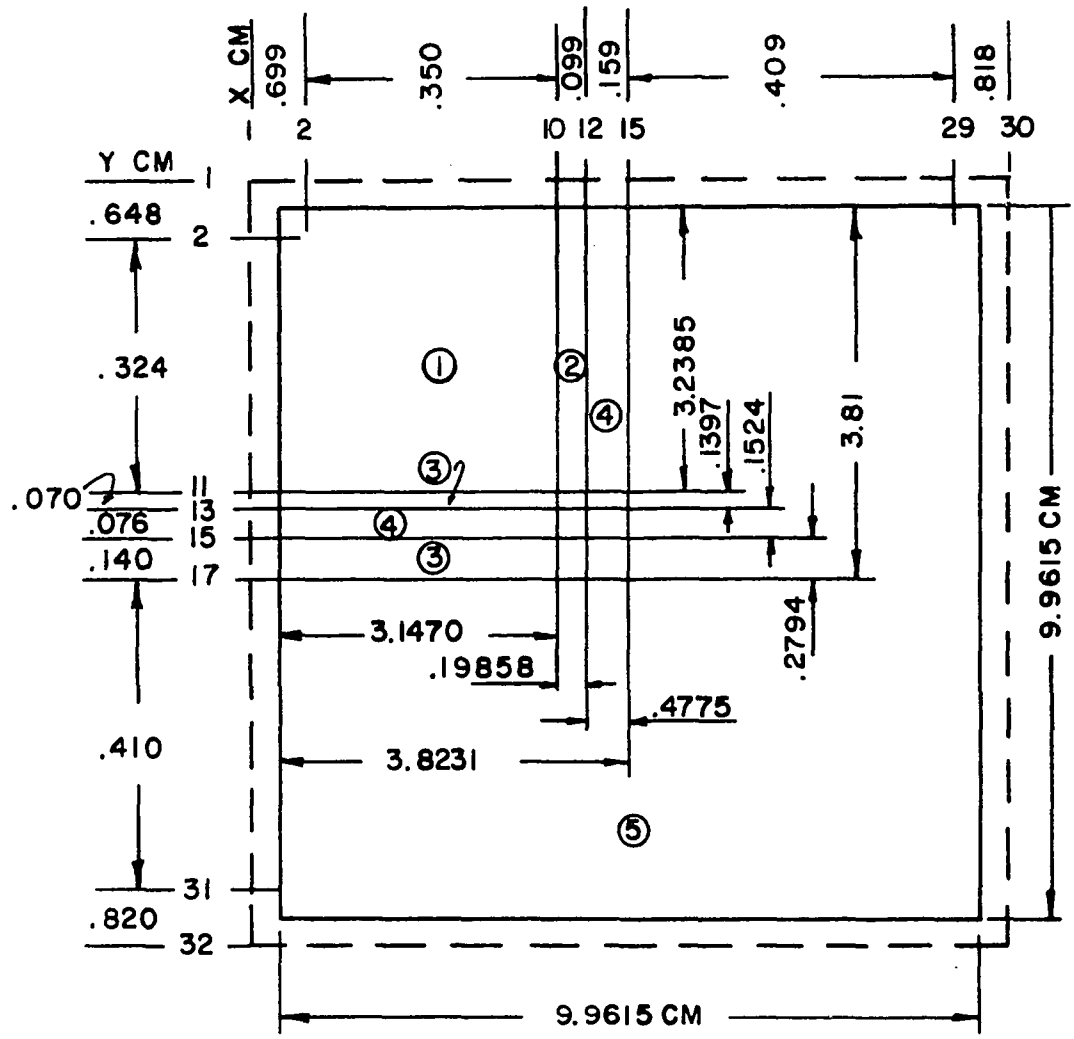

Figure V-4. 13 element cell - 397 cm^2

axes. Material 1 is the fuel slab cell which contains 0.020 inches of fuel matrix, 0.020 inches of aluminum cladding and 0.110 inches of moderator. Material 2 is the mixture of the unfueled edge of fuel plates and heavy water. Material 3 represents the D_2O within the fuel element region and Material 4 represents the aluminum side plates and outside non-fuel plates. Material 5 represents the D_2O in the cell but outside of the fuel element region.

Figures V-2 to V-4 also show the spatial mesh spacings which were used for two dimensional calculations to generate few group neutron cross sections for the fuel element cell. The points outside the physical boundaries represent fictitious points that are required for the EXTERMINATOR-2 code for reflecting boundary conditions. The fuel slab cell region shown in Material 1 is adjusted in dimensions to account for the slight curvature of the fuel plates. Conservation of mass is preserved.

Figure V-5 shows the radially homogenized axial regions of the reactor with dimensions indicated for each region. Except for the core region, all the regions contained aluminum, heavy water and void with one region including some graphite. Materials A, B, C, D, and E are axial reflectors and Materials F and G are radial reflectors. Material F contained the graphite. The cadmium of the control rods, in their up position, is in Material E.

2. Region composition

The cell dimensions and composition of the initial critical ALRR fuel plate are shown in Table V-1. The average fuel loading per element for the initial core was 176.5 grams uranium containing 164.5 grams U-235 for an enrichment of 93.2 percent.

Table V-1

Cell Dimensions and Composition of Initial Critical ALRR Fuel Plate

	Inches	Cm
Fuel length	23.5	59.69
Average fuel width	2.478	6.294
Fuel matrix thickness	0.02	0.0508
Volume of fuel matrix	1.165	19.086
Clad thickness	0.02	0.0508
Water channel thickness	0.11	0.2794
Plate thickness	0.06	0.1524
U volume per plate		0.6303
Al volume per plate		18.456
U-235 concentration in fuel	$.0014732 \times 10^{24}$ atoms/cc	
U-238 concentration in fuel	$.0001066 \times 10^{24}$ atoms/cc	
Al concentration in fuel	$.05782 \times 10^{24}$ atoms/cc	
D_2O in moderator 99.7 mol % D_2O	$.03312 \times 10^{24}$ molecules/cc (68°F)	
H_2O in moderator	$.0001003 \times 10^{24}$ molecules/cc (68°F)	
D/H in moderator 99.7 mol % D_2O	332.33	

Table V-2 lists volume fractions of water and aluminum for materials in the ALRR fuel element cells which were shown in Figures V-2 to V-4. Material 2 represents the homogenized unfueled edge of the fuel plate and water in the coolant channel.

Table V-2

ALRR Fuel Element Cell Composition
(See Figures V-2 to V-4)

Material Identification		Volume Fraction Al	Water[a]
1	Fuel slab cell (See Table V-1)		
2	Unfueled edge of fuel plate and water	.3529	.6471
3	Pure water	0.0	1.0
4	Pure aluminum	1.0	0.0
5	Pure water	0.0	1.0

[a] 99.7 mol % D_2O (D/H - 332.33) at 68°F.

Table V-3 lists the composition of the non-fuel regions shown in Figure V-5. Material A is in the bottom, light water reflector region but includes the heavy water fill and drain pipes. This accounts for the low D/H ratio in this region. Material B is within the heavy water tank and includes the lower aluminum grid plate. Material C includes the lower unfueled regions of the fuel elements. Material D includes the upper unfueled regions of the fuel elements and the

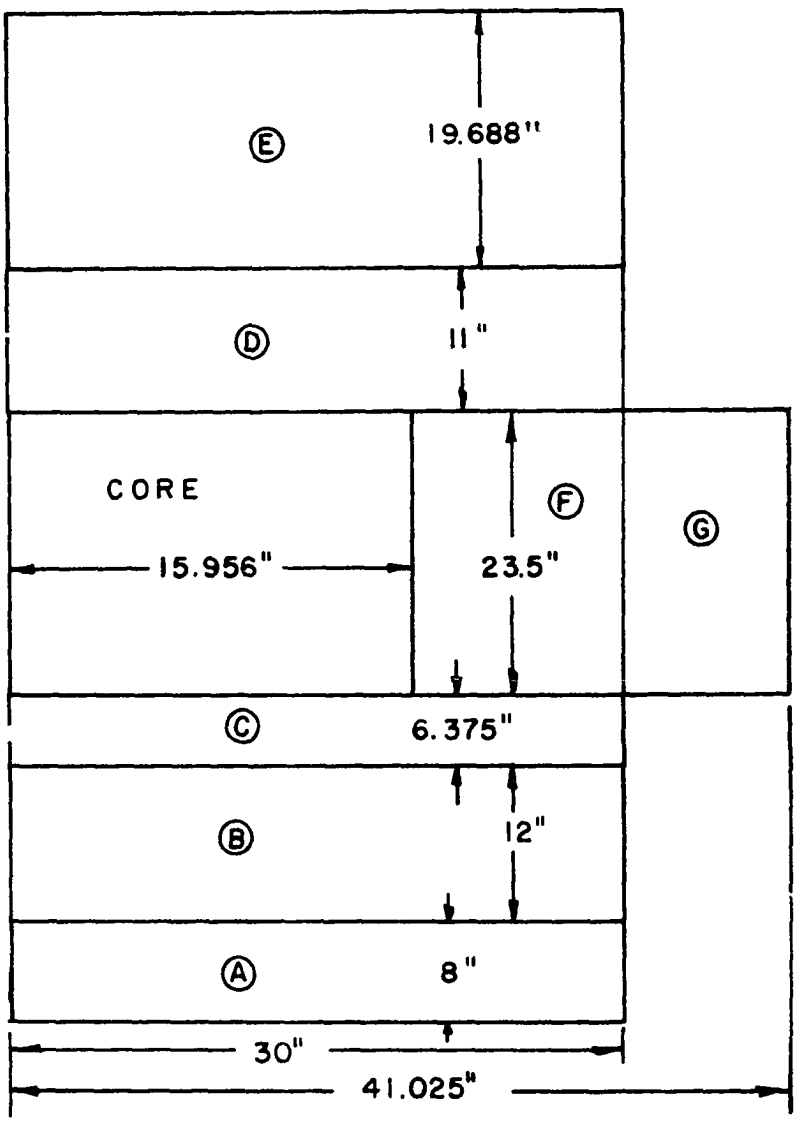

Figure V-5. Radially homogenized ALRR regions

Table V-3

Composition of Non-fuel Regions
(See Figure V-5)

Material Identification	Volume Fractions[a] Al	Water[b]	Graphite
A	.1259	.8741[c]	
B	.1022	.8881	
C	.0609	.8934	
D	.0760	.9156	
E	.0247	.9718	
F	.0558	.8564	.0521
G	.1094	.7112[d]	

[a]Remainder of volume is void.

[b]99.7 mol % D_2O except as noted.

[c]D/H = .1945.

[d]D/H = .4318.

aluminum extension pieces of the control rods. Material E includes the fuel element hold down units. The cadmium control rods in this region were neglected at this time and accounted for later by use of a distributed poison. Material F within the D_2O tank contains all the horizontal beam tubes most of which are filled with graphite. It also contains parts of the vertical experimental tubes. Material G is the light water reflector region outside of the heavy water tank. However, it does contain a heavy water section that protrudes into the light water thermal shield at the thermal column.

This accounts for the low D/H ratio in this region. The D/H ratios are quoted because they are used as input to the LEOPARD code.

3. Fuel region cross sections

The four group neutron cross sections for 24 element ALRR fuel cell were calculated by the LEOPARD code and the results for 84°F and 1 atmosphere are shown in Table V-4. The initial critical experiments were conducted during the summertime when the average water temperature was 84°F. The neutron energy breakpoints in LEOPARD are 821×10^3 ev, 5.53×10^3 ev and 0.625 ev, and the fraction of fission neutrons born in the first two groups are 0.7516 and 0.2484, respectively. The resonance shielding factor (L) for U-238 was assumed to be unity since the contribution of U-238 would be small because of the highly enriched fuel. The cross section values for Materials 1 and 5 were taken directly from the LEOPARD code output forms. Materials 2, 3 and 4 are within one mean free path (λ) of the Material 1 fuel slab region and would be influenced by the flux in Material 1. Their macroscopic cross sections were computed from the microscopic cross sections listed in the LEOPARD output of Material 1 and their corresponding number densities for Materials 2, 3, and 4.

Once the few group neutron cross sections for the elements in the fuel cell are obtained (Table V-4), the few group neutron cross sections for the fuel element are obtained by a two

Table V-4

Four Group Neutron Cross Sections for 24 Element ALRR Fuel Cell

Description	g	D cm	Σ_a cm^{-1}	Σ_R^a cm^{-1}	$\nu\Sigma_f$ cm^{-1}
Material 1	1	2.070	1.475 -03	5.791 -02	1.861 -03
Fuel Slab Cell	2	1.336	5.186 -04	2.101 -02	8.019 -04
	3	1.539	6.318 -03	8.227 -03	9.058 -03
	4	1.063	5.232 -02	0.0	1.035 -01
Material 2	1	2.081	1.254 -03	5.763 -02	1.324 -03
.3529 Al	2	1.346	8.948 -05	2.114 -02	0.0
.6471 water	3	1.583	4.868 -04	1.039 -02	0.0
	4	1.211	2.483 -03	0.0	0.0
Material 3	1	1.834	1.764 -03	8.026 -02	2.047 -03
Water	2	1.117	4.780 -08	3.056 -02	0.0
99.7 mol %	3	1.192	2.137 -06	1.592 -02	0.0
D_2O	4	0.884	5.222 -05	0.0	0.0
Material 4	1	2.763	3.182 -04	1.614 -02	0.0
Al	2	2.161	2.535 -04	3.909 -03	0.0
	3	3.964	1.376 -03	2.637 -04	0.0
	4	3.771	6.934 -03	0.0	0.0
Material 5	1	1.916	1.865 -03	8.055 -02	2.168 -03
Water	2	1.208	4.887 -08	3.348 -02	0.0
99.7 mol %	3	1.196	2.878 -06	2.009 -02	0.0
D_2O	4	0.794	9.038 -05	0.0	0.0

[a]Notation 5.7914 -02 equals 5.7914×10^{-2}.

dimensional cell calculation using EXTERMINATOR-2 code. The fuel cell was shown in Figure V-2. A buckling of 10^{-8} to simulate an infinite cell was used and a k_{eff} convergence level of 0.0005 was assumed.

The regionwise average neutron fluxes from the cell calculation are flux weighted with the material neutron cross sections to obtain a single set of few group neutron cross section for the fuel element to be used in the R-θ reactor calculations. Table V-5 gives the average group fluxes, the

Table V-5

Average Group Flux and Few Group Neutron Cross Sections for 24 Element Cell Fuel Element

A. Average neutron relative fluxes

Material/group	1	2	3	4	Volume or Area
1	.15370	.37609	.54970	.88661	10.191
2	.12916	.35752	.54961	.85418	.64307
3	.12338	.35389	.54962	.96333	1.4019
4	.12164	.35239	.54954	.96718	2.3292
5	.09017	.32570	.54809	1.0743	39.171

B. Few group neutron cross sections for fuel element

Group	D cm	Σ_a cm^{-1}	Σ_R cm^{-1}	$\nu\Sigma_f$ cm^{-1}
1	2.1201	1.3350 -03	5.4118 -02	1.6051 -03
2	1.3929	4.1204 -04	1.9292 -02	5.7135 -04
3	1.6570	4.6628 -03	7.7896 -03	6.3384 -03
4	1.1908	3.6974 -02	0.0	7.0568 -02

material areas (same as material volumes for an infinite cell) and the resultant few group neutron cross sections for the fuel element in the cell. The flux weighting used is shown in Equation V-1

$$\bar{\Sigma}_x = \frac{\sum_{j=1}^{4} \Sigma_{xj} \bar{\Phi}_j V_j}{\sum_{j=1}^{4} \bar{\Phi}_j V_j} \qquad \text{(V-1)}$$

where x equals absorption (a), removal (R) or neutron source ($\nu\Sigma_f$) and j is the number of regions for the cross section terms and in Equation V-2

$$\frac{1}{\bar{D}_x} = \frac{\sum_{j=1}^{4} \frac{\bar{\Phi}_j V_j}{D_{xj}}}{\sum_{j=1}^{4} \bar{\Phi}_j V_j} \qquad \text{(V-2)}$$

for the diffusion terms. These equations are used for each neutron group.

The cell in Figure V-2 produced a k_∞ of 1.84265.

4. Non-fuel region cross sections

The non-fuel regions shown in Figure V-5 were treated as homogeneous mixtures of aluminum, heavy water and graphite and void if present and the few group neutron cross sections were calculated with the LEOPARD code.

Table V-6 shows the resulting few group neutron cross sections for these non-fuel regions. The Group 1 fission

Table V-6

Four Group Neutron Cross Sections for ALRR Homogenized Non-fuel Regions

Material	g	D cm	Σ_a cm^{-1}	Σ_R cm^{-1}	$\nu\Sigma_f$ cm^{-1}
A	1	2.2450	1.4313 -03	9.0961 -02	5.1473 -04
	2	1.1020	3.5930 -05	1.1524 -01	0.0
	3	0.7121	9.2082 -04	1.1339 -01	0.0
	4	0.2018	1.5295 -02	0.0	0.0
B	1	1.9940	1.6671 -03	7.3233 002	1.8971 -03
	2	1.2573	2.6424 -05	3.0062 -02	0.0
	3	1.3021	1.8804 -04	1.7781 -02	0.0
	4	0.8755	1.2917 -03	0.0	0.0
C	1	2.0453	1.6730 -03	7.2985 -02	1.9199 -03
	2	1.2892	1.5766 -05	3.0113 -02	0.0
	3	1.3120	1.1332 -04	1.7913 -02	0.0
	4	0.8778	8.0653 -04	0.0	0.0
D	1	1.9759	1.7158 -03	7.5018 -02	1.9638 -03
	2	1.2455	1.9648 -05	3.0902 -02	0.0
	3	1.2748	1.4064 -04	1.8349 -02	0.0
	4	0.8542	9.8620 -04	0.0	0.0
E	1	1.9369	1.8157 -03	7.8697 -02	2.1000 -03
	2	1.2211	6.4163 -06	3.2623 -02	0.0
	3	1.2216	4.7735 -05	1.9509 -02	0.0
	4	0.8134	3.8323 -04	0.0	0.0
F	1	2.0345	1.5995 -03	7.1068 -02	1.8369 -03
	2	1.2615	1.4443 -05	2.9435 -02	0.0
	3	1.2728	1.0390 -04	1.7513 -02	0.0
	4	0.8733	7.5895 -04	0.0	0.0
G	1	2.6774	1.2400 -03	7.2128 -02	7.1107 -04
	2	1.3295	2.9783 -05	8.2398 -02	0.0
	3	0.9417	6.6826 -04	7.9278 -02	0.0
	4	0.2837	1.0667 -02	0.0	0.0

cross sections represents the neutron production due to (n,2n) reactions in deuterium above the 2.23 Mev threshold energy. The values in regions C, D, and E are for 24 fuel elements. The remaining regions are not affected by the number of fuel elements present.

5. 13 element core two group neutron cross sections

The previous sections considered four group cross sections for the 24 element core. This section lists the two group cross sections used in the 13 element, minimal critical mass core. This core required half-core symmetry and only two groups were used because of the large number of mesh points.

Table V-7 lists the fuel cell cross sections. Table V-8 lists the average group fluxes and the two-group cross sections for the 13 element cell fuel element. Table V-9 lists the two group cross sections for the homogenized non-fuel regions.

B. Results

1. Initial studies of 24 and 18 element cores

Some initial studies were made using the 24 element core because this arrangement allowed for one-sixth core symmetry and was easier to analyze than a full core without symmetry.

Some studies were made of the 24 element core shown in Figure V-6. The jagged element was felt to be a better reproduction of the true fuel element. This was later shown not to

Table V-7

Two Group Neutron Cross Sections for 13 Element ALRR Fuel Cell

Description	g	D cm	Σ_a cm^{-1}	Σ_R cm^{-1}	$\nu\Sigma_f$
Material 1 Fuel Slab Cell	1	1.5262	3.272 -03	3.737 -03	4.683 -03
	2	1.0635	5.232 -02	0.0	1.035 -01
Material 2 .3529 Al .6471 Water	1	1.5688	5.131 -04	7.255 -03	1.299 -04
	2	1.1123	4.075 -03	0.0	0.0
Material 3 Water 99.7 mol % D_2O	1	1.2756	1.964 -04	1.125 -02	2.263 -04
	2	0.7943	9.038 -05	0.0	0.0
Material 4 Al	1	3.6373	7.312 -04	5.128 -05	0.0
	2	3.8266	5.581 -03	0.0	0.0
Material 5 Water 99.7 mol % D_2O	1	1.2756	1.964 -04	1.125 -02	2.263 -04
	2	0.7943	9.038 -05	0.0	0.0

Table V-8

Average Group Flux and Two Group Neutron Cross Sections for 13 Element Cell Fuel Element

A. Average relative neutron flux

Material	1	2	3	4	5
Group					
1	1.1064	1.0562	1.0480	1.0446	0.9753
2	0.8894	0.9579	0.9685	0.9716	1.0776
Area	10.191	0.6431	1.4019	2.3292	39.171

B. Few group neutron cross sections for fuel element

Group	D cm	Σ_a cm^{-1}	Σ_R cm^{-1}	$\nu\Sigma_f$ cm^{-1}
1	1.6447	2.480 -03	4.011 -03	3.356 -03
2	1.1690	3.680 -02	0.0	7.053 -02

Table V-9

Few Group Neutron Cross Sections for ALRR Homogenized Non-fuel Regions

Material	g	D cm	Σ_a cm^{-1}	Σ_R cm^{-1}	$\nu\Sigma_f$ cm^{-1}
A	1	1.3362	7.854 -04	3.866 -02	1.652 -04
	2	0.2018	1.529 -02	0.0	0.0
B	1	1.3584	2.862 -04	9.982 -03	1.955 -04
	2	0.8755	1.292 -03	0.0	0.0
C	1	1.3803	2.421 -04	1.004 -02	1.989 -03
	2	0.8778	8.065 -04	0.0	0.0
D	1	1.3375	2.629 -04	1.029 -02	2.031 -03
	2	0.8542	9.862 -04	0.0	0.0
E	1	1.2959	2.179 -04	1.093 -02	2.185 -04
	2	0.8134	3.832 -04	0.0	0.0
F	1	1.3482	2.293 -04	9.817 -03	1.909 -04
	2	0.8733	7.589 -04	0.0	0.0
G	1	1.5905	6.165 -04	2.831 -02	2.108 -04
	2	0.2837	1.067 -02	0.0	0.0

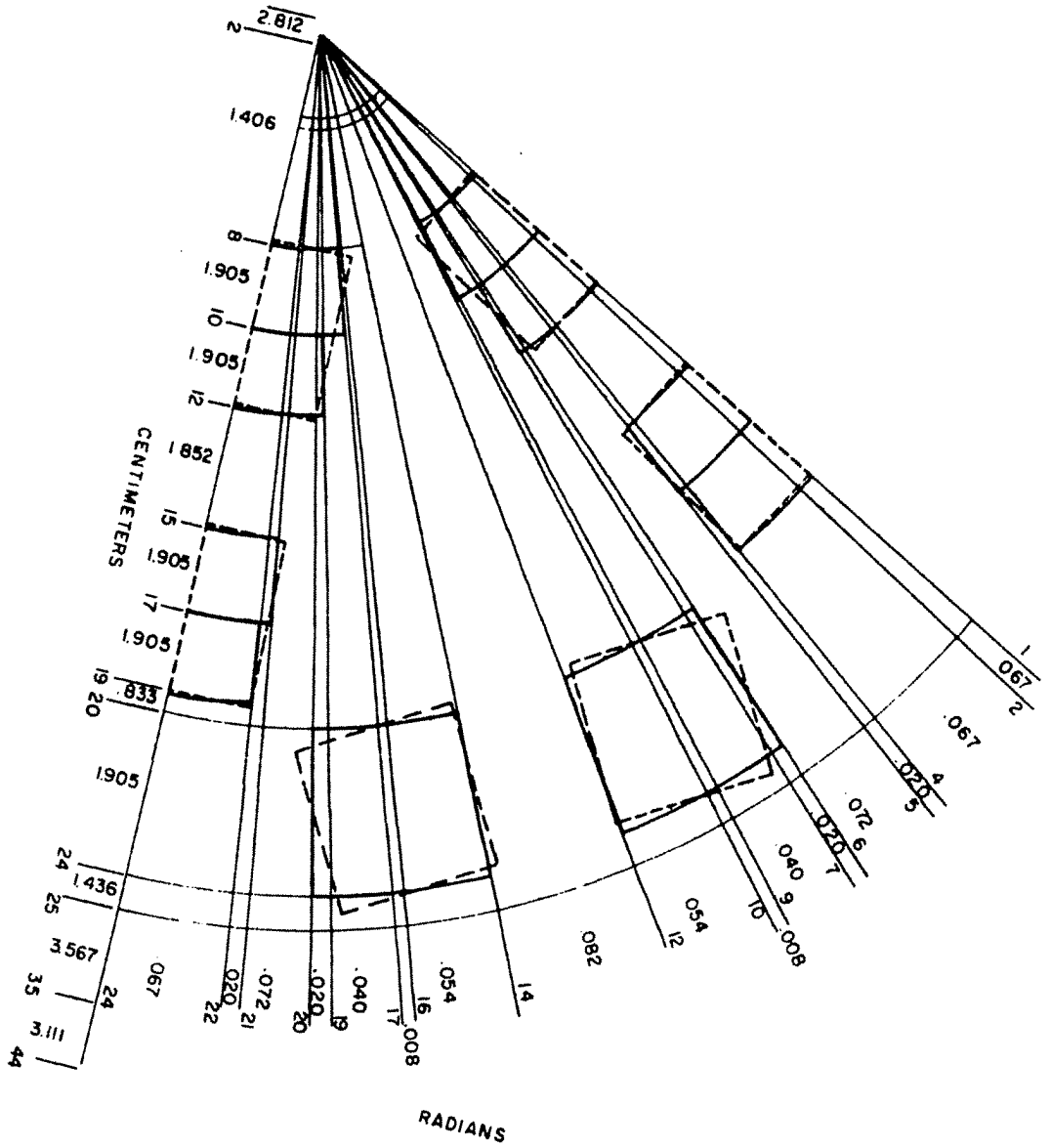

Figure V-6. One sixth region, jagged element core - R-θ geometry

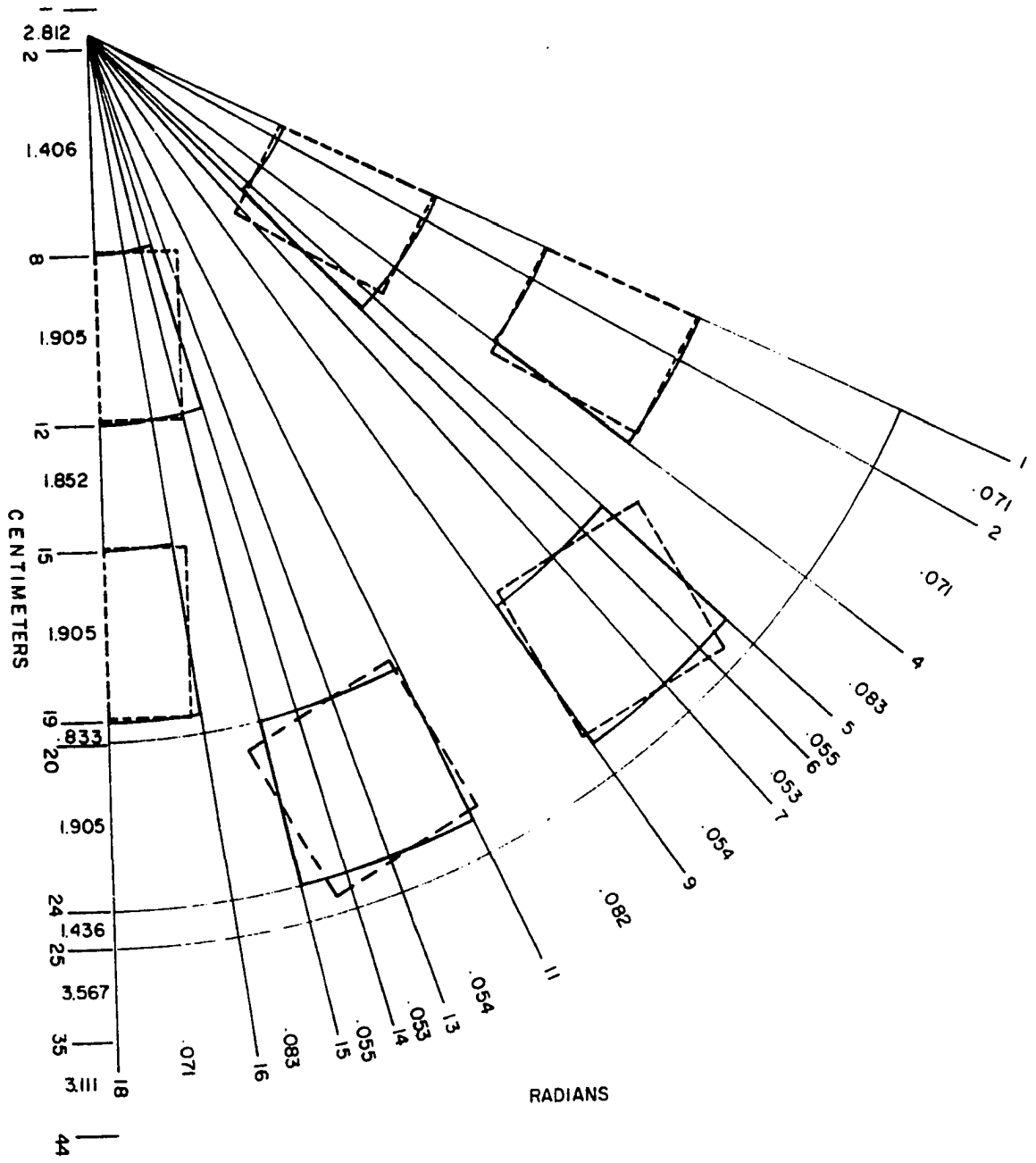

Figure V-7. One sixth region, simple element core - R-θ geometry

make a significant difference from the smooth element core shown in Figure V-7.

A study was made to be sure the flux did go to zero (a factor of 1000 below its highest value) at the boundary. In the radial direction, the number of mesh points was increased from 40 to 44 to satisfy this criteria. The 44 radial mesh points were then used in further calculations. The four additional mesh points were added to the outer H_2O radial reflector region.

The effect on k_{eff} of varying the reflector savings was then evaluated. This was shown to have a tremendous effect with k_{eff} varying from 1.1464 for a reflector savings of 26 cm to 1.2288 for a reflector savings of 40 cm. This indicates that k_{eff} is greatly influenced by the axial buckling.

The effect of going from the 24x44 mesh jagged-edged fuel element to the 18x44 smooth-edged fuel element was shown to be negligible with k_{eff} being 1.19093 for the jagged-edged case and 1.19041 for the smooth-edged case. The smooth-edged case was used in all further calculations.

The initial core had the central thimble filled with carbon. Calculations indicated that going from graphite to D_2O increased k_{eff} by 0.0028. Removing the central thimble increased k_{eff} by a calculated value of 0.0060 versus a measured value of 0.0070.

The original 13 element core was non-symmetric and required shifting one element to get one-half core symmetry.

This condition was studied using an 18 element core. The element in the outer fuel ring was shifted from an off-center to an on-center position. This change gave a change in k_{eff} of 0.01008 for six elements in ring 3. The effect of changing one element on k_{eff} would only be 0.00168 which is small for our study. The element was shifted to the on-center position and one-half core symmetry was used.

2. Distributed poison in Region E

With the control rods in their up position, the cadmium in the rods was located in Region E of Figure V-5. To account for this cadmium, a distributed poison that had the same negative worth of 0.6 percent $\Delta k/k$ as the remaining worth of removing the six control rods was assumed to exist in this region. First the poison search routine in FOG 3 was used to get an approximate value for this distributed poison. Then an iteration was done with FOG 2 until the change in k_{eff} was close to 0.006. This iteration was done for the 2 group and 4 group programs.

This iteration changed the absorption cross section in Region E from 0.000383 cm^{-1} for the no poison case to 0.00723 cm^{-1} for the two group case and to 0.0064 cm^{-1} for the four group condition. These values were then used for Σ_a in Region E for the FOG 2 buckling iteration search to determine the axial buckling terms for the EXTERMINATOR-2 code. It was

shown that the buckling terms were not too critical for the Σ_a term in Region E once Σ_a was near its final value.

3. Results for 24 element core

A two dimensional R-θ few group neutron diffusion calculation was set up for the four-element one-sixth core geometry shown in Figure V-7 with the subdivided homogenized regions represented by the appropriate few group cross sections. The control rods were fully out of the core and their normal positions occupied by heavy water. The one-sixth core was represented by four material regions; they are the fuel element, the core D_2O, the D_2O reflector region and the H_2O reflector region.

The initial guess for the geometric buckling was assumed to be energy independent and the same as the axial geometric buckling based on an active fuel length of 23.5 inches and an axial reflector savings of 32 cm at each end. The group independent geometric buckling was 6.5×10^{-4} cm^{-2}. The fluxes were assumed to vanish at the outer boundaries.

The regionwise fluxes from the first one-sixth core two dimensional calculation were used to obtain a single set of flux weighted few group neutron cross sections for the core region. The one-region core few group cross sections were then used for the radial and axial one dimensional calculation to obtain the group dependent axial bucklings from the converged axial flux distribution using FOG 2. The geometries

for this radial and axial buckling iteration calculations are shown in Figure V-8. In these one dimensional calculations, zero flux conditions were applied at the outer boundaries.

Once the axial bucklings were obtained from the buckling iteration problem, the one-sixth core two dimensional calculation was repeated with the new set of axial bucklings. Then the new one-region core few group cross sections obtained from the results of the second two dimensional calculation was used for the subsequent buckling iteration problem. This process of alternating two dimensional and buckling iteration calculations provides a reasonable convergence of the axial bucklings within two or three loops. The axial bucklings were obtained from the FOG buckling iteration calculation. The k_{eff}'s were obtained from the one-sixth core R-θ calculation with the axial bucklings from FOG 2 by the EXTERMINATOR-2 code. Since the cross sections converged rapidly during the first two trials, the calculations were terminated and a k_{eff} of 1.1507 after the second trial was taken as a converged value which is equal to a reactivity of 13.1 percent.

The 24 element core contained 3948 grams of U-235.

4. Results for 13 element core

The original cold, clean, minimum critical mass reactor contained 13 fuel elements with 2139 grams of uranium 235 and has a measured k_{eff} of 1.0063. Figure V-9 shows the location of the fuel elements for this core. Since this core is non-

A. RADIAL

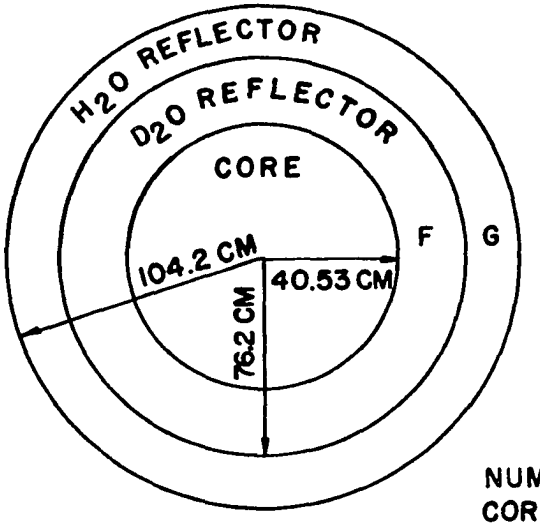

NUMBER OF MESHES
CORE : 32
REFLECTOR F: 28
REFLECTOR G: 22

B. AXIAL

REGION	1	2	3	4	5	6
	A	B	C	CORE	D	E
NUMBER OF MESHES	16	24	13	48	22	40
REGION THICKNESS, CM.	20.32	30.32	16.19	59.69	27.94	50.01
REGION THICKNESS, IN.	8	12	6.38	23.5	11	19.69

Figure V-8. Geometries for buckling iteration calculation

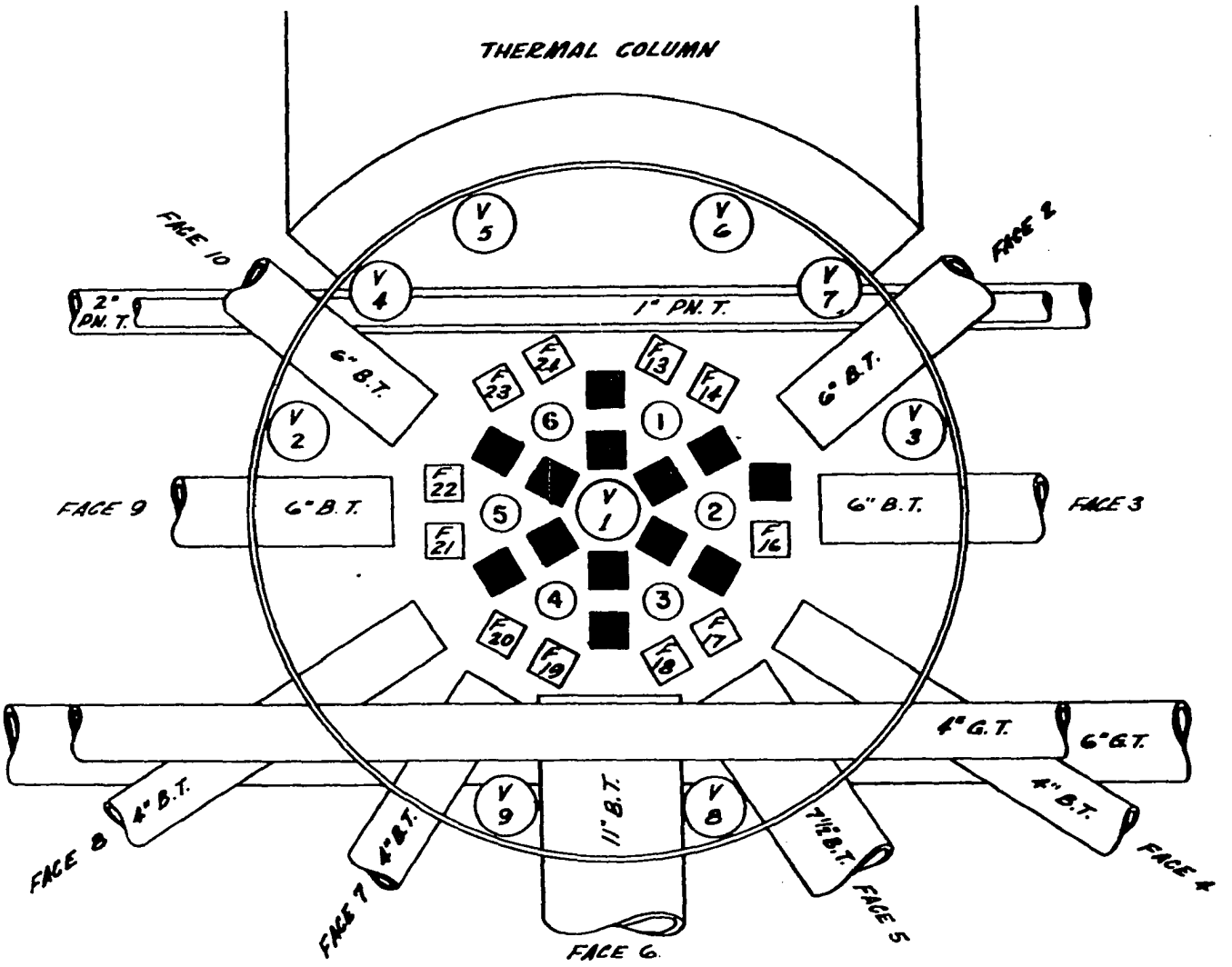

Figure V-9. Geometric relation between the core, control rods and some of the experimental thimbles for 13 element core

symmetric, a sample calculation was made to check the effect of moving the odd fuel element in ring 3 from an off-center to an on-center position. This calculation indicated an increase in k_{eff} of less than 0.0017. The element was considered to be on-center and half-core symmetry was used in the calculations. Figure V-10 shows the arrangement of this half-core symmetry design used in the calculations.

Only two neutron groups were used in the 13 element core. This core had 50 x 44 mesh points and 4 neutron groups could not be handled by our computer. Also, the 4 group case would increase the cost per computer run.

A sample problem was run for the 24 element case of going from 4 to 2 groups of neutrons. The 2 group case had an increase in k_{eff} of 0.02 that was independent of fixed reflector savings. This bias was included in the 13 element 2 group calculations as an increase in k_{eff} of 0.011 assuming a linear effect in k_{eff} and number of fuel elements. Allowing for the effect of shifting the 13th element to the on-center position increases this bias to a k_{eff} of 0.0127.

The two group neutron cross sections from LEOPARD are listed in Table V-10. The relative average neutron fluxes for the core D_2O and fuel regions as shown in Table V-11 and the flux averaged few group neutron cross sections are shown in Table V-12. The average cross sections of Table V-12 were used in Fog 2 for the iteration method described previously.

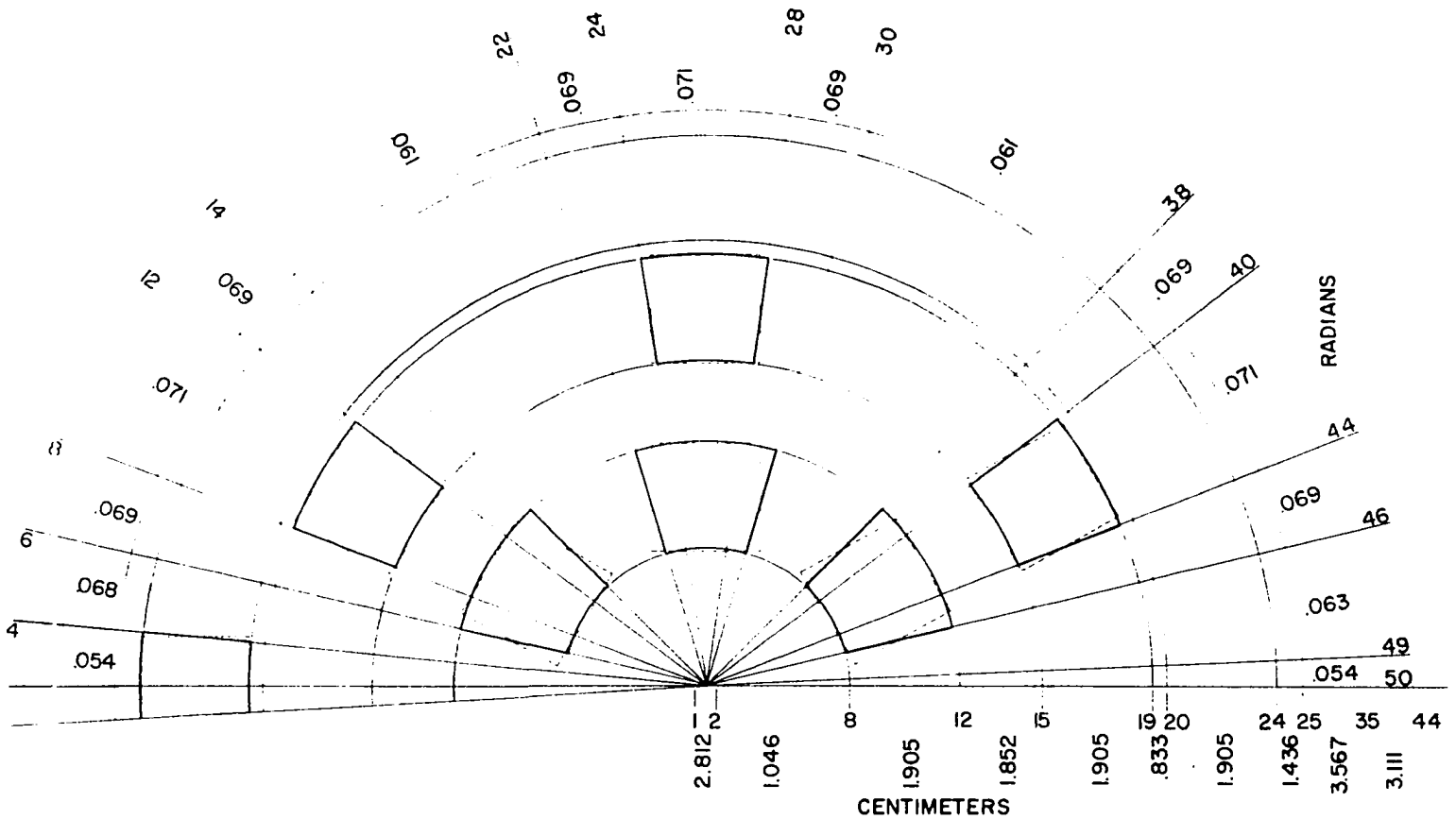

Figure V-10. Mesh spacing for 13 element core

Table V-10

Two Group Neutron Cross Sections for 13 Element Core

Description	g	D cm	Σ_a cm^{-1}	Σ_R cm^{-1}	$\nu\Sigma_f$ cm^{-1}
Material 1	1	1.5905	6.165-04	2.831-02	2.108-04
H_2O reflector	2	0.3146	1.250-01	0.0	0.0
Material 2	1	1.3482	2.293-04	9.817-03	1.909-04
D_2O reflector	2	0.8733	8.753-04	0.0	0.0
Material 3	1	1.2756	1.964-04	1.125-02	2.263-04
Core D_2O	2	0.7943	9.038-05	0.0	0.0
Material 4	1	1.6403	2.504-03	4.006-03	3.397-03
Fuel	2	1.1695	3.676-02	0.0	7.045-02

Table V-11

Average Neutron Flux (Relative)

Material/Group	1	2	Area, cm^2
3	.002366	.00394	2188
4	.003944	.003375	392.5

Table V-12

Few Group Neutron Cross Sections for Core

Group	D cm	Σ_a cm^{-1}	Σ_R cm^{-1}	$\nu\Sigma_f$ cm^{-1}
1	1.3444	7.257-04	9.216-04	9.539-04
2	0.8297	4.973-03	0.0	9.384-03

The iteration technique produced a k_{eff} of 1.0253. Subtracting the above bias makes k_{eff} equal to 1.0126. Accounting for the worth of the central thimble and replacing the heavy water in the central thimble with graphite makes k_{eff} equal to 1.0038, which compared to the measured value of 1.0063 gives a calculated error in k_{eff} of 0.0025.

VI. SELECTION OF CONSTANTS FOR USE IN THE ALRR REACTIVITY EQUATION

In the next chapter, a neutron poison is utilized to determine the excess reactivity of the 24 element core. This chapter discusses the reactivity equation used and the selection of constants used in the equation.

The equation which relates reactivity to stable reactor period in U-235 fueled, heavy-water moderated reactors was solved using delayed neutron data for use in thermal reactors and for changes to parameters in the equations. The results are plotted in various figures and the reactivity in cents versus the stable reactor period are tabulated.

A. Theory

The reactivity (ρ) is related to the stable reactor period (T) by the relation (Glasstone and Edlund 22a, p. 298).

$$\rho = \frac{\ell}{\ell+T} + \frac{T}{\ell+T} \sum_{i=1}^{n} \frac{\gamma_i \beta_i}{1+\lambda_i T} \qquad \text{(VI-1)}$$

where ℓ is the prompt neutron lifetime,

T is the stable reactor period,

β_i is the yield of the ith delayed neutron group,

γ_i is the effectiveness of the ith delayed neutron group as compared to prompt neutrons. (Delayed neutrons have lower leakage probabilities than prompt neutrons because they are emitted at lower energies.) This term was added to the basic equation.

λ_i is the decay constant for the ith group, and

n is the number of the delayed neutron group.

(There are six groups from U-235).

A reactor which is just critical on prompt neutrons alone is said to have an excess reactivity of one dollar. The reactivity in dollars is:

$$\$ = \frac{\rho}{\gamma\beta} , \qquad \text{(VI-2)}$$

where β is the total delayed neutron fraction, and

γ is the average effectiveness of the delayed neutrons. Equations 1 and 2 are combined to give

$$\$ = \frac{\ell}{\gamma\beta(\ell+T)} + \frac{T}{\ell+T} \sum_{i=1}^{n} \frac{\gamma_i\beta_i}{\gamma\beta(1+\lambda_i T)} . \qquad \text{(VI-3)}$$

The γ_i for the individual delayed neutron groups differ only slightly from the average γ in thermal reactors and in practical calculations, the measured delayed neutron fractions β_i/β can be substituted for $\gamma_i\beta_i/\gamma\beta$ (Keepin 22b, p. 193). With this approximation, Equation 3 now becomes

$$\$ = \frac{\ell}{\gamma\beta(\ell+T)} + \frac{T}{\ell+T} \sum_{i=1}^{n} \frac{\beta_i}{\beta(1+\lambda_i T)} . \qquad \text{(VI-4)}$$

In general, photoneutron activity can be treated as individual groups formed directly from fission (Keepin 22b, p. 195). It is assumed that all delayed neutrons have the same effectiveness. Therefore, the nine D_2O photoneutron groups can be treated simply as additional groups of delayed neutrons making

(n) in Equation 4 equal to 15.

Allowance should be made for an effective irradiation time, buildup factor for each delayed neutron group (Keepin 22b, p. 195), prior to a reactivity change. Most periods in this report were between 20 and 60 seconds and the waiting times prior to these step changes were long enough to reduce this source of error to less than 3%.

B. Data Used

1. Delayed neutrons

Less than one percent of the neutrons which are emitted following fission are called delayed neutrons.

Keepin, Wimett and Zeigler (23) measured periods, relative abundances and yields of delayed neutrons from thermal fission of U-235. Six exponential periods were found sufficient for optimum fit of all data. There may be a dozen or more delayed-neutron precursors of appreciable yield in fission. However, six delayed groups have always provided ample details in thermal reactor kinetic calculations.

Table 1 lists the delayed neutron data for thermal fission of U-235 (Keepin 22b, p. 90) based on the work of Keepin, Wilmett and Zeigler (23).

a. Photoneutrons In a heavy water moderated system, gamma rays above a threshold energy of 2.23 Mev can interact with deuterium and produce neutrons known as photoneutrons. Delayed high energy gamma rays emitted during the decay of

Table VI-1

Delayed Neutron Data for Thermal Fission in U-235

Group	Half-life sec.	Decay Constant λ_i sec.$^{-1}$	Absolute Group Yield %	Relative Abundance a_i	Delayed Fraction β_i
1	0.230	3.01	0.066	0.042	0.000273
2	0.610	1.14	0.182	0.115	0.0007475
3	2.30	0.301	0.624	0.395	0.0025675
4	6.22	0.111	0.310	0.196	0.001274
5	22.72	0.0305	0.346	0.219	0.0014235
6	55.72	0.0124	0.052	0.033	0.0002145
				Total	0.0065

some fission fragments cause delayed photoneutrons having the same periods and abundances as their precursors.

Table 2 lists the group constants for delayed photoneutrons from U-235 fission gamma rays in heavy water. This table obtained from (Keepin 22b, p. 146) reports Bernstein et al. (24) results normalized to the latest accepted delayed neutron data for thermal fission in U-235. The 12.8 day long-lived photoneutron activity measured by Ergen (25) is included in the group constants.

The effects of varying the various parameters in Equation 4 has been adequately covered elsewhere, e.g., Keepin (22b). However, the effects of varying parameters unique to the Ames Laboratory Research Reactor (ALRR) type reactors will be considered.

2. Gamma ray transmission

Photoneutrons in heavy water are caused by gamma rays, which originate in the fuel elements, that have an energy greater than 2.23 Mev. Removal of these gamma rays or reduction in their energy below this threshold value by structural materials in the reactor reduces the contribution of photoneutrons from this process. The percent of these gamma rays which enter the heavy water and cause photoneutrons is called the gamma ray transmission.

The ALRR is a heterogeneous, highly enriched, heavy water moderated and cooled reactor with aluminum clad MTR type fuel

Table VI-2

Delayed Photoneutrons from U-235 Fission Gamma Rays in Heavy Water

Group	Half-life	Decay Constant λ_i sec.$^{-1}$	Photoneutrons Per Fission (10^{-5})	Delayed Fraction β_i (10^{-5})
1	2.5 S	2.77×10^{-1}	158.0	65.1
2	41 S	1.69×10^{-2}	49.5	20.4
3	2.4 M	4.81×10^{-3}	17.0	7.00
4	7.7 M	1.50×10^{-3}	8.14	3.36
5	27 M	4.28×10^{-4}	5.01	2.07
6	1.65H	1.17×10^{-4}	5.65	2.34
7	4.4 H	4.37×10^{-5}	0.78	0.323
8	53 H	3.63×10^{-6}	0.25	0.103
9	12.8 D	6.26×10^{-7}		0.05
			Total	100.75

elements. Similar reactors of this type are the Massachusetts Institute of Technology Reactor (MITR) and the Georgia Institute of Technology Research Reactor (GTRR). The quoted gamma ray transmission values for these reactors are 69 percent for the MITR and 72 percent for the GTRR (Graham and Harmer 26, p. 68).

A gamma ray transmission value of 70 percent was assumed for the ALRR because of its similarities to the above reactors and comparisons made between results using values of 60, 70 and 80 percent are shown in Figure VI-1.

These curves were obtained from Equation 4 with a prompt neutron lifetime for the ALRR of 5×10^{-4} seconds, an effective delayed neutron fraction of 0.0075, with 100 percent of the delayed neutron fractions from U-235 shown in Table 1 and either 60, 70, or 80 percent of the delayed photoneutron fractions shown in Table 2. Figure VI-1 indicates little error introduced in reactivity values for slight variations in gamma ray transmission for reactor periods less than 100 seconds.

3. Relative abundance of photoneutrons

Evidence exists, Church (27), that the shortest-lived, 2.5 second photoneutron group should have an abundance of about 20 percent of that reported by Bernstein et al. (24). Figure VI-2 shows the effect of this reduction, Curve D_2O-.2, compared to the original data, Curve D_2O=1., where 100 percent of the 2.5 second delayed-neutron abundance was used. A gamma

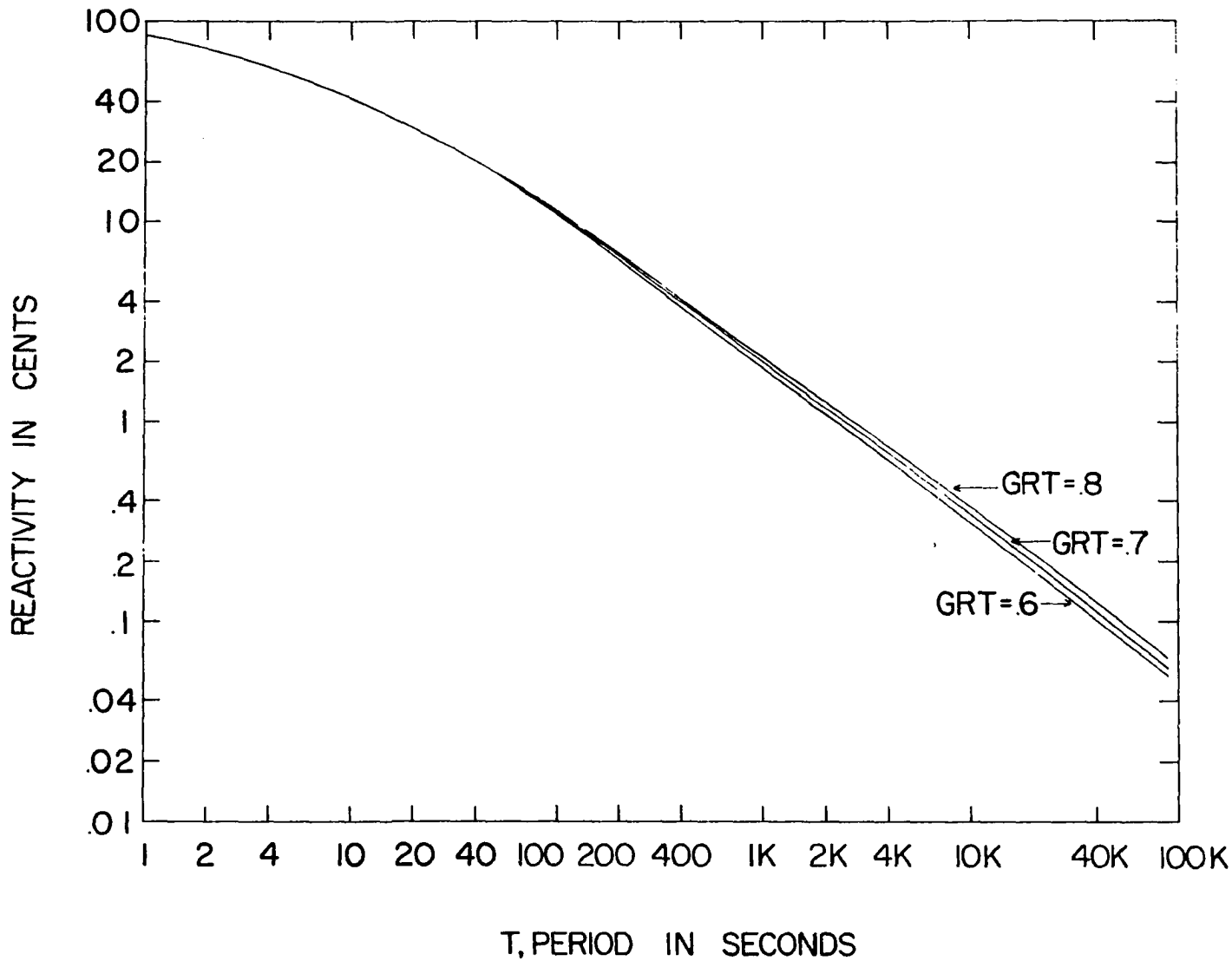

Figure VI-1. Reactivity in cents versus stable reactor period as a function of gamma ray transmission

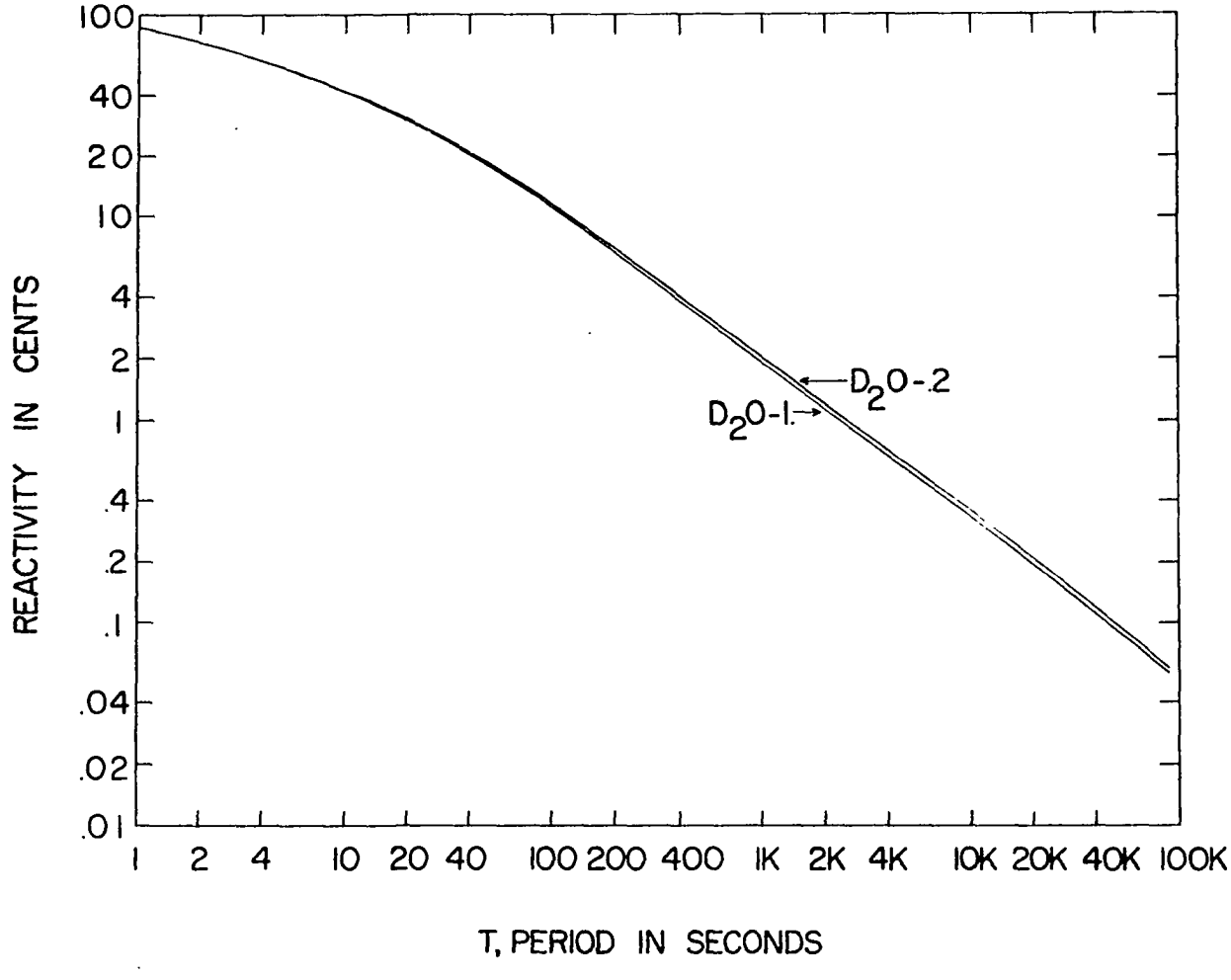

Figure VI-2. Reactivity in cents versus stable reactor period as a function of the abundance of 2.5 second photoneutron

ray transmission value of 70 percent was used for both curves. The reduction in group abundance results in a slightly higher reactivity value for the same reactor period.

Table 3 lists the reactivity in cents versus positive periods from 10 to 540 seconds using 100 percent of the 2.5 second (D_2O-1.) delayed neutron relative abundance, while Table 4 lists equivalent data for the 20 percent (D_2O-0.2) case.

Buildup errors can be reduced by allowing long irradiation times, 10 to 30 minutes, prior to a reactivity change and by using reactor periods that are less than 100 seconds.

Table VI-3

100 Percent Photoneutron Abundance

U-235 THERMAL+D2O-1
REACTIVITY IN CENTS VERSUS POSITIVE PERIOD FOR ALRR

SEC	.0	.1	.2	.3	.4	.5	.6	.7	.8	.9
10	41.50	41.32	41.14	40.97	40.79	40.62	40.45	40.29	40.12	39.96
11	39.80	39.64	39.48	39.32	39.17	39.02	38.87	38.72	38.57	38.42
12	38.27	38.13	37.99	37.85	37.71	37.57	37.43	37.30	37.16	37.03
13	36.90	36.77	36.64	36.51	36.38	36.26	36.13	36.01	35.89	35.76
14	35.64	35.52	35.41	35.29	35.17	35.06	34.94	34.83	34.72	34.61
15	34.50	34.39	34.28	34.17	34.06	33.96	33.85	33.75	33.64	33.54
16	33.44	33.34	33.24	33.14	33.04	32.94	32.84	32.75	32.65	32.56
17	32.46	32.37	32.27	32.18	32.09	32.00	31.91	31.82	31.73	31.64
18	31.55	31.47	31.38	31.29	31.21	31.12	31.04	30.95	30.87	30.79
19	30.71	30.62	30.54	30.46	30.38	30.30	30.22	30.15	30.07	29.99
20	29.91	29.84	29.76	29.69	29.61	29.54	29.46	29.39	29.32	29.24
21	29.17	29.10	29.03	28.96	28.89	28.82	28.75	28.68	28.61	28.54
22	28.47	28.40	28.34	28.27	28.20	28.14	28.07	28.01	27.94	27.88
23	27.81	27.75	27.69	27.62	27.56	27.50	27.43	27.37	27.31	27.25
24	27.19	27.13	27.07	27.01	26.95	26.89	26.83	26.77	26.71	26.66
25	26.60	26.54	26.48	26.43	26.37	26.32	26.26	26.20	26.15	26.09
26	26.04	25.98	25.93	25.88	25.82	25.77	25.72	25.66	25.61	25.56
27	25.51	25.46	25.40	25.35	25.30	25.25	25.20	25.15	25.10	25.05
28	25.00	24.95	24.90	24.85	24.80	24.76	24.71	24.66	24.61	24.56
29	24.52	24.47	24.42	24.38	24.33	24.28	24.24	24.19	24.15	24.10
30	24.05	24.01	23.96	23.92	23.88	23.83	23.79	23.74	23.70	23.66
31	23.61	23.57	23.53	23.48	23.44	23.40	23.36	23.31	23.27	23.23
32	23.19	23.15	23.11	23.07	23.03	22.99	22.94	22.90	22.86	22.82
33	22.78	22.74	22.70	22.67	22.63	22.59	22.55	22.51	22.47	22.43
34	22.39	22.36	22.32	22.28	22.24	22.21	22.17	22.13	22.09	22.06
35	22.02	21.98	21.95	21.91	21.88	21.84	21.80	21.77	21.73	21.70
36	21.66	21.63	21.59	21.56	21.52	21.49	21.45	21.42	21.38	21.35
37	21.31	21.28	21.25	21.21	21.18	21.15	21.11	21.08	21.05	21.01
38	20.98	20.95	20.92	20.88	20.85	20.82	20.79	20.75	20.72	20.69
39	20.66	20.63	20.60	20.56	20.53	20.50	20.47	20.44	20.41	20.38
40	20.35	20.32	20.29	20.26	20.23	20.20	20.17	20.14	20.11	20.08
41	20.05	20.02	19.99	19.96	19.93	19.90	19.87	19.84	19.82	19.79
42	19.76	19.73	19.70	19.67	19.64	19.62	19.59	19.56	19.53	19.50
43	19.48	19.45	19.42	19.39	19.37	19.34	19.31	19.29	19.26	19.23
44	19.21	19.18	19.15	19.13	19.10	19.07	19.05	19.02	18.99	18.97
45	18.94	18.92	18.89	18.86	18.84	18.81	18.79	18.76	18.74	18.71
46	18.69	18.66	18.64	18.61	18.59	18.56	18.54	18.51	18.49	18.46
47	18.44	18.42	18.39	18.37	18.34	18.32	18.30	18.27	18.25	18.22
48	18.20	18.18	18.15	18.13	18.11	18.09	18.06	18.04	18.01	17.99
49	17.97	17.94	17.92	17.90	17.88	17.85	17.83	17.81	17.79	17.76
50	17.74	17.72	17.70	17.67	17.65	17.63	17.61	17.59	17.56	17.54
51	17.52	17.50	17.48	17.46	17.43	17.41	17.39	17.37	17.35	17.33
52	17.31	17.29	17.26	17.24	17.22	17.20	17.18	17.16	17.14	17.12
53	17.10	17.08	17.06	17.04	17.02	17.00	16.98	16.96	16.94	16.92
54	16.90	16.88	16.86	16.84	16.82	16.80	16.78	16.76	16.74	16.72

Table VI-3 (continued)

U-235 THERMAL+D2O-1
REACTIVITY IN CENTS VERSUS POSITIVE PERIOD FOR ALRR

SEC	.0	.1	.2	.3	.4	.5	.6	.7	.8	.9
55	16.70	16.68	16.66	16.64	16.62	16.60	16.58	16.56	16.55	16.53
56	16.51	16.49	16.47	16.45	16.43	16.41	16.39	16.38	16.36	16.34
57	16.32	16.30	16.28	16.26	16.25	16.23	16.21	16.19	16.17	16.16
58	16.14	16.12	16.10	16.08	16.07	16.05	16.03	16.01	16.00	15.98
59	15.96	15.94	15.92	15.91	15.89	15.87	15.86	15.84	15.82	15.80
60	15.79	15.77	15.75	15.74	15.72	15.70	15.68	15.67	15.65	15.63
61	15.62	15.60	15.58	15.57	15.55	15.53	15.52	15.50	15.48	15.47
62	15.45	15.44	15.42	15.40	15.39	15.37	15.35	15.34	15.32	15.31
63	15.29	15.27	15.26	15.24	15.23	15.21	15.20	15.18	15.16	15.15
64	15.13	15.12	15.10	15.09	15.07	15.05	15.04	15.02	15.01	14.99
65	14.98	14.96	14.95	14.93	14.92	14.90	14.89	14.87	14.86	14.84
66	14.83	14.81	14.80	14.78	14.77	14.75	14.74	14.72	14.71	14.70
67	14.68	14.67	14.65	14.64	14.62	14.61	14.59	14.58	14.56	14.55
68	14.54	14.52	14.51	14.49	14.48	14.47	14.45	14.44	14.42	14.41
69	14.40	14.38	14.37	14.35	14.34	14.33	14.31	14.30	14.28	14.27
70	14.26	14.24	14.23	14.22	14.20	14.19	14.18	14.16	14.15	14.14
71	14.12	14.11	14.10	14.08	14.07	14.06	14.04	14.03	14.02	14.00
72	13.99	13.98	13.96	13.95	13.94	13.93	13.91	13.90	13.89	13.87
73	13.86	13.85	13.84	13.82	13.81	13.80	13.78	13.77	13.76	13.75
74	13.73	13.72	13.71	13.70	13.68	13.67	13.66	13.65	13.63	13.62
75	13.61	13.60	13.59	13.57	13.56	13.55	13.54	13.52	13.51	13.50
76	13.49	13.48	13.46	13.45	13.44	13.43	13.42	13.40	13.39	13.38
77	13.37	13.36	13.35	13.33	13.32	13.31	13.30	13.29	13.27	13.26
78	13.25	13.24	13.23	13.22	13.21	13.19	13.18	13.17	13.16	13.15
79	13.14	13.13	13.11	13.10	13.09	13.08	13.07	13.06	13.05	13.04
80	13.02	13.01	13.00	12.99	12.98	12.97	12.96	12.95	12.94	12.92
81	12.91	12.90	12.89	12.88	12.87	12.86	12.85	12.84	12.83	12.82
82	12.81	12.79	12.78	12.77	12.76	12.75	12.74	12.73	12.72	12.71
83	12.70	12.69	12.68	12.67	12.66	12.65	12.64	12.63	12.62	12.60
84	12.59	12.58	12.57	12.56	12.55	12.54	12.53	12.52	12.51	12.50
85	12.49	12.48	12.47	12.46	12.45	12.44	12.43	12.42	12.41	12.40
86	12.39	12.38	12.37	12.36	12.35	12.34	12.33	12.32	12.31	12.30
87	12.29	12.28	12.27	12.26	12.25	12.24	12.23	12.22	12.21	12.20
88	12.19	12.19	12.18	12.17	12.16	12.15	12.14	12.13	12.12	12.11
89	12.10	12.09	12.08	12.07	12.06	12.05	12.04	12.03	12.02	12.01
90	12.01	12.00	11.99	11.98	11.97	11.96	11.95	11.94	11.93	11.92
91	11.91	11.90	11.89	11.89	11.88	11.87	11.86	11.85	11.84	11.83
92	11.82	11.81	11.80	11.80	11.79	11.78	11.77	11.76	11.75	11.74
93	11.73	11.72	11.72	11.71	11.70	11.69	11.68	11.67	11.66	11.65
94	11.65	11.64	11.63	11.62	11.61	11.60	11.59	11.58	11.58	11.57
95	11.56	11.55	11.54	11.53	11.53	11.52	11.51	11.50	11.49	11.48
96	11.47	11.47	11.46	11.45	11.44	11.43	11.42	11.42	11.41	11.40
97	11.39	11.38	11.37	11.37	11.36	11.35	11.34	11.33	11.32	11.32
98	11.31	11.30	11.29	11.28	11.28	11.27	11.26	11.25	11.24	11.24
99	11.23	11.22	11.21	11.20	11.20	11.19	11.18	11.17	11.16	11.16

Table VI-3 (continued)

U-235 THERMAL+D2O-1
REACTIVITY IN CENTS VERSUS POSITIVE PERIOD FOR ALRR

SEC	0	1	2	3	4	5	6	7	8	9
100	11.15	11.07	10.99	10.92	10.84	10.77	10.70	10.62	10.55	10.48
110	10.42	10.35	10.28	10.22	10.15	10.09	10.02	9.96	9.90	9.84
120	9.78	9.72	9.66	9.61	9.55	9.49	9.44	9.39	9.33	9.28
130	9.23	9.17	9.12	9.07	9.02	8.97	8.93	8.88	8.83	8.78
140	8.74	8.69	8.65	8.60	8.56	8.51	8.47	8.43	8.38	8.34
150	8.30	8.26	8.22	8.18	8.14	8.10	8.06	8.02	7.99	7.95
160	7.91	7.87	7.84	7.80	7.77	7.73	7.70	7.66	7.63	7.59
170	7.56	7.53	7.49	7.46	7.43	7.40	7.36	7.33	7.30	7.27
180	7.24	7.21	7.18	7.15	7.12	7.09	7.06	7.03	7.01	6.98
190	6.95	6.92	6.89	6.87	6.84	6.81	6.79	6.76	6.73	6.71
200	6.68	6.66	6.63	6.61	6.58	6.56	6.53	6.51	6.49	6.46
210	6.44	6.42	6.39	6.37	6.35	6.32	6.30	6.28	6.26	6.24
220	6.21	6.19	6.17	6.15	6.13	6.11	6.09	6.07	6.05	6.03
230	6.01	5.99	5.97	5.95	5.93	5.91	5.89	5.87	5.85	5.83
240	5.81	5.79	5.77	5.76	5.74	5.72	5.70	5.68	5.67	5.65
250	5.63	5.61	5.60	5.58	5.56	5.55	5.53	5.51	5.50	5.48
260	5.46	5.45	5.43	5.41	5.40	5.38	5.37	5.35	5.34	5.32
270	5.31	5.29	5.28	5.26	5.25	5.23	5.22	5.20	5.19	5.17
280	5.16	5.14	5.13	5.12	5.10	5.09	5.07	5.06	5.05	5.03
290	5.02	5.01	4.99	4.98	4.97	4.95	4.94	4.93	4.91	4.90
300	4.89	4.88	4.86	4.85	4.84	4.83	4.81	4.80	4.79	4.78
310	4.77	4.75	4.74	4.73	4.72	4.71	4.69	4.68	4.67	4.66
320	4.65	4.64	4.63	4.62	4.60	4.59	4.58	4.57	4.56	4.55
330	4.54	4.53	4.52	4.51	4.50	4.49	4.48	4.47	4.45	4.44
340	4.43	4.42	4.41	4.40	4.39	4.38	4.37	4.36	4.35	4.34
350	4.33	4.33	4.32	4.31	4.30	4.29	4.28	4.27	4.26	4.25
360	4.24	4.23	4.22	4.21	4.20	4.20	4.19	4.18	4.17	4.16
370	4.15	4.14	4.13	4.12	4.12	4.11	4.10	4.09	4.08	4.07
380	4.06	4.06	4.05	4.04	4.03	4.02	4.02	4.01	4.00	3.99
390	3.98	3.98	3.97	3.96	3.95	3.94	3.94	3.93	3.92	3.91
400	3.91	3.90	3.89	3.88	3.87	3.87	3.86	3.85	3.84	3.84
410	3.83	3.82	3.82	3.81	3.80	3.79	3.79	3.78	3.77	3.77
420	3.76	3.75	3.74	3.74	3.73	3.72	3.72	3.71	3.70	3.70
430	3.69	3.68	3.68	3.67	3.66	3.66	3.65	3.64	3.64	3.63
440	3.62	3.62	3.61	3.60	3.60	3.59	3.59	3.58	3.57	3.57
450	3.56	3.55	3.55	3.54	3.54	3.53	3.52	3.52	3.51	3.51
460	3.50	3.49	3.49	3.48	3.48	3.47	3.46	3.46	3.45	3.45
470	3.44	3.44	3.43	3.42	3.42	3.41	3.41	3.40	3.40	3.39
480	3.39	3.38	3.37	3.37	3.36	3.36	3.35	3.35	3.34	3.34
490	3.33	3.33	3.32	3.32	3.31	3.31	3.30	3.29	3.29	3.28
500	3.28	3.27	3.27	3.26	3.26	3.25	3.25	3.24	3.24	3.23
510	3.23	3.22	3.22	3.21	3.21	3.20	3.20	3.19	3.19	3.19
520	3.18	3.17	3.17	3.17	3.16	3.16	3.15	3.15	3.14	3.14
530	3.13	3.13	3.12	3.12	3.11	3.11	3.11	3.10	3.10	3.09
540	3.09	3.08	3.08	3.07	3.07	3.07	3.06	3.06	3.05	3.05

Table VI-4

20 Percent of 2.5 Second Photoneutron Abundance

U-235 THERMAL+D2O-.2
REACTIVITY IN CENTS VERSUS POSITIVE PERIOD FOR ALRR

SEC	.0	.1	.2	.3	.4	.5	.6	.7	.8	.9
10	42.26	42.08	41.91	41.73	41.56	41.39	41.22	41.06	40.89	40.73
11	40.57	40.41	40.25	40.10	39.94	39.79	39.64	39.49	39.34	39.20
12	39.05	38.91	38.77	38.63	38.49	38.35	38.21	38.08	37.94	37.81
13	37.68	37.55	37.42	37.29	37.16	37.04	36.91	36.79	36.67	36.55
14	36.43	36.31	36.19	36.07	35.95	35.84	35.73	35.61	35.50	35.39
15	35.28	35.17	35.06	34.95	34.84	34.74	34.63	34.53	34.42	34.32
16	34.22	34.12	34.02	33.92	33.82	33.72	33.62	33.52	33.43	33.33
17	33.24	33.14	33.05	32.96	32.86	32.77	32.68	32.59	32.50	32.41
18	32.32	32.24	32.15	32.06	31.98	31.89	31.81	31.72	31.64	31.56
19	31.47	31.39	31.31	31.23	31.15	31.07	30.99	30.91	30.83	30.75
20	30.68	30.60	30.52	30.45	30.37	30.30	30.22	30.15	30.07	30.00
21	29.93	29.85	29.78	29.71	29.64	29.57	29.50	29.43	29.36	29.29
22	29.22	29.15	29.09	29.02	28.95	28.88	28.82	28.75	28.69	28.62
23	28.56	28.49	28.43	28.36	28.30	28.24	28.17	28.11	28.05	27.99
24	27.93	27.87	27.81	27.74	27.68	27.62	27.57	27.51	27.45	27.39
25	27.33	27.27	27.21	27.16	27.10	27.04	26.99	26.93	26.87	26.82
26	26.76	26.71	26.65	26.60	26.54	26.49	26.44	26.38	26.33	26.28
27	26.22	26.17	26.12	26.07	26.02	25.96	25.91	25.86	25.81	25.76
28	25.71	25.66	25.61	25.56	25.51	25.46	25.41	25.37	25.32	25.27
29	25.22	25.17	25.13	25.08	25.03	24.98	24.94	24.89	24.84	24.80
30	24.75	24.71	24.66	24.62	24.57	24.53	24.48	24.44	24.39	24.35
31	24.30	24.26	24.22	24.17	24.13	24.09	24.04	24.00	23.96	23.92
32	23.87	23.83	23.79	23.75	23.71	23.67	23.62	23.58	23.54	23.50
33	23.46	23.42	23.38	23.34	23.30	23.26	23.22	23.18	23.14	23.11
34	23.07	23.03	22.99	22.95	22.91	22.87	22.84	22.80	22.76	22.72
35	22.69	22.65	22.61	22.57	22.54	22.50	22.46	22.43	22.39	22.36
36	22.32	22.28	22.25	22.21	22.18	22.14	22.11	22.07	22.04	22.00
37	21.97	21.93	21.90	21.86	21.83	21.80	21.76	21.73	21.69	21.66
38	21.63	21.59	21.56	21.53	21.49	21.46	21.43	21.40	21.36	21.33
39	21.30	21.27	21.23	21.20	21.17	21.14	21.11	21.08	21.04	21.01
40	20.98	20.95	20.92	20.89	20.86	20.83	20.80	20.77	20.74	20.71
41	20.68	20.65	20.62	20.59	20.56	20.53	20.50	20.47	20.44	20.41
42	20.38	20.35	20.32	20.29	20.26	20.24	20.21	20.18	20.15	20.12
43	20.09	20.07	20.04	20.01	19.98	19.95	19.93	19.90	19.87	19.84
44	19.82	19.79	19.76	19.74	19.71	19.68	19.65	19.63	19.60	19.57
45	19.55	19.52	19.50	19.47	19.44	19.42	19.39	19.36	19.34	19.31
46	19.29	19.26	19.24	19.21	19.19	19.16	19.14	19.11	19.08	19.06
47	19.03	19.01	18.99	18.96	18.94	18.91	18.89	18.86	18.84	18.81
48	18.79	18.77	18.74	18.72	18.69	18.67	18.65	18.62	18.60	18.58
49	18.55	18.53	18.50	18.48	18.46	18.44	18.41	18.39	18.37	18.34
50	18.32	18.30	18.27	18.25	18.23	18.21	18.18	18.16	18.14	18.12
51	18.10	18.07	18.05	18.03	18.01	17.99	17.96	17.94	17.92	17.90
52	17.88	17.85	17.83	17.81	17.79	17.77	17.75	17.73	17.71	17.68
53	17.66	17.64	17.62	17.60	17.58	17.56	17.54	17.52	17.50	17.48
54	17.46	17.44	17.42	17.40	17.37	17.35	17.33	17.31	17.29	17.27

Table VI-4 (continued)

U-235 THERMAL+D2O-.2
REACTIVITY IN CENTS VERSUS POSITIVE PERIOD FOR ALRR

SEC	.0	.1	.2	.3	.4	.5	.6	.7	.8	.9
55	17.25	17.23	17.21	17.19	17.18	17.16	17.14	17.12	17.10	17.08
56	17.06	17.04	17.02	17.00	16.98	16.96	16.94	16.92	16.90	16.89
57	16.87	16.85	16.83	16.81	16.79	16.77	16.75	16.73	16.72	16.70
58	16.68	16.66	16.64	16.62	16.61	16.59	16.57	16.55	16.53	16.52
59	16.50	16.48	16.46	16.44	16.43	16.41	16.39	16.37	16.35	16.34
60	16.32	16.30	16.28	16.27	16.25	16.23	16.21	16.20	16.18	16.16
61	16.15	16.13	16.11	16.09	16.08	16.06	16.04	16.03	16.01	15.99
62	15.98	15.96	15.94	15.93	15.91	15.89	15.88	15.86	15.84	15.83
63	15.81	15.79	15.78	15.76	15.75	15.73	15.71	15.70	15.68	15.66
64	15.65	15.63	15.62	15.60	15.59	15.57	15.55	15.54	15.52	15.51
65	15.49	15.48	15.46	15.44	15.43	15.41	15.40	15.38	15.37	15.35
66	15.34	15.32	15.31	15.29	15.28	15.26	15.25	15.23	15.22	15.20
67	15.19	15.17	15.16	15.14	15.13	15.11	15.10	15.08	15.07	15.05
68	15.04	15.02	15.01	14.99	14.98	14.96	14.95	14.94	14.92	14.91
69	14.89	14.88	14.86	14.85	14.84	14.82	14.81	14.79	14.78	14.77
70	14.75	14.74	14.72	14.71	14.70	14.68	14.67	14.65	14.64	14.63
71	14.61	14.60	14.58	14.57	14.56	14.54	14.53	14.52	14.50	14.49
72	14.48	14.46	14.45	14.44	14.42	14.41	14.40	14.38	14.37	14.36
73	14.34	14.33	14.32	14.30	14.29	14.28	14.27	14.25	14.24	14.23
74	14.21	14.20	14.19	14.17	14.16	14.15	14.14	14.12	14.11	14.10
75	14.09	14.07	14.06	14.05	14.04	14.02	14.01	14.00	13.99	13.97
76	13.96	13.95	13.94	13.92	13.91	13.90	13.89	13.87	13.86	13.85
77	13.84	13.83	13.81	13.80	13.79	13.78	13.77	13.75	13.74	13.73
78	13.72	13.71	13.69	13.68	13.67	13.66	13.65	13.63	13.62	13.61
79	13.60	13.59	13.58	13.56	13.55	13.54	13.53	13.52	13.51	13.50
80	13.48	13.47	13.46	13.45	13.44	13.43	13.42	13.40	13.39	13.38
81	13.37	13.36	13.35	13.34	13.33	13.31	13.30	13.29	13.28	13.27
82	13.26	13.25	13.24	13.23	13.21	13.20	13.19	13.18	13.17	13.16
83	13.15	13.14	13.13	13.12	13.11	13.10	13.08	13.07	13.06	13.05
84	13.04	13.03	13.02	13.01	13.00	12.99	12.98	12.97	12.96	12.95
85	12.94	12.93	12.92	12.90	12.89	12.88	12.87	12.86	12.85	12.84
86	12.83	12.82	12.81	12.80	12.79	12.78	12.77	12.76	12.75	12.74
87	12.73	12.72	12.71	12.70	12.69	12.68	12.67	12.66	12.65	12.64
88	12.63	12.62	12.61	12.60	12.59	12.58	12.57	12.56	12.55	12.54
89	12.53	12.52	12.51	12.50	12.49	12.48	12.47	12.46	12.45	12.45
90	12.44	12.43	12.42	12.41	12.40	12.39	12.38	12.37	12.36	12.35
91	12.34	12.33	12.32	12.31	12.30	12.29	12.28	12.28	12.27	12.26
92	12.25	12.24	12.23	12.22	12.21	12.20	12.19	12.18	12.17	12.16
93	12.16	12.15	12.14	12.13	12.12	12.11	12.10	12.09	12.08	12.07
94	12.07	12.06	12.05	12.04	12.03	12.02	12.01	12.00	11.99	11.99
95	11.98	11.97	11.96	11.95	11.94	11.93	11.92	11.91	11.91	11.90
96	11.89	11.88	11.87	11.86	11.85	11.85	11.84	11.83	11.82	11.81
97	11.80	11.79	11.79	11.78	11.77	11.76	11.75	11.74	11.74	11.73
98	11.72	11.71	11.70	11.69	11.68	11.68	11.67	11.66	11.65	11.64
99	11.63	11.63	11.62	11.61	11.60	11.59	11.59	11.58	11.57	11.56

Table VI-4 (continued)

U-235 THERMAL+D2O-.2
REACTIVITY IN CENTS VERSUS POSITIVE PERIOD FOR ALRR

SEC	0	1	2	3	4	5	6	7	8	9
100	11.55	11.47	11.39	11.31	11.24	11.16	11.09	11.01	10.94	10.87
110	10.80	10.73	10.66	10.59	10.53	10.46	10.39	10.33	10.27	10.21
120	10.14	10.08	10.02	9.96	9.91	9.85	9.79	9.74	9.68	9.63
130	9.57	9.52	9.47	9.41	9.36	9.31	9.26	9.21	9.16	9.11
140	9.07	9.02	8.97	8.93	8.88	8.83	8.79	8.75	8.70	8.66
150	8.62	8.57	8.53	8.49	8.45	8.41	8.37	8.33	8.29	8.25
160	8.21	8.17	8.14	8.10	8.06	8.03	7.99	7.95	7.92	7.88
170	7.85	7.81	7.78	7.75	7.71	7.68	7.65	7.61	7.58	7.55
180	7.52	7.49	7.46	7.43	7.40	7.37	7.34	7.31	7.28	7.25
190	7.22	7.19	7.16	7.13	7.11	7.08	7.05	7.02	7.00	6.97
200	6.94	6.92	6.89	6.87	6.84	6.81	6.79	6.76	6.74	6.71
210	6.69	6.67	6.64	6.62	6.59	6.57	6.55	6.53	6.50	6.48
220	6.46	6.43	6.41	6.39	6.37	6.35	6.33	6.30	6.28	6.26
230	6.24	6.22	6.20	6.18	6.16	6.14	6.12	6.10	6.08	6.06
240	6.04	6.02	6.00	5.98	5.96	5.95	5.93	5.91	5.89	5.87
250	5.85	5.84	5.82	5.80	5.78	5.77	5.75	5.73	5.71	5.70
260	5.68	5.66	5.65	5.63	5.61	5.60	5.58	5.56	5.55	5.53
270	5.52	5.50	5.49	5.47	5.45	5.44	5.42	5.41	5.39	5.38
280	5.36	5.35	5.33	5.32	5.31	5.29	5.28	5.26	5.25	5.23
290	5.22	5.21	5.19	5.18	5.16	5.15	5.14	5.12	5.11	5.10
300	5.08	5.07	5.06	5.05	5.03	5.02	5.01	4.99	4.98	4.97
310	4.96	4.94	4.93	4.92	4.91	4.90	4.88	4.87	4.86	4.85
320	4.84	4.82	4.81	4.80	4.79	4.78	4.77	4.76	4.74	4.73
330	4.72	4.71	4.70	4.69	4.68	4.67	4.66	4.65	4.63	4.62
340	4.61	4.60	4.59	4.58	4.57	4.56	4.55	4.54	4.53	4.52
350	4.51	4.50	4.49	4.48	4.47	4.46	4.45	4.44	4.43	4.42
360	4.41	4.40	4.39	4.38	4.37	4.37	4.36	4.35	4.34	4.33
370	4.32	4.31	4.30	4.29	4.28	4.27	4.27	4.26	4.25	4.24
380	4.23	4.22	4.21	4.20	4.20	4.19	4.18	4.17	4.16	4.15
390	4.15	4.14	4.13	4.12	4.11	4.10	4.10	4.09	4.08	4.07
400	4.06	4.06	4.05	4.04	4.03	4.03	4.02	4.01	4.00	3.99
410	3.99	3.98	3.97	3.96	3.96	3.95	3.94	3.93	3.93	3.92
420	3.91	3.91	3.90	3.89	3.88	3.88	3.87	3.86	3.86	3.85
430	3.84	3.83	3.83	3.82	3.81	3.81	3.80	3.79	3.79	3.78
440	3.77	3.77	3.76	3.75	3.75	3.74	3.73	3.73	3.72	3.71
450	3.71	3.70	3.69	3.69	3.68	3.68	3.67	3.66	3.66	3.65
460	3.64	3.64	3.63	3.63	3.62	3.61	3.61	3.60	3.60	3.59
470	3.58	3.58	3.57	3.57	3.56	3.55	3.55	3.54	3.54	3.53
480	3.53	3.52	3.51	3.51	3.50	3.50	3.49	3.49	3.48	3.47
490	3.47	3.46	3.46	3.45	3.45	3.44	3.44	3.43	3.43	3.42
500	3.41	3.41	3.40	3.40	3.39	3.39	3.38	3.38	3.37	3.37
510	3.36	3.36	3.35	3.35	3.34	3.34	3.33	3.33	3.32	3.32
520	3.31	3.31	3.30	3.30	3.29	3.29	3.28	3.28	3.27	3.27
530	3.26	3.26	3.25	3.25	3.24	3.24	3.23	3.23	3.22	3.22
540	3.22	3.21	3.21	3.20	3.20	3.19	3.19	3.18	3.18	3.17

VII. CORE POISONING EXPERIMENT

A. Introduction

Aluminum strips containing boron carbide were uniformly distributed in the 24 element core as a means of evaluating excess reactivity. The boron carbide strips would change the rod bank positions and incremental bank worths at these positions were used to measure incremental bank worths with integrations of these data being used to obtain the core excess reactivity.

Figure VII-1 shows the B_4C-Al poison strips, the poison positioning piece and the aluminum hold-down unit. The hold-down units were used as a safety precaution even though the low power critical runs did not require water flow. The aluminum poison strips were .040" x .25" x 24" long and contained 3.39 percent boron as boron carbide.

The initial core contained 24 fuel elements with the central thimble voided. Each fuel element had 4 pieces of poison -- 96 pieces total. Figure VII-2 shows the poison locations for the initial run.

Control rod positions are indicated in percent of rod withdrawal with 100 percent corresponding to 28 inches of travel. At "0" percent, the lower end of the cadmium in the rods is 6.5 inches above the bottom of the fuel region. At 100 percent, the lower edge of the cadmium is 11 inches above the active core region.

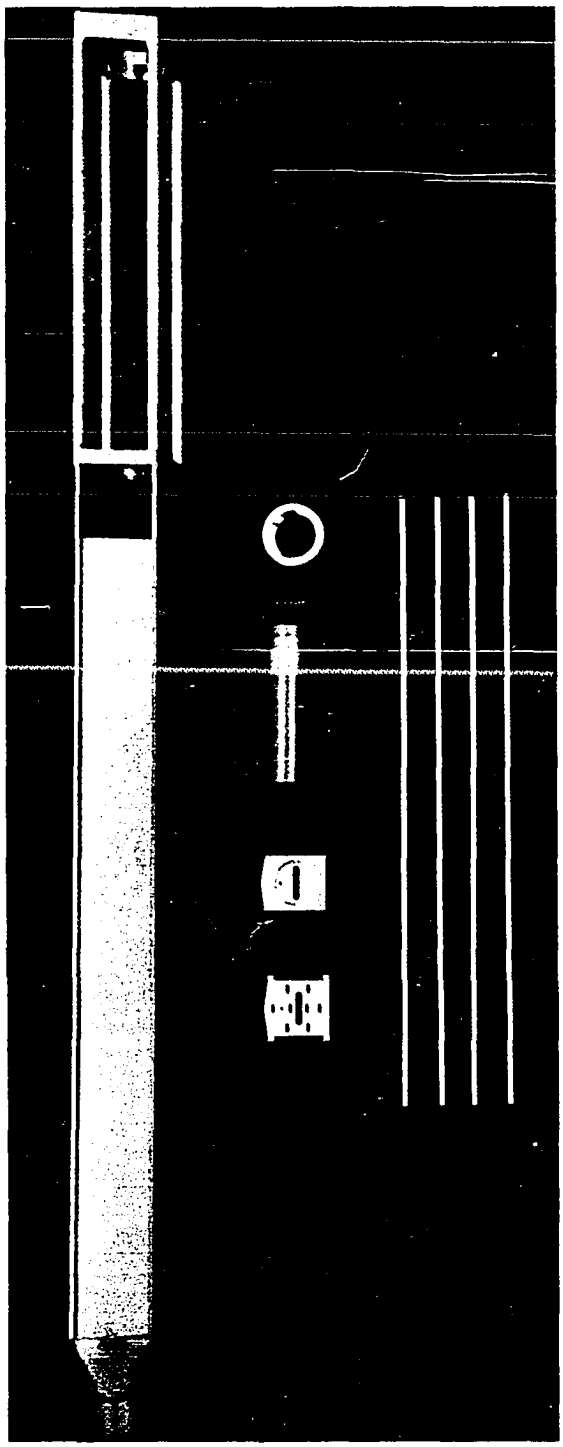

Figure VII-1. Fuel element, B_4C-Al poison strips, poison positioning piece and hold-down unit

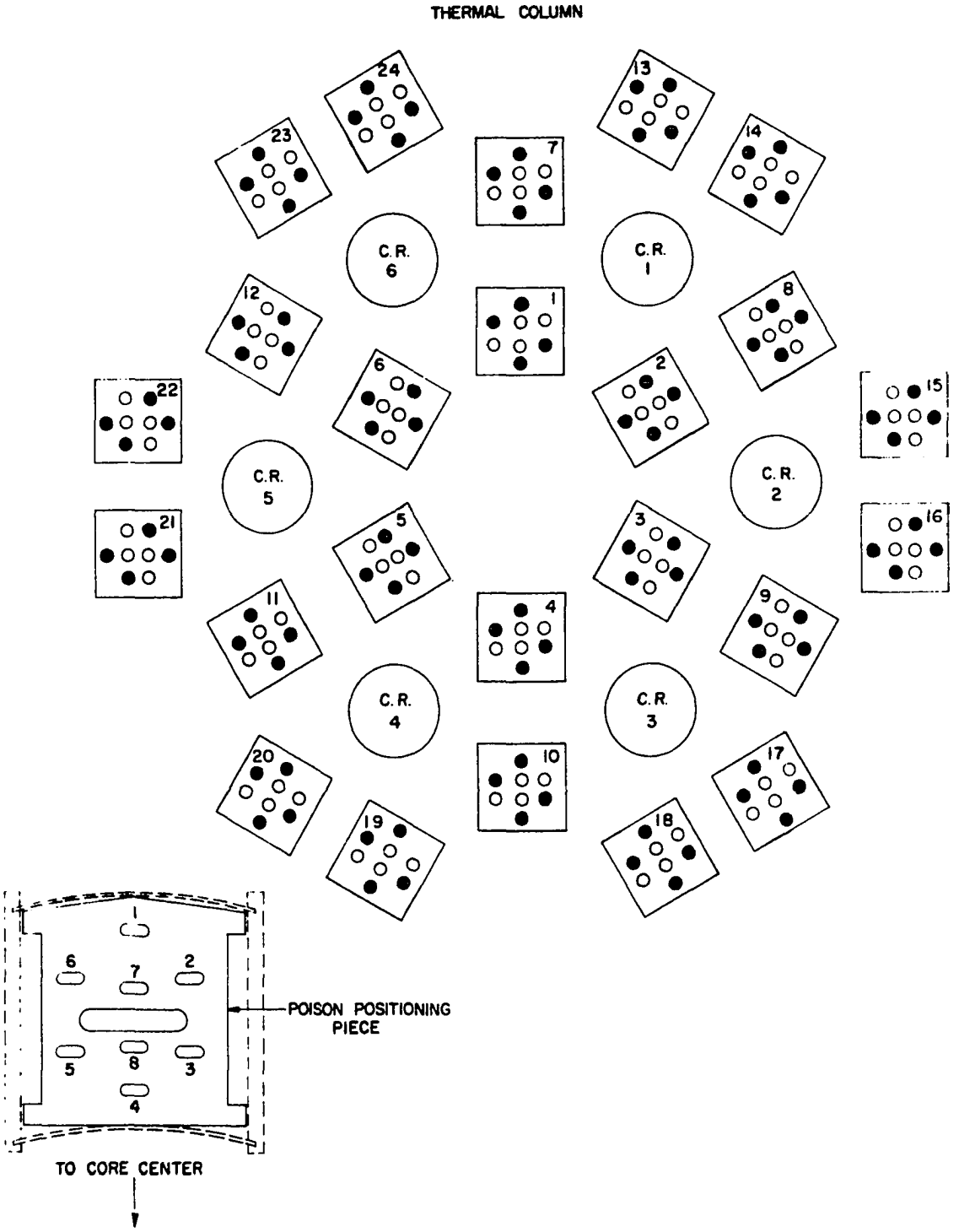

Figure VII-2. 24 element core with 96 poison strips

Less error is introduced by using shorter periods with longer waiting times as indicated in Chapter VI. This also requires larger rod travel with resultant decreased relative rod measurement errors.

Incremental bank worths were obtained for critical conditions as poison was uniformly removed from the reactor. Data were obtained from cores containing 96, 84, 72, 48, 24, 12 and "0" poison pieces. Incremental bank worth results were obtained with integration under these curves being used to obtain the rod bank excess reactivity curves. The reactivity values were obtained from data in the previous chapter.

B. Details of Experiment

The poison strips were .040" x .25" x 24" long and contained 3.39% boron as boron carbide. Table VII-1 lists the amount of boron and carbon contained in this material as obtained by chemical analysis. The remainder of this material was aluminum.

Table VII-1

Chemical Analysis of B_4C - Al Poison

Sample No.	1	2	3	4	Averages
Boron w/o	3.38	3.40	3.40	--	3.393
Carbon w/o	1.09	1.01	1.20	1.09	1.098

The carbon content was higher than the chemical composition of boron carbide would indicate. There was no free carbon in the samples, so the additional carbon must have come from the commercial grade aluminum used to make the strips. A spectrographic analysis indicated trace amounts of the following impurities: Cr, Cu, Fe, Ga, Mg, Mu, Ni and Si.

An aluminum positioning piece, see Figures VII-1 and VII-2, was placed on top of the fuel plates in each element to locate the poison pieces between the fuel plates. Only positions 1, 3, 4, and 6 were used during this series of experiments.

Aluminum hold-down units were placed on top of the poison strips to prevent movement of these strips during an experiment or during insertion of a fuel element into the D_2O system. The hold-down units served as an added safety precaution to prevent motion of the poison during the experiment even though the "zero" power critical runs did not require water circulation through the fuel elements.

C. Core Conditions

These experiments were conducted in the 24 element core with the central thimble voided. Data were obtained from cores containing 96, 84, 72, 48, 24, 12 and "0" pieces of poison. Figures VII-2 to VII-8 show the locations of the poison pieces for the various cores and Table VII-2 lists the amount of boron present in each core loading.

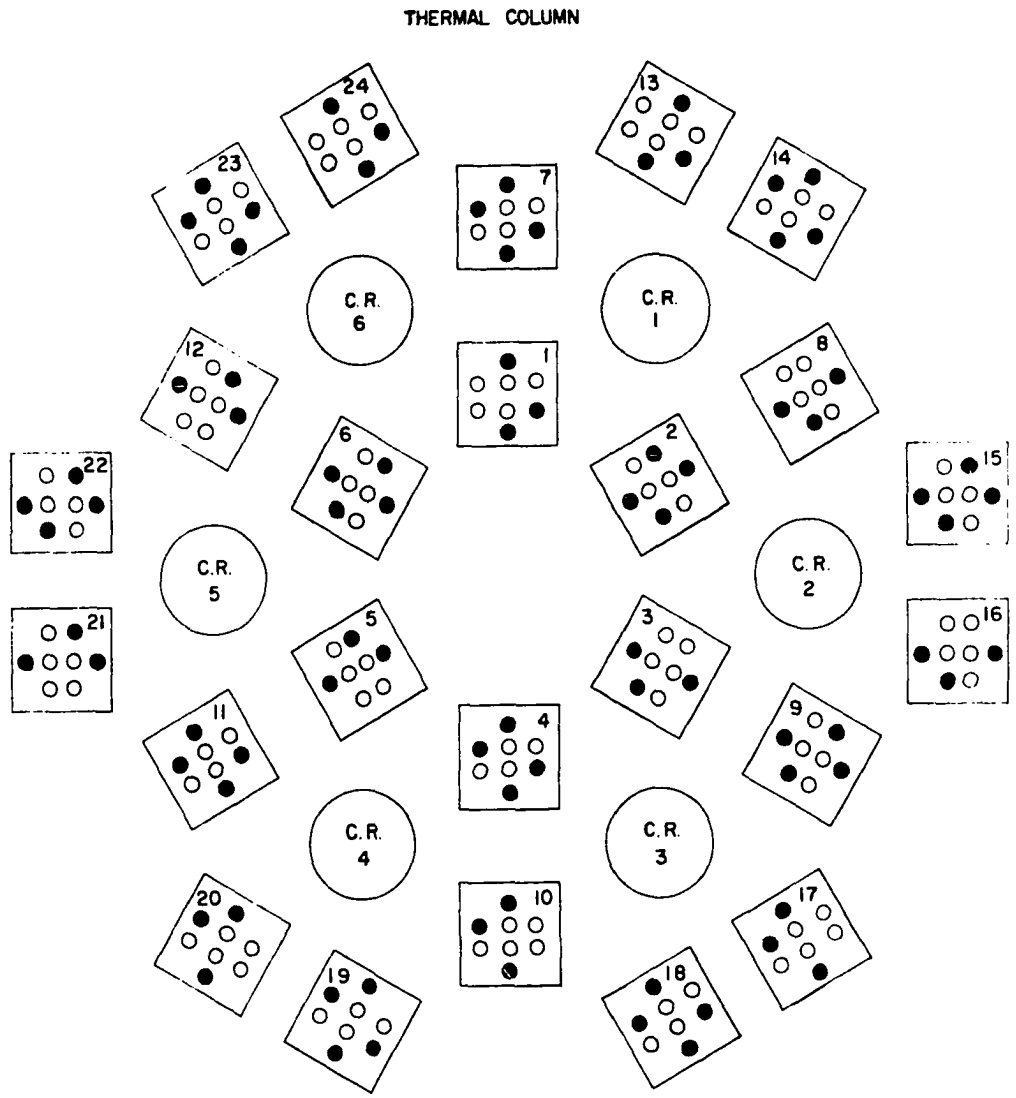

Figure VII-3. 24 element core with 84 poison strips

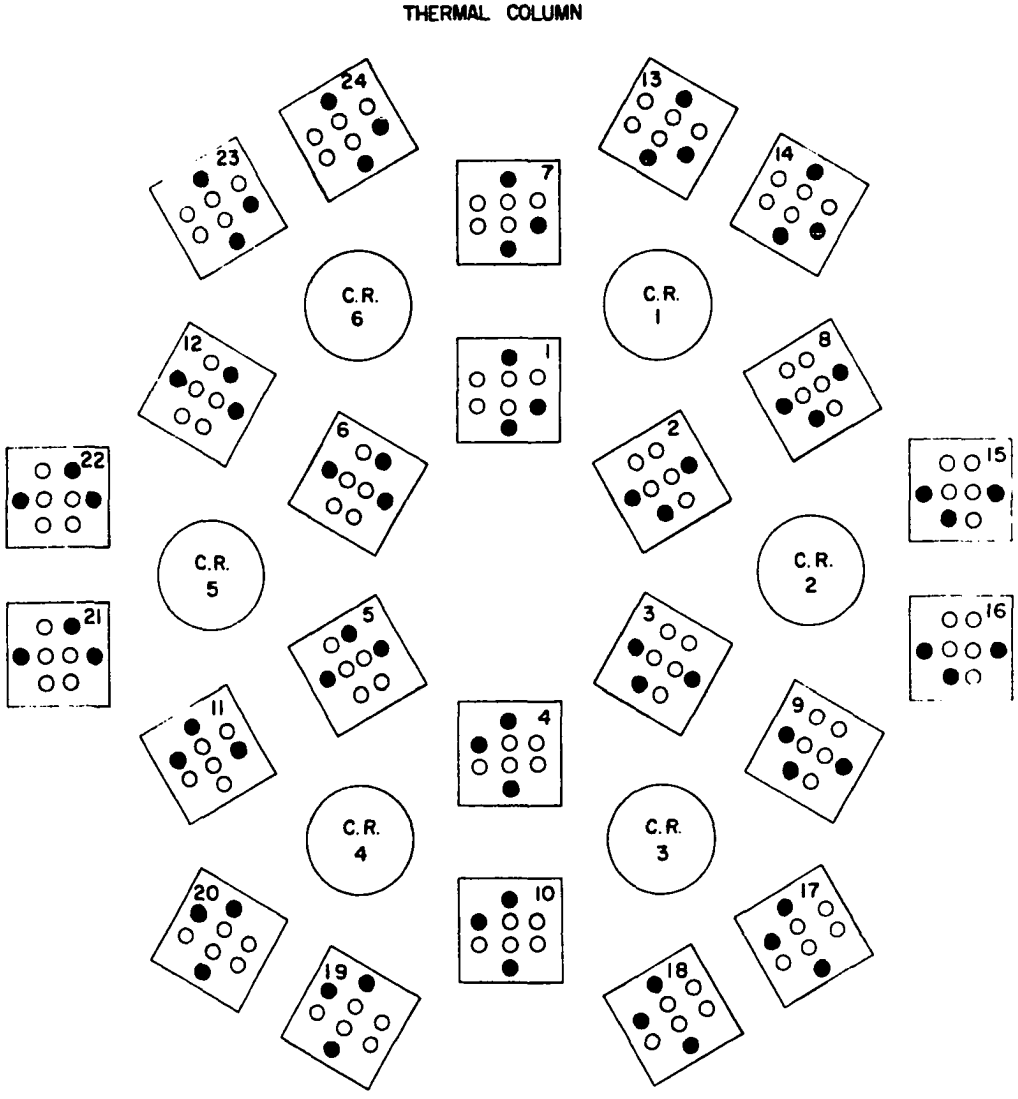

Figure VII-4. 24 element core with 72 poison strips

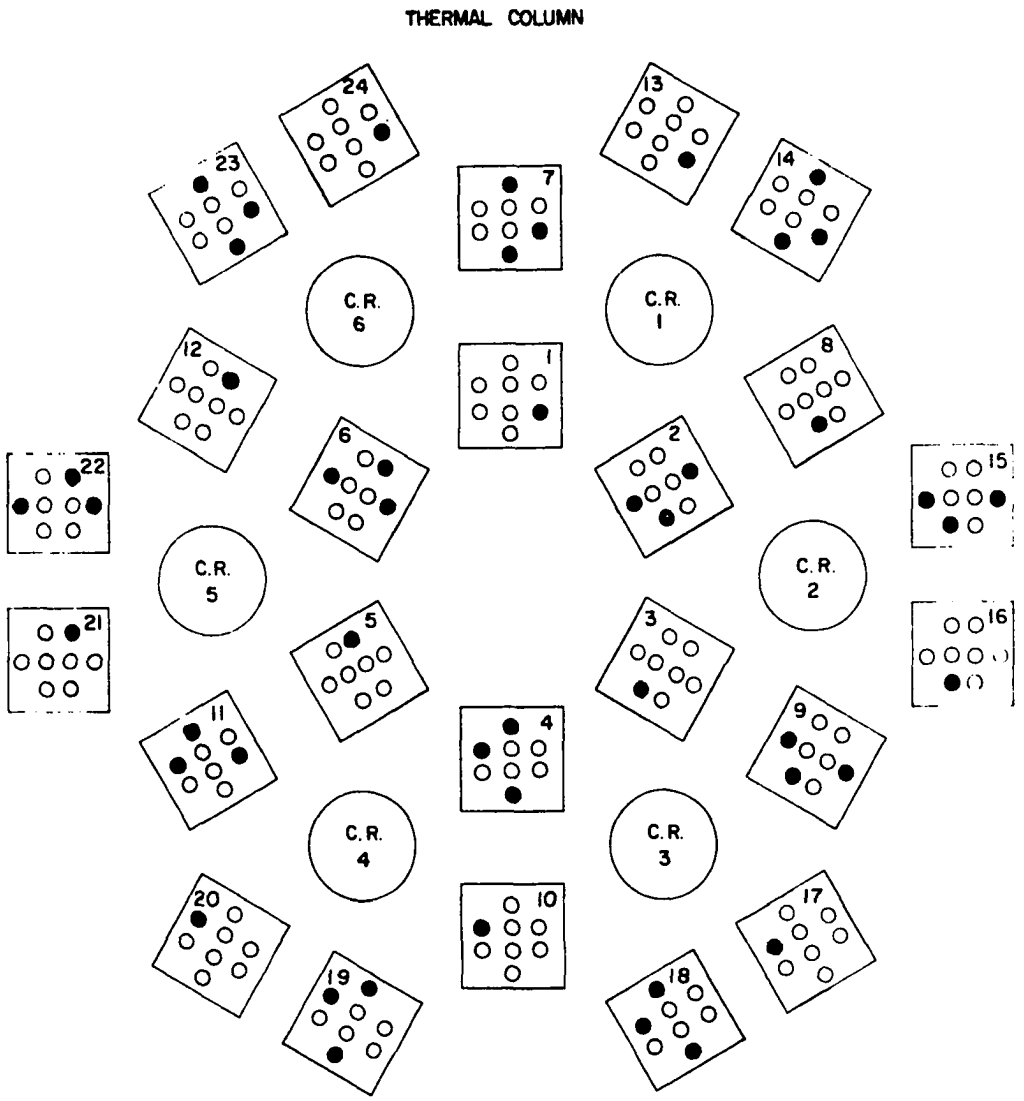

Figure VII-5. 24 element core with 48 poison strips

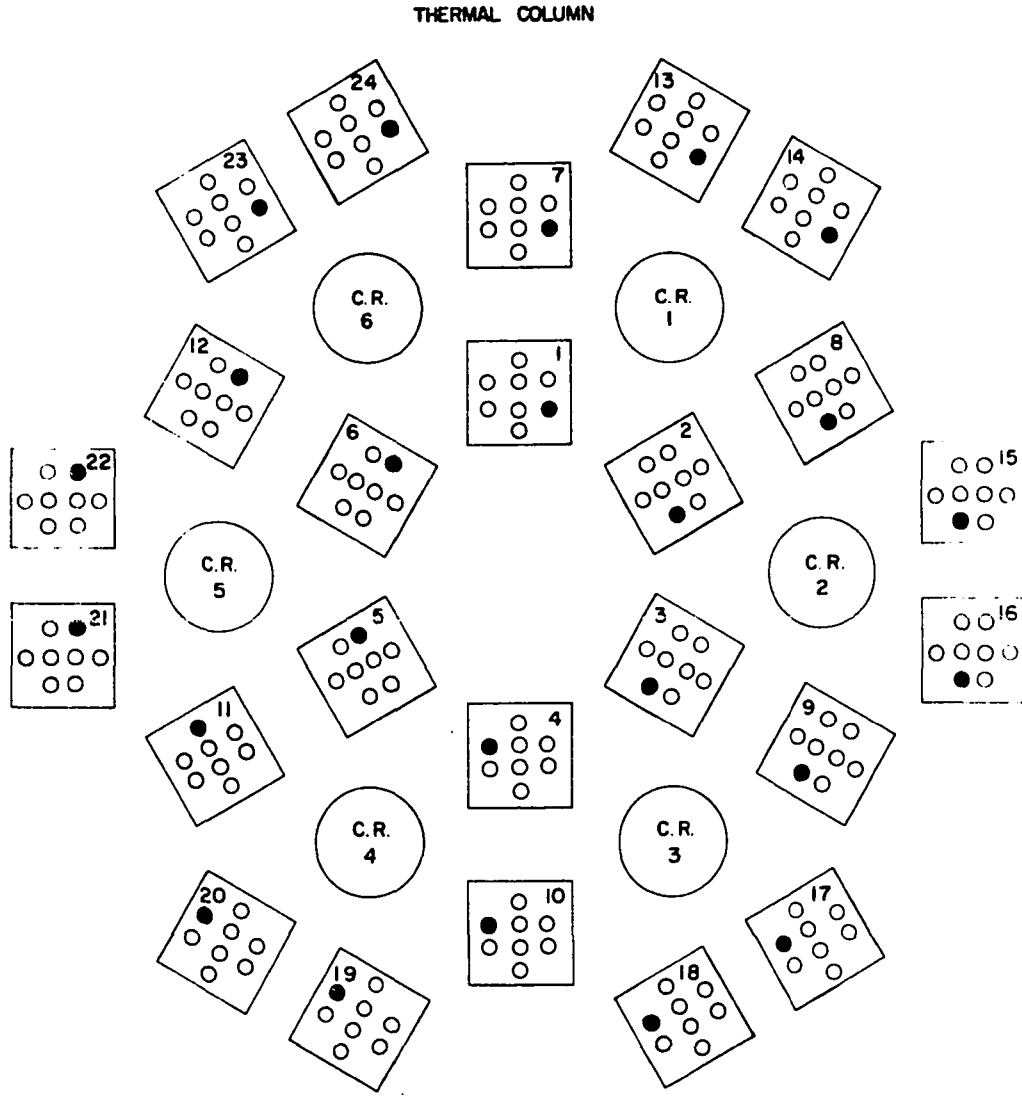

Figure VII-6. 24 element core with 24 poison strips

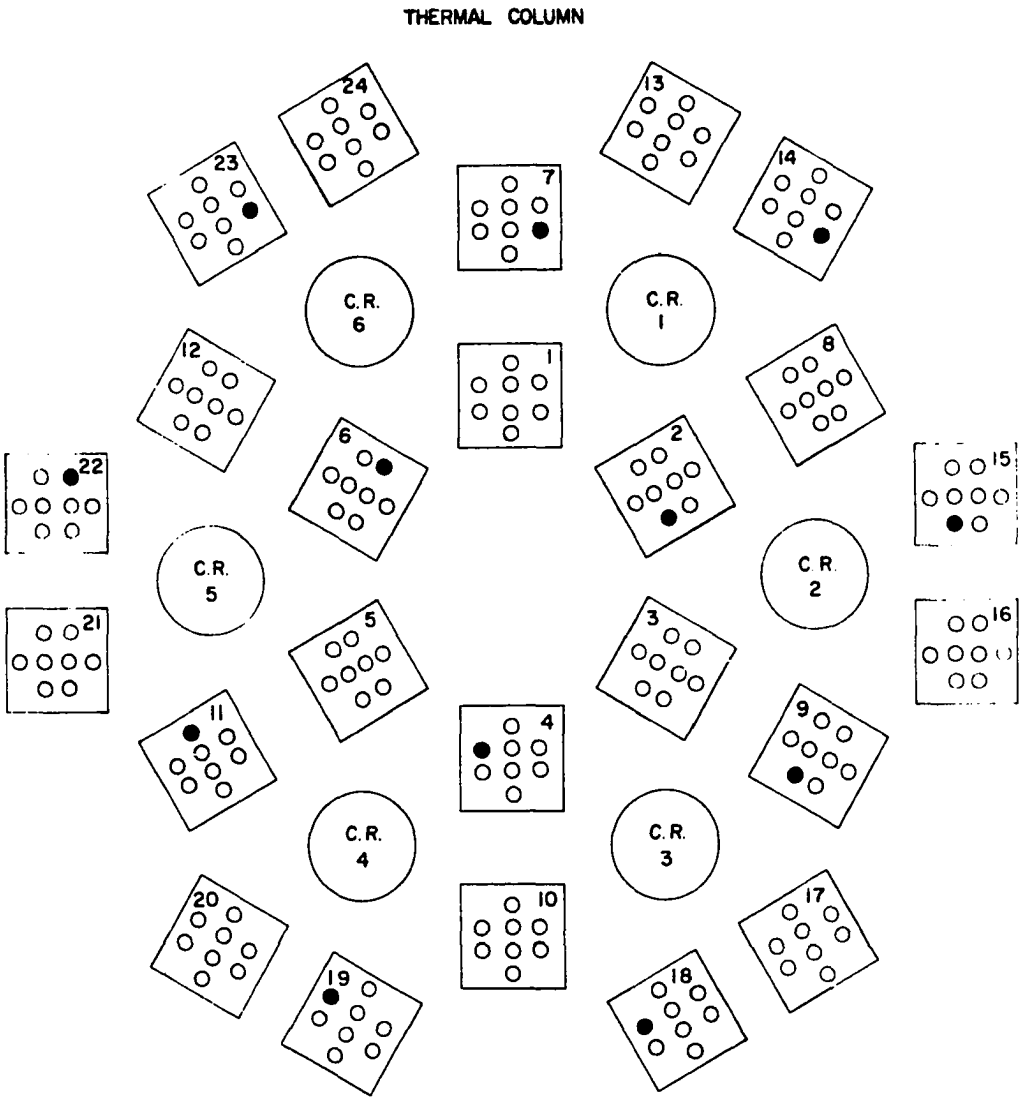

Figure Vii-7. 24 element core with 12 poison strips

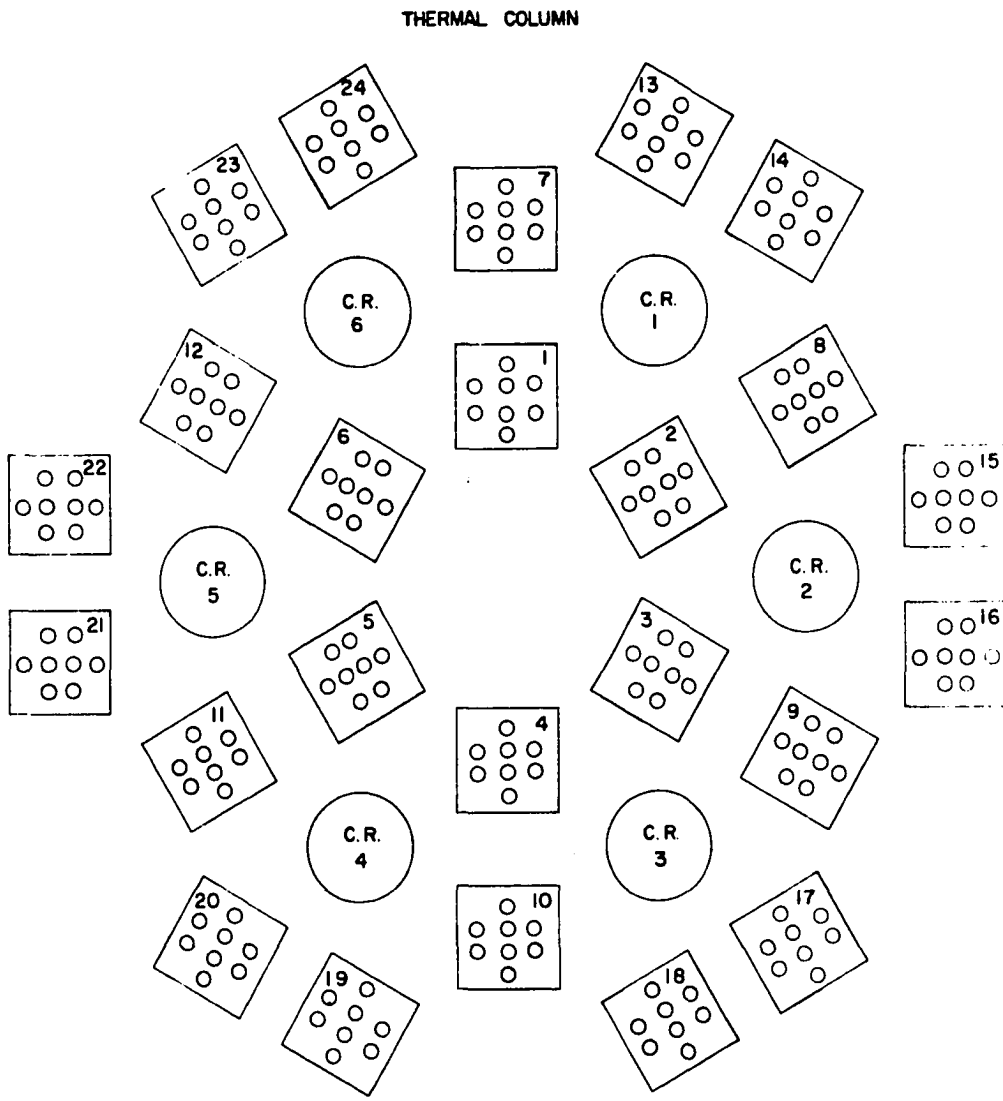

Figure VII-8. 24 element core with "0" poison strips

Table VII-2

Amount of Boron for Each Loading

Number Pieces	Grams B_4C-Al	Grams B
96	972	33.0
84	851	28.8
72	729	24.7
48	487	16.5
24	243	8.24
12	121	4.10

D. Experimental Data

Incremental control rod and 6 rod bank worths were measured for each poison loading. The following method was used to obtain these measurements for each core condition:

1. Go critical with the six rods in a banked position.
2. Insert the regulating rod a short distance estimated to be worth less than 30 cents and maintain criticality by adjusting the remaining five rod bank.
3. Withdraw the regulating rod to the new bank position. Measure the reactor period and obtain its corresponding worth in cents of reactivity.
4. Calculate the incremental bank worths for their corresponding travel.

The incremental rod bank worths are shown in Figure VII-9 with the integral of these curves shown in Figure VII-10. The lower curves assume all delayed neutron fractions are present.

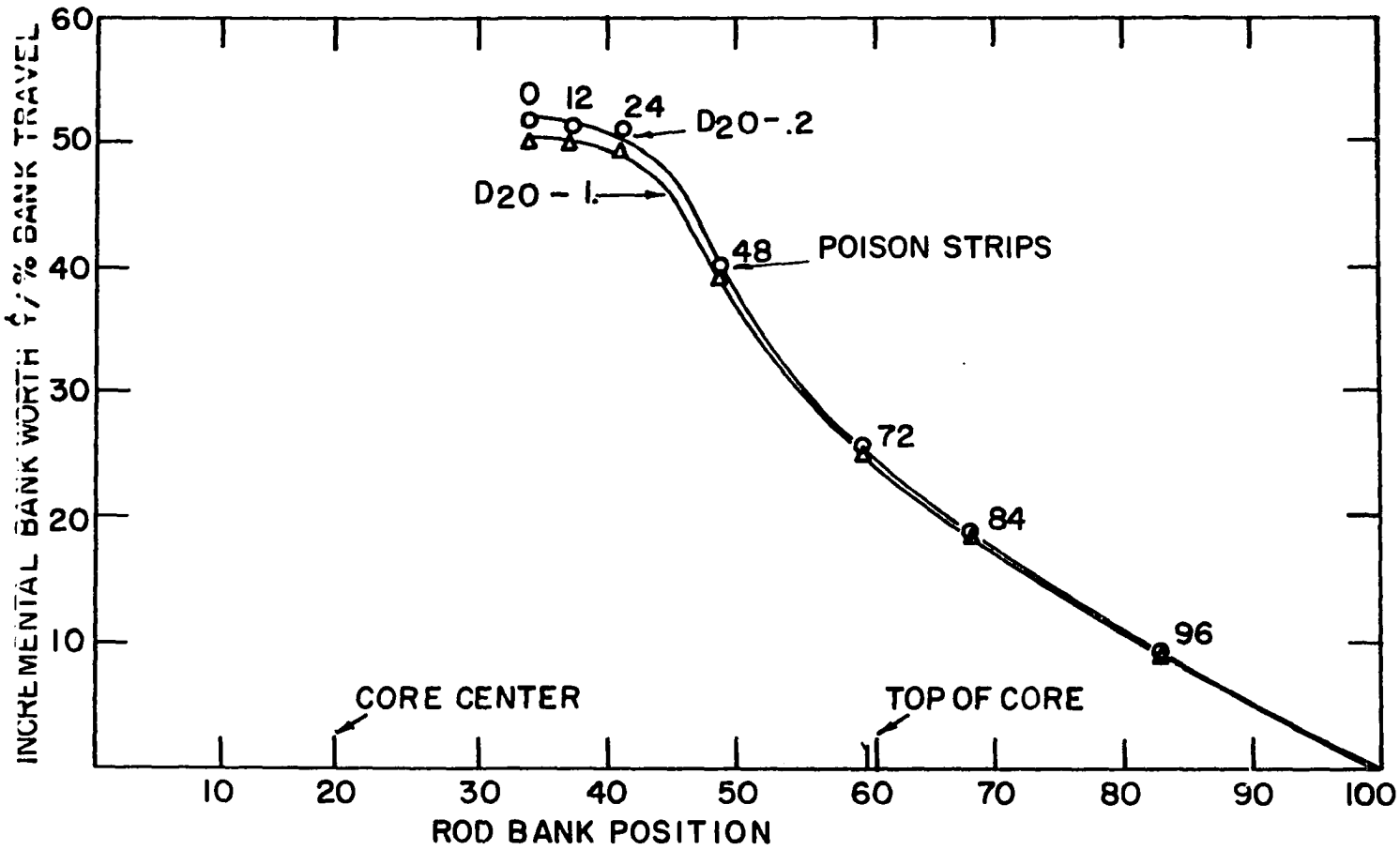

Figure VII-9. Incremental bank worth versus rod bank position as a function of the abundance of the 2.5 second photoneutron and number of poison strips

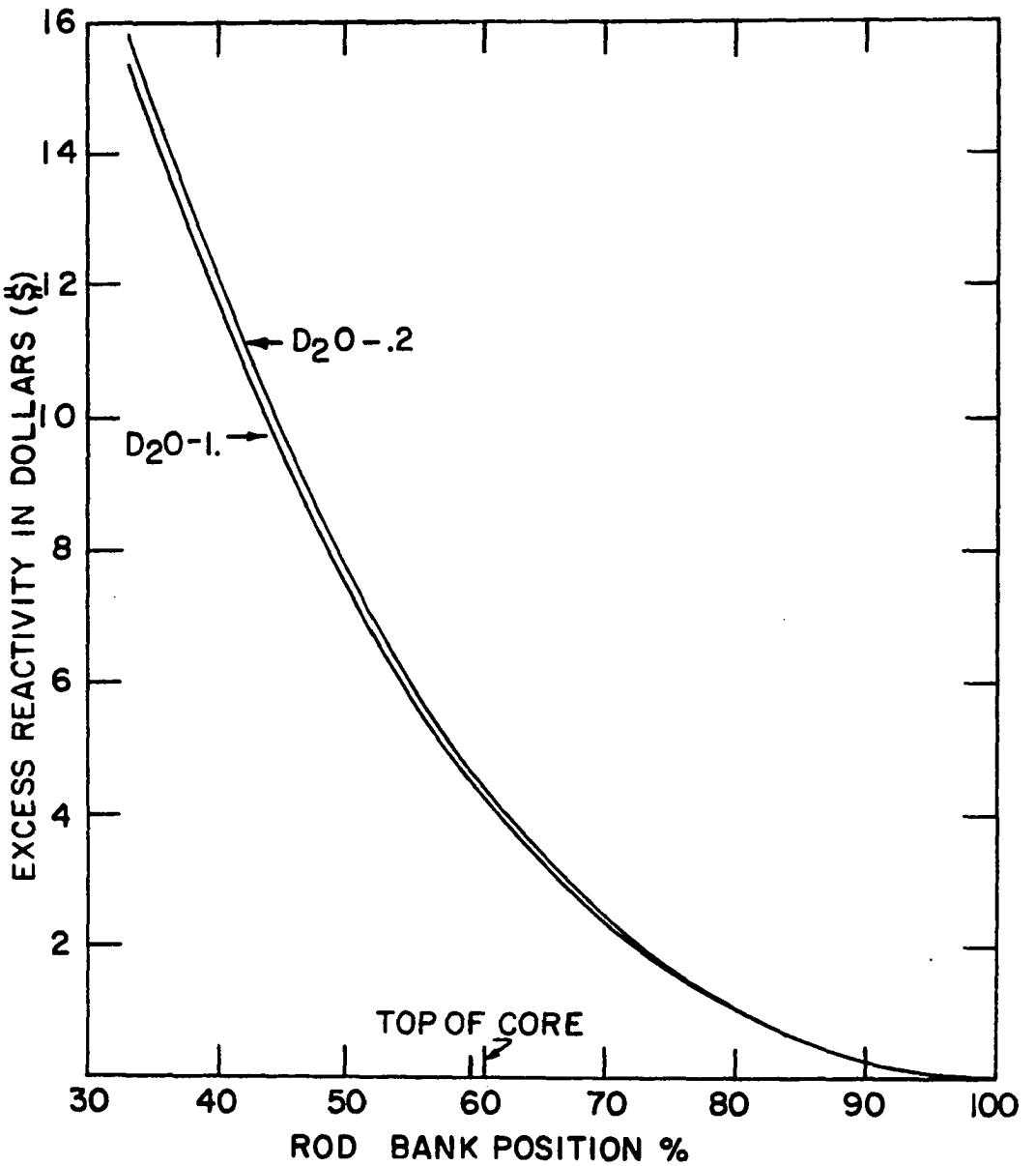

Figure VII-10. Integrated bank worth versus rod bank position as a function of the abundance of the 2.5 second photoneutron

The upper curves assume that only 20 percent of the 2.5 second photoneutrons are present as indicated in Chapter VI.

Using the upper curve, the excess reactivity is 15.8 dollars with the center thimble voided. The thimble is worth .007 $\Delta k/k$ and flooding the central thimble is worth .0113 $\Delta k/k$. Changing to dollar system makes the total excess reactivity 17.8 dollars based on a β_{eff} of .0091 used during the initial critical experiments.

Several members of the Ames Laboratory Reactor Division have measured β/ℓ using the rod oscillator method. The values of β/ℓ have remained fairly consistent. The method assumed the value of β_{eff} of .0091 in the Hazards Report as a means of determining the value of ℓ. However, the use of the ℓ value of 5.3×10^{-4} seconds given in the Hazards Report would make β_{eff} equal to 0.0073. This gives a variation in β_{eff} of 20 to 24 percent depending on which value of β_{eff} is assumed correct. This would also vary the value of reactivity from 13.0 percent to 16.2 percent for the 24 element core depending on the value of β_{eff} used.

VIII. SUMMARY AND CONCLUSIONS

The design procedures used in this dissertation are similar to the technique used for the design of light water moderated reactors. The LEOPARD code, modified for plate-type fuel elements, was used to generate few group neutron cross section sections. The diffusion code EXTERMINATOR-2 was used to solve the cell calculations and normal spatial calculations in R-θ geometry. The FOG program was used for its buckling iteration and poison search features.

The 24 element core was solved using one-sixth core symmetry and four neutron groups. The 13 element minimum critical mass core was solved using one-half core symmetry and only two neutron groups because of its large mesh size of 50x 44 mesh points. Going to four groups would increase program costs.

The 24 element core gave a calculated k_{eff} of 1.1507 which is equal to a reactivity of 13.1 percent. Measured values, using borated poison strips, gave reactivity values that varied from 13 to 16.2 percent depending on the value of β_{eff} used. The calculated value would agree with a β_{eff} of 0.0074. More emphasis should be placed on calculating or measuring the value of β_{eff} and of the neutron lifetime ℓ to better determine the measured value of k_{eff} from the poison experiment so it can be used to check the calculated value.

The calculated value of k_{eff} was 1.0038 for the 13 ele-

ment core. This value agrees reasonable well with the measured value for k_{eff} of 1.0063. Attempts should be made to use four neutron groups to attempt to get better agreement with measured value without depending on the four group to two group bias in k_{eff}.

The control rods, in their fully withdrawn position, were worth a k_{eff} of 0.006. The FOG 3 poison search routine was used to add a distributed poison to this rodded region to have the same worth.

More emphasis should be placed on the super cell technique in the LEOPARD code that accounts for the extra material in the core region. A parallel method should be developed for plate type fuel elements to give better group cross sections to be used in the other codes.

IX. LITERATURE CITED

1. AMF ATOMICS, "Final Hazards Summary Report for Ames Laboratory Research Reactor, Ames, Iowa," American Machine & Foundry Company (March 1964).

2. Y. S. KIM, "Development of Design Procedures to Determine Reactor Physics Characteristics of High-Enriched Heavy Water Moderator Reactors," NUS-652, NUS Corporation (March 1970).

3. T. J. THOMPSON, M. BENEDICT, et al., "Final Hazards Summary Report to the Advisory Committee on Reactor Safeguards on a Research Reactor for the Massachusetts Institute of Technology," MIT-5007, Massachusetts Institute of Technology (1956).

4. C. L. LARSON, "Reactivity Studies of a Heavy Water Moderated, Highly Enriched Uranium Reactor," Sc.D. Thesis, Massachusetts Institute of Technology (July 1959).

5. R. P. MORGAN, "Estimation of Void Coefficients in MIT Reactor," M.S. Thesis, Massachusetts Institute of Technology (1959).

6. E. BARNETT, et al., "The MIT Nuclear Reactor Startup," Transactions of the American Nuclear Society 2, 74 (June 1959).

7. R. L. MATHEWS, "Flux Distributions in the MIT Reactor," Ph.D. Thesis, Massachusetts Institute of Technology (1964).

8. W. W. GRAHAM and D. M. WALKER, "Safety Analysis Report for the 5 MW Georgia Tech Research Reactor," GT-NE-7 (1967).

9. NATIONAL BUREAU OF STANDARDS, "Final Safety Analysis Report on the National Bureau of Standards Reactor," NBSR9 (April 1966).

10. R. F. BARRY, "LEOPARD - A Spectrum Dependent Non-Spatial Depletion Code for the IBM-7094," WCAC-3269-26 (1963).

11. H. BOHL, JR. and A. P. HEMPHILL, "MUFT-5, A Fast Neutron Spectrum Program for the Philco 2000," WAPD-TM-218 (1961).

12. H. AMSTER and J. B. KALLAGAN, "KATE-1, A Program for Calculating Wigner-Wilkins and Maxwellian Averaged

Thermal Constants on Philco-2000, WAPD-TM-232 (1960).

13. R. L. HELLENS, "Neutron Slowing Down in Group Diffusion Theory," WAPD-114 (1956).

14. E. GRUELING, et al., "A Multigroup Approximation to the Boltzmann Equation for Critical Reactors," NDA-10-96 (circa 1955).

15. E. P. WIGNER and J. E. WILKINS, "Effect of the Temperature of the Moderator on the Velocity Distribution of Neutrons with Numerical Calculations for H as Moderator," AECD-2275 (1948).

16. A. AMOUYAL, P. BENOIST and J. HOROWITZ, "Nouvelle Methods de Determination du Facteur d'Utilization Thermique d'Une Cellule," J. Nucl. Energy, 6, 79 (1957).

17. C. P. BHALLA, "Thermal Flux Disadvantage Factors for Slab Geometry," Nucl. Sci. Eng., 12, 311 (1962).

18. M. H. THEYS, "Integral Transport Theory of Thermal Utilization Factor in Infinite Slab Geometry," Nucl. Sci. Eng., 7, 58 (1960).

19. D. SCHIFF and S. STEIN, "Escape Probability and Capture Fraction for Gray Slabs," WAPD-149 (1956).

20. H. P. FLATT, "The FOG One Dimensional Neutron Diffusion Equation Codes," NAA-SR-6104 (1961).

21. T. B. FOWLER, et al., "EXTERMINATOR-2, A Fortran-IV Code for Solving Multigroup Neutron Diffusion Equations in Two Dimensions," ORNL-4078 (1967).

22a. S. GLASSTONE and M. C. EDLUND, The Elements of Nuclear Reactor Theory, D. Van Nostrand Company, Inc., New York (1952).

22b. G. R. KEEPIN, Physics of Nuclear Kinetics, Addison-Wesley Publishing Co., Inc., Reading Mass. (1965).

23. G. R. KEEPIN, T. F. WIMETT and R. K. ZEIGLER, "Delayed Neutrons from Fissionable Isotopes of Uranium, Plutonium and Thorium," Physical Review, 107, 1044 (1957).

24. S. BERNSTEIN, et al., "Yield of Photoneutrons from U-235 Fission Products in Heavy Water," Physical Review, 71, 573 (1947).

25. W. K. ERGEN, "Hard Gamma Emitters among Fission Fragments," ANP-59 (1951).

26. W. W. GRAHAM and D. S. HARMER, "The Determination of Effective Delayed Neutron and Photoneutron Kinetics Parameters in a Highly Enriched Heavy-Water Reactor," TID-22730 (1965).

27. J. P. CHURCH, "Evaluation of Published Delayed-Neutron Parameters for Uranium-235 and Uranium-235 Heavy Water Systems," Nucl. Sci. Eng. 43, 229 (1971).

X. ACKNOWLEDGEMENTS

I wish to express my sincere gratitude to Dr. R. A. Danofsky for his counseling and guidance. I wish to express my gratitude to Dr. Y. S. Kim of NUS Corporation for his suggestions and help with the alterations to the LEOPARD computer code and particularly to Dr. O. Gailar of Purdue University for his many suggestions during the course of this dissertation. I also wish to thank the members of Ames Laboratory for all the services rendered and to the members of my family for their great patience.